SINGLE-BOLTED CONNECTIONS FOR ORTHOTROPIC FIBRE-REINFORCED COMPOSITE STRUCTURAL MEMBERS

BY

CHARLES N. ROSNER

A Thesis
Submitted to the Faculty of Graduate Studies
in Partial Fulfilment of the Requirements
for the Degree of

MASTER OF SCIENCE

Department of Civil Engineering
University of Manitoba
Winnipeg, Manitoba

(c) September, 1992

Canada

SINGLE-BOLTED CONNECTIONS FOR ORTHOTROPIC FIBRE-REINFORCED

COMPOSITE STRUCTURAL MEMBERS

BY

CHARLES N. ROSNER

A practicum submitted to the Faculty of Graduate Studies of the University of Manitoba in partial fulfillment of the requirements of the degree of

MASTER OF SCIENCE

(c)   1992

ABSTRACT

Although the high strength-to-weight ratio makes fibre-reinforced composite materials extremely attractive to the structural engineer, there is a lack of research, and consequently, a lack of criteria needed to design structures, especially connections, using these materials. The design of bolted connections for orthotropic fibre-reinforced composite materials requires much more attention in comparison to the connections used for standard isotropic homogenous structural steels. In light of this, an experimental investigation was conducted at the University of Manitoba to study the behaviour of connections fabricated from a glass-fibre-reinforced composite material. A total of 102 single-bolt double-shear lap connections was tested. The effects of the various geometric parameters including, the connection width, edge distance, material thickness, and fibre orientation were studied. Based on the research findings a design procedure is introduced which accounts for material orthotropy, pseudo-yielding capability, and other factors that influence the connection behaviour. The experimental results were used to correlate and refine a proposed analytical model introduced to describe the behaviour of single-bolted connections in composite materials. The proposed design procedure is capable of predicting the ultimate load and failure modes of a connection with any geometry. Because of the generic nature of the model, the design guidelines can be applied to a multitude of composite material systems. Due to the model's simplicity, the proposed design procedure is ideal for future design codes.

ACKNOWLEDGEMENTS

TABLE OF CONTENTS

LIST OF TABLES

LIST OF FIGURES

CHAPTER 1 INTRODUCTION

1.1 GENERAL

The high strength-to-weight ratio of fibre-reinforced composites makes them extremely attractive as a building material for civil engineering applications. The structural integrity and strength of a building using advanced composite materials is mainly controlled by the strength of the connections rather than the strength of the members. Several types of connections are currently used for structures. These include bolted, bonded, combined bolted-bonded, and interlocking connections. For civil engineering applications bolted connections are easy to assemble and disassemble, easy to maintain, and are usually cost-effective when compared to other types of connections. Therefore, bolted connections are the most practical for civil structural applications.

The main problem with achieving the full potential of fibre-reinforced composite materials in civil engineering applications, is the lack of the designer's familiarity with the material. Although much research has been conducted on the behaviour of this material for the aeronautical and automotive industries, there has been very little research conducted for the civil engineering field, especially in the area of bolted connections.

Research done by the aeronautical and automotive industries has mostly dealt with thin composite laminates where the ratio of the hole diameter to the thickness

of the member is high enough to induce very little deformation of the bolt through the thickness of the material. However, connections for civil structures involve relatively thick members due to the nature of the applied load. Therefore the through-thickness effects could be significant. In addition, connections for civil structures are required to carry unusually high loads for long periods of time, in often fluctuating and extreme environmental conditions without the benefit of periodic inspections. Slender structural members which are mainly used in building construction are inherently fabricated via the pultrusion process making their behaviour different from the multi-angle laminate skins typically used in the aeronautical and automotive fields.

The design of bolted connections with fibre-reinforced composites is much more complex than with standard structural materials such as steel. Bolted connections not only sever the reinforcing fibres and thus reduce the overall strength of the composite, but also introduce high stress concentrations which promote fracture. Material orthotropy and heterogeneity further complicate the situation, as well as the fact that the behaviour of fibre-reinforced composites lies somewhere between that of perfectly elastic behaviour and fully plastic behaviour and therefore cannot be characterized by either.

1.2 OBJECTIVE

The main objectives of this research program are:

1. to investigate the behaviour of bolted connections in fibre-reinforced composite materials;

2. to develop a model to predict the ultimate load and mode of failure of single-bolted connections in fibre-reinforced composite materials; and

3. to introduce a simple design procedure which can be used in a design code.

1.3 SCOPE

A comprehensive experimental and analytical investigation was conducted at the University of Manitoba to study and determine the behaviour of bolted connections in composite materials for civil engineering applications. The investigation studied the behavioral effects of various geometric parameters including the width, edge distance, material thickness and fibre orientation of the connection. The investigation emphasized the behaviour of single-bolt double-shear lap connections fabricated from a glass fibre-reinforced composite material. Based on the research findings, a design procedure was developed. The proposed design methodology is capable of predicting the ultimate capacity and failure mode of single-bolt double-shear connections.

CHAPTER 2 LITERATURE REVIEW

2.1 INTRODUCTION TO COMPOSITES

Fibre-reinforced composite materials consist of high strength fibres embedded in a matrix. Although each constituent maintains its unique material properties and characteristics, together they produce a material that has properties that cannot be achieved by either component acting alone. The fibres used for composite materials may consist of glass, carbon, or aramid materials, while the matrix may consist of polymers, metals, or ceramics. The fibres are the principal load-carrying members. The main functions of the matrix consist of keeping the fibres in the desired location and orientation, transferring load between the fibres, and protecting the fibres from the environment.

In civil engineering structural applications, where the composites are utilized in the form of plates and structural shapes, most fibre-reinforced composites consist of glass fibres surrounded in either a polyester or vinylester plastic matrix. Although other materials could be used to produce higher performance composites, they are very expensive. Due to the potential for the use of large quantities of composite materials in civil engineering applications, glass-fibre-reinforced plastic composites (GFRP) are the most economical. To date, several companies are producing GFRP structural sections and many standard shapes and sizes are commercially available.

Fibre-reinforced composite materials are fairly new to the civil structural field.

Green (1) discusses the use of these materials in the construction industry and how the high strength-to-weight ratio and corrosion resistance of fibre-reinforced composites makes them extremely attractive as a building material. Sheard (2) explains that one of the main reasons why the use of these materials has not grown dramatically is the lack of knowledge of their behaviour. Proposals as well as the transfer of fibre-reinforced composite technology as it pertains to civil structures, have been made by several authors including Ahmad and Plecnik (3), Meier (4), (5), and Plecnik, Ballinger, Rao, and Ahmad (6). Preliminary research has been conducted to determine the behaviour of fibre-reinforced composite structural members by Barbero (7); Meier, Muller, and Puck (8); Bank (9), (10) and Mosallam (11).

Many fibre-reinforced composite materials offer material properties and strengths comparable to the mild steels typically used for civil applications. The high strength-to-weight ratio of fibre-reinforced composites makes them extremely attractive as a building material.

Since fibre-reinforced composites are generally orthotropic and heterogenous, the design of structural components and connections is more complicated in comparison to the traditional structural steels which are isotropic and homogenous.

Most composite materials utilize continuous unidirectional fibres oriented in a particular direction. The axes of orthotropy or the principal material axes coincide with the longitudinal and transverse axes of the unidirectional fibres. The material strengths and elastic properties are higher in the direction of the principal fibres and

are lower when measured at any angle with respect to this axis, Mallick (12). In general the lowest strengths are measured at 90° to the unidirectional fibres. The principal material directions are normally designated by an orthogonal coordinate system. The first axis, axis-1, is located in the plane of the composite lamina and is parallel to the unidirectional fibres, the second axis, axis-2 is also located in the plane of the lamina and is transverse to the unidirectional fibres, and the third axis, axis-3, designates the direction of the thickness as shown in Fig. 2.1. For in-plane analysis the four independent elastic constants are the longitudinal and transverse elastic moduli E_{11}, E_{22}, the in-plane shear modulus G_{12}, and major Poisson ratio v_{12}.

Besides the directional dependence of the material properties, the design of structures using fibre-reinforced composites is complicated by the fact that the material is heterogenous. Fibre-reinforced composites are elastic up to failure which is quite different than the behaviour of typical structural steels which are capable of large plastic deformations before failure. However, due to the heterogenous nature of the fibre-reinforced composite material, the various failure mechanisms at the microscopic level, can produce a pseudo-yielding effect. Although this pseudo-yielding capability of composites is not nearly as great as the yielding for ductile structural steels, it is enough to warrant special consideration in the design of composite structures, and in particular, the design of bolted connections in composite materials.

2.2 BOLTED CONNECTIONS IN COMPOSITE MATERIALS

In civil structural applications, the mechanical fastener connection is the easiest to assemble and disassemble, and is usually the most cost effective compared to bonding and other types of connections. Cosenza (13) as well as Godwin and Matthews (14) discuss various types of fasteners and the problems associated with each. Although there are several types of mechanical fasteners, the three basic kinds consist of screws, rivets, and bolts. Screws have low load-carrying capacity and therefore are not practical for structural purposes. Rivets can provide adequate strength, however the riveting operation can damage the composite material in addition to the fact that the clamping forces are difficult to control, Godwin and Matthews (14). Typically bolts have the highest strength and do not cause damage to the composite material during assembly. With properly sized washers and applied torques, the clamping forces can be controlled, Bickford (15). Therefore bolts are considered the most practical fasteners for civil structural applications.

Recently, some initial research has been conducted on structural bolted connections with respect to civil applications by Bank, Mosallam, and McCoy (16), who investigated beam-column connections fabricated from glass fibre-reinforced pultruded sections. However, most research on the behaviour of bolted connections in composite materials has been conducted in the aeronautical and automotive fields as shown in literature surveys by Tsiang (17) and Vinson (18). There are several primary aspects of mechanically fastened connections that researchers have concentrated on. These include the effects of various parameters such as type of

material, type of fastener, and joint geometry. In addition, complications associated with the material anisotropy, heterogeneity, bolt-to-hole interactions, pseudo-yielding capabilities, stress concentrations, failure modes, and failure criteria have all been studied to some degree. The complexity of bolted connection behaviour is discussed by Matthews (19), Bord (20), and Oplinger (21).

For bolted connections one of the major design considerations is the high stress concentrations in the vicinity of the bolt hole. Drilling holes to fabricate a connection could considerably weaken the composite member due to the discontinuity of the principal load-carrying fibres. This fact, coupled with the orthotropy of composite materials, generally leads to stress concentrations around the bolt hole higher than what is generally experienced in isotropic structural steels. An exact stress solution was developed for an infinitely wide, isotropic, elastic plate with an unloaded hole, attributed to Kirsh by Timoshenko (22). Lekhnitskii (23) extended this solution to encompass orthotropic materials. It must be noted however, that these solutions are for unloaded holes and the stress distribution for a plate loaded through a hole is quite different. A solution for an infinite, elastic, isotropic plate loaded through a hole was developed by Bickley (24). By the method of superposition, De Jong (25) developed an approximate solution for an orthotropic plate with finite dimensions. However, to date there is no exact closed-form solution available for an orthotropic plate of finite dimensions loaded through a hole. Therefore the stress distributions are currently determined via numerical procedures or experimental evaluation.

2.3 FAILURE MODES

Bolted connections for fibre-reinforced composite members experience similar failure modes to those of bolted connections fabricated using structural steels. The basic failure modes include net tension, shear-out, and bearing as shown in Fig. 2.2. In addition to these basic failure modes, some fibre-reinforced composite materials are susceptible to a fourth mode known as cleavage or splitting failure, which is also shown in Fig. 2.2. Combinations of the basic modes of failure are also possible.

Bearing failure is usually the most desired failure mode since it is the most ductile and is not catastrophic. To achieve bearing failure, the geometry of the connection usually consists of large edge distances and widths. The basic geometric parameters consist of the connection width "w", the edge distance "e", the hole diameter "d", and the material thickness "t" as shown in Fig. 2.2. In general, the edge distances and widths needed to achieve bearing failure are much larger for composite materials than structural steels.

2.4 EXPERIMENTAL RESEARCH

2.4.1 Single-Bolt Connections

The experimental work conducted by Collings (26) included both single-bolt and multi-bolt connections using carbon-fibre-reinforced composite materials (CFRP). For the single-hole connections, Collings investigated different parameters including the effects of the stacking sequence of multi-angled composites, the hole diameter, the end distance of the connection, the connection width, the lateral

constraint of the bolt, and the composite laminate thickness. The results of his investigation showed that with increasing width-to-hole diameter ratios (w/d), the failure mode changed from net tension failure to bearing failure at (w/d) values between 3 and 7 for different laminate lay-ups. For increasing edge distance-to-hole diameter ratios (e/d), the mode of failure changed from shear-out to bearing failure at (e/d) values between 3 and 5 for different laminate lay-ups. Bearing strength was shown to be dependent on several variables including the degree of lateral constraint and laminate thickness. Collings found that increased lateral constraint increased bearing strength as much as 60-70% up to a lateral pressure of 22 MPa (3190 psi), after which little further strength could be obtained. At a pressure of 22 MPa (3190 psi) the effects of hole size became negligible. With lateral constraint greater than 22 MPa (3190 psi) the thickness of the composite members had no effect on the bearing strength. It was found that the bearing strength decreased with increasing diameter-to-thickness ratios (d/t) without the presence of lateral constraint.

Kretsis and Matthews (27) conducted research on GFRP as well as CFRP composites to examine the effects of the fibre-matrix system on the behaviour of connections. Similar to the work of Collings, the investigation included a parametric study to examine the effects of the connection width, edge distance, hole diameter, and laminate thickness as well as the effects of lateral pressure on the connection bearing strength. Test results indicated that lateral constraint increased the bearing strength for both GFRP and CFRP composites. The results showed that decreasing hole-diameter-to-thickness ratios (d/t), increased the bearing strength. However,

high lateral pressure did not suppress the effects of thickness for GFRP material as it did for CFRP material. This behaviour possibly suggests the presence of some instability effects in the material at the microscopic level, which is independent of lateral pressure. This theory was supported by observations of "out of plane" buckling which had occurred for specimens with (d/t)>3. For civil structural applications, where the members are usually quite thick, these problems are irrelevant. The results showed that as the width increased, the mode of failure changed from net tension failure to bearing failure at approximately (w/d)=3. The bearing strength of the CFRP material was noted to be about 19% higher than for the GFRP material. Similarly, as the edge distance increased the mode of failure changed from shear-out failure to bearing failure at approximately (e/d)=3. Kretsis and Matthews concluded that the effects of all the variables examined were similar for both GFRP and CFRP, although the effect of laminate thickness was more pronounced for GFRP because its lower stiffness favoured instability effects which reduced strength. It should be noted that the CFRP specimens were 20% stronger than the GFRP specimens.

Godwin and Matthews (14) provided a review compiled from numerous sources of work conducted on mechanically fastened joints. The review entails a detailed summary of various material, fastener, and design parameters of composite joints. In general their findings showed that with increasing bolt torque, the bearing strength of the connection increased provided that the bolts were not over tightened and did not crush the material. It was found that to achieve bearing failure the

(e/d) ratio must be within the range of 3 to 5 depending on the laminate lay-up. The review indicated that the recommended minimum (w/d) ratio by various researchers ranged between 3 to 8. The effect of (d/t) was shown to be negligible in the presence of lateral constraint. For pin-loaded plates, (d/t) should be less than 1 to achieve full bearing strength. Other important design parameters included the interactions of multi-hole joints which showed that single-hole results could not be extrapolated to complex connections. It was also found that the direction of load bearing with respect to the fibres could have a great influence on the bearing strength of the material. In general, it can be concluded that generous edge distances and widths and adequately tightened bolts will provide the maximum bearing strength possible for composite bolted connections.

Smith, Ashby and Pascoe (28) modelled the effects of clamping force induced by tightened bolts. Accounting for friction forces and lateral constraints it was found that bearing stresses at the onset of failure increased with increasing clamping forces, friction forces and washer sizes.

2.4.2 Multi-Bolt Connections

The transition from single-bolt to multi-bolt connections is complicated and does not consist of simple extrapolation. Several researchers have conducted experimental and analytical work in the area of multi-fastener connections. The bearing/bypass load ratio is a major factor in the behaviour of multi-fastener connections as reported by Ramkumar (29) and Tang (30). The bearing/bypass load

ratio is the ratio of the load resisted by a particular bolt in a connection to the load resisted by other bolts behind it. Ramkumar's work showed that for both static and cyclic load conditions there was a linear reduction in connection strength with increasing bearing/bypass load ratios.

Collings (26) conducted work on single and multi-bolt composite connections. Several multi-bolt configurations were tested to study the interaction between holes and their effects on the tensile strength of the connection. Collings concluded that there was no interaction among the bolt holes for large pitch and gauge spacings and that the behaviour of multi-fastener connections could be determined from single-hole data.

Agarwal (31) also conducted work on multi-fastener connections, examining the effect of the number of bolts in a row (perpendicular to the applied load), the number of bolts in tandem (parallel to the applied load), the interaction of stress fields or load distribution, and the effects of bolt pattern. The specimens were fabricated from graphite-epoxy composite. He concluded that by increasing the number of bolts in tandem, the net tension strength could be slightly increased. However, the effect of the number of bolts per row was the opposite, since the net tensile strength was reduced up to 15% with an increased number of bolts per row. The study was based on an analytical analysis used to predict the connection strength. Using a finite element method for single-bolt connections, the most critical row of bolts, and hence failure strength, was predicted. Strain gauge measurements showed also that for connections with two rows of bolts, the load was

shared equally by the two rows. However, for connections of three rows or more, the first row resisted the smallest amount of load. Based on the experimental results, the analytical method seemed to predict the failure loads for connections with two bolts per row quite well, however it became increasingly nonconservative for connections with three or more bolts per row or for staggered patterns. This suggested that for complex bolt configurations, the interaction between bolt-holes was significant and could not be neglected in the analysis. These findings somewhat contradicted the results reported by Collings (26).

Results by Pyer and Matthews (32) also confirmed Agarwal's findings which indicate that multi-holed connections are complicated and that an analysis based on the behaviour of single-hole connections could be inaccurate.

2.4.3 Environmental Effects

Environmental effects on fibre-reinforced composite connections were studied by Kim and Whitney (33). Kim and Whitney conducted environmental tests at 127°C (260°F) and 1.5% water content to determine their effects on the bearing strength of composite bolted connections by comparing them to tests at room temperature and dry conditions. The test specimens were made from graphite-epoxy composite material. They found that the presence of 1.5% water content reduced the bearing strength by 10% while a temperature of 127°C (260°F) reduced the bearing strength by 30%. They found that the temperature seemed to be the most critical factor affecting connection strength. Combined moisture-temperature effects

could not be determined.

Bailie, Duggan, Bradshaw, and McKenzie (34) also conducted high temperature tests at 450°K (350°F) on various graphite-epoxy composites. They found that the strength of the connection could be reduced substantially if the temperature approached the glass transition temperature of the material.

Ramkumar (29) conducted tests to determine the effect of moisture degradation. Compared to the dry condition, he found that at a water content of 1.2%, the strength reduction was minimal for connections loaded in tension, but was as high as 12% for connections loaded in compression.

Crews (35) conducted bearing tests in air and submerged in water to determine the effects of moisture. Using different clamping torques, it was found that lateral pressure could increase the static strength by 100% in comparison to the pin bearing case. Moisture seemed to have no effect on the static strength. However moisture could reduce the fatigue strength by 40%.

Carbon epoxy laminates are at the extreme cathodic end of the galvanic series causing corrosion problems for all less noble metals that come in contact with them. Tanis and Poullos (36) conducted corrosion tests on various fastener materials to determine which material was most compatible with graphite-epoxy composites. They found that aluminum and steel based alloys were the least compatible while nickel and titanium based alloys were the most compatible. Glass fibre composites do not induce corrosion in steel bolts, and therefore corrosion is not of great concern for this material.

2.4.4 Design Considerations

Due to the many design considerations that must be taken into account, the analysis and design of bolted connections in fibre-reinforced composite materials can be overwhelming. This is especially so for design from a purely theoretical standpoint. Despite the complexity of bolted connection behaviour, simply design procedures are needed to allow for practical use of these materials.

Simple equations based on static equilibrium and idealized stress distributions were given by Chamis (37) for preliminary design of bolted connections. Due to the oversimplification of his method, these equations should only be used for initial "sizing" of a connection and should be verified by appropriate experimental or analytical analysis.

Johnson and Matthews (38) conducted experimental tests to determine the load limit of bolted connections. The definition of failure is arbitrary and can be defined as the maximum load capacity of a connection or some predetermined elongation of the hole. From their results, Johnson and Matthews determined that a factor of safety of 2 should be used for bolted connections in composite materials.

Hart-Smith (39), (40) introduced a simply analysis theory based on the stress concentrations at loaded bolt holes to predict the behaviour of bolted connections. He discussed both single-fastener and multi-fastener connections and the relevant theory and design factors for both. The analysis is semi-empirical and is based on the elastic stress concentration factors at a loaded hole. These elastic stress concentration factors were expressed in terms of connection geometry. This

expression was derived from experimental tests and theoretical deductions for isotropic materials. The analysis proposed that the stress concentrations that occur in orthotropic fibre-reinforced composite materials could be related to the elastic stress concentrations through a correlation factor which could be determined from experimental tests. By testing a limited number of specimens for a given composite material, the analysis could be generalized for all connection geometries. Obviously such a analysis procedure is extremely useful and is the basis for the design procedure presented in Chapter 5.

2.5 ANALYTICAL RESEARCH

In most of the analytical research, finite element methods are usually used to determine the stress and strain distributions in bolted connections in fibre-reinforced composite materials. A multitude of finite element computer programs are currently available. Some are very general in nature and others are highly specialized, utilizing special elements and procedures to analyze specific aspects of bolted connection behaviour such as bolt-to-hole contact stresses. Although the actual finite element methods used may differ, a basic analytical procedure is common to most research. This procedure starts with the use of a finite element method to model a bolted connection and determine the stresses and strains. For laminated materials, which use multi-angle lay-ups, classical lamination theory is usually used to determine the stresses and strains in each individual lamina. Once the stresses or strains have been determined for the laminate or the individual lamina, the

stresses or strains are typically compared to a failure criterion, such as the maximum stress criterion or maximum strain criterion, to determine if the material has failed at some point in the connection. To account for stress redistributions, a failure hypothesis, such as that derived by Nuismer and Whitney (41), (42), may be used to determine which stresses should be compared to the failure criterion to determine if ultimate failure of the connection has occurred. In the case of composites consisting of several lamina, the connection is generally considered to have failed when the first lamina has failed. This is known as first-ply-failure. In other situations the stiffness of the failed ply may be reduced and the entire finite element procedure repeated until all plies have failed before the entire connection is considered to have failed.

2.5.1 Failure Hypothesis

Placing holes in fibre-reinforced composites considerably weakens the member due to the high stress concentrations and brittle nature of the material. However, since fibre-reinforced composites have some capability of redistributing stresses, the stress concentration factors developed by elastic theory are usually too conservative. Several hypothesises have been developed to describe the inelastic behaviour of composites with holes.

Waddoups, Eisenmann, and Kaminski (43) applied classical fracture mechanics to predict the behaviour of a notched laminated composite material. Although fibre-reinforced composites are generally statically brittle, several mechanisms exist

that prohibit the cracks from propagating and allow the redistribution of stresses. Waddoups, Eisenmann, and Kaminski proposed the existence of intense energy regions on either side of the hole perpendicular to the loading direction. Modelling these regions as through cracks, they developed a procedure based on linear elastic fracture mechanics for predicting the strength of a notched composite material.

Whitney and Nuismer (41), (42) developed two stress hypotheses that avoided the use of fracture mechanics to predict the behaviour of notched composites. These theories are the "point-stress" criterion and the "average-stress" criterion. Nuismer and Whitney noted that the stress concentrations due to the presence of a hole were actually dependent on the size of the hole. Compared to an unnotched member, they found that members with small holes did not experience as great a strength reduction as members with large holes. Although they had presented the stress hypotheses to account for this hole size effect, the stress hypothesis can also be interpreted as accounting for the pseudo-yielding capability of fibre-reinforced composite materials.

According to the point stress criterion, it is assumed that failure occurs when the stress at some distance "d_o" away from the hole reaches or exceeds the strength of the unnotched material, F_{tu}, as shown in Fig. 2.3. This distance d_o is called the characteristic distance and is determined through experimental tests. Nuismer and Whitney presented this dimension as a material property which "represents the distance over which the material must be critically stressed in order to find a sufficient flaw size to initiate failure" (41).

According to the average stress criterion, failure of the laminate occurs when the average stress over a characteristic distance "a_o" reaches or exceeds the unnotched material strength as shown in Fig. 2.4. Similar to d_o, the distance a_o is assumed to be a material property and is determined through experimental tests. The value a_o is basically considered to be the distance over which the material is capable of redistributing stresses before catastrophic failure will occur.

To determine the ultimate failure of a connection, the stresses located either at the critical distance d_o, or the average stresses over the distance a_o are compared to a material failure criterion to determine if the strength of the material has actually been exceeded.

To characterize the "hole size" effect, Pipes, Wetherhold, and Gillespie (44) proposed a model that gave the notched strength of a composite material as a function of the size of the hole. Two parameters consisting of a notch-sensitivity parameter and an exponential parameter were used to relate the notched strength of the material to the hole radius. These parameters were determined experimentally and were considered material properties.

2.5.2 Material Failure Criteria

In the design of a connection or structural component the stresses or strains are compared to the allowable stress or strain capacity of a material to determine the failure. For isotropic structural steels, the tensile yield strength is generally used for design purposes. However, for orthotropic unidirectional composites, there are

five independent in-plane strengths that characterise the material:

F_{t11} = Longitudinal tensile strength

F_{t22} = Transverse tensile strength

F_{c11} = Longitudinal compressive strength

F_{c22} = Transverse compressive strength

F_{s12} = In-plane shear strength

Corresponding to each of the five material strengths there are also five maximum strains that can be used to predict the failure of a composite material.

For isotropic structural steels, the Tresca maximum shear stress criterion or the Von Mises distortional energy yielding criterion are used to determine the yielding surface for a given multi-axial stress state. Since fibre-reinforced composites are orthotropic and do not exhibit extensive yielding, these failure criteria are not applicable and therefore several new failure criteria have been developed. Some of the more notable failure criteria include the Maximum stress, Maximum strain, Azzi-Tsai-Hill, Tsai-Wu, and Yamada failure theories. Mallick (12) points out that the Maximum stress and Maximum strain theories are the simplest to use. These theories basically state that failure will occur when any stress or strain in the principal material directions exceeds the allowable strength or strain capacity of the material. Hill (45) had extended the Von Mises Criterion to predict the yielding of orthotropic metals. Azzi and Tsai (46) incorporated Hill's theory to predict the fracture failure of orthotropic composite materials. Tsai and Wu (47) proposed a quadratic tensor polynomial failure criterion which accounted for the interaction

between the various strengths of a composite material. The quadratic polynomial expression was based on the tensor of material strengths allowing strength interaction terms to be included in the criterion. Yamada (48) proposed a criterion based on the assumption that, at final failure, all of the lamina in a composite laminate had failed by cracking along the fibres. As a result all transverse strength was considered ineffective and only the longitudinal and shear strengths were required.

2.5.3 Finite Element Methods

Many finite element computer programs have been developed by researchers to analyze the behaviour of bolted connections in composite materials. Although most finite element programs are based on anisotropic elastic theory, they do vary widely in terms of applications and investigations of particular connection configurations as noted by Snyder, Burns, and Venkayya (49), Garbo (50), and Pataro (51). Programs that are generic in nature can be applied to a variety of connection situations, but do not account for certain aspects of the connection problem. To refine the analysis, researchers have developed other programs to account for these factors, such as clearance effects, bolt-hole interactions, and non-linear contact problems.

Several researchers have used various failure theories to analyze composite bolted connections. Agarwal (52) used the maximum strain criterion and a modified version of the average stress hypothesis to determine the failure strength and failure

mode of single-bolted connections.

Soni (53) did not use any failure hypothesis, but compared the maximum stress at the edge of the bolt hole with the Tsai-Wu failure criterion. The location of the failure along the bolt hole determined what the final failure mode would be. Although he used a last-ply failure stress to predict the ultimate strength of the connections, his predictions were relatively conservative.

Garbo, Hong, and Kim (54) used the point stress failure hypothesis and the maximum strain failure criterion to analyze bolted connections for various CFRP materials used in helicopter applications.

Lee and Chen (55) used the maximum strain failure criterion and accounted for the stress redistributions with a progressive laminate failure instead of using a failure hypothesis.

Waszczak and Cruse (56) developed a synthesis procedure for optimizing single and multi-bolted connections.

York, Wilson, and Pipes (57) used the Pipes-Wetherhold-Gillespie modified point stress failure criterion to predict the net tension strength of composite bolted connections. Their analysis had shown that the (e/d) ratio had little effect on the stress distribution along the net section but the (w/d) ratio had a pronounced effect. The stress concentrations adjacent to the hole were shown to increase with increasing (w/d) ratios.

The failure strength and failure mode of single-bolted connections in composite materials was analyzed by Chang, Scott, and Springer (58) using a

modified version of the Whitney and Nuismer's point stress hypothesis together with Yamada's criterion for material failure. Failure of the laminate was assumed to have occurred when the first ply failed. A knowledge of where the laminate failed with respect to the bolt hole gave insight into the mode of failure, being either bearing, net tension, or shear-out failure. A parametric study showed that strength increased with increasing width-to-hole diameter ratios (w/d) and with increasing edge distance-to-hole diameter ratios (e/d). Subsequent experimental work on both single-bolt and double-bolt connections, in series and in parallel, by the same authors (59) showed that the method was accurate within 10% of the experimental results. Based on their analytical work Chang, Scott, and Springer (60) proposed a simple design procedure which predicted the ultimate load and mode of failure for connections with more than two bolts through the use of interaction coefficients. However, the accuracy of predicting the behaviour of these complex connections was not confirmed by experimental results.

Wong and Matthews (61) noted that in the study of basic problems in composite behaviour, the through thickness stresses in thin laminates could be neglected and a two-dimensional analysis was justified. This was especially the case for bolted connections where the composite was transversely restrained by washers. Using a two dimensional finite element model, they analyzed the maximum strains at the bolt hole and conducted a parametric study on the effects of width and edge distance. They showed that with increasing values of the (w/d) and (e/d) ratios, the maximum strains adjacent to the hole boundary became constant at (w/d) and (e/d)

values between 2 to 5.

The effects of bolt friction, clearance, material properties and connection geometry were studied by Rowlands, Rahman, Wilkinson, and Chiang (62) for both single and double-bolt connections using a finite element procedure. Their results showed that bolt friction had little effect on the stresses around the hole, and that the behaviour of the connections varied little for (w/d) and (e/d) ratios greater than 4. Bolt clearance had a marked effect as the radial stresses increased dramatically with increased clearance.

Using a general finite element program, Wang and Han (63) tried a more universal finite element approach to determine the load distribution in multi-bolted connections. Their analysis showed that there are generally stress interactions between the bolt holes, and the load distribution among the bolts is not linear.

A three dimensional finite element procedure was used by Lucking, Hoa, and Sankar (64) to investigate the effect of the (d/t) ratio on the interlaminar stresses near the hole. Their results showed that the interlaminar stresses could be significant.

In light of the complicated stress interactions taking place at the bolt hole, several researchers have developed finite element programs to account for the specific problems in dealing with the contact stress analysis.

Dutta (65) developed a program that accounted for the through thickness effects as well as the pin-to-plate contact problem.

Naik and Crews (66) investigated the effect of clearance using an inverse

formulation finite element approach. The clearance problem is difficult to analyze, because it involves a contact region that is nonlinear with bearing load. By comparing the overall deformations of the connections, they concluded clearance would have little effect on overall connection stiffness.

Hyer and Klang (67) used a finite element method which accounted for the effects of clearance, friction, and bolt elasticity. They found that bolt elasticity had little effect on stresses. Friction tended to decrease the maximum radial stresses and shift them away from the centre-line of the connection while increasing the magnitude of tangential stresses and shifting their location slightly. As for the effects of clearance, their results indicated that with increased clearance, radial stresses increased and the peak tangential stresses were spread over a larger distance. The peak tangential stresses basically occurred at the end of the contact arc which was also shown in the solution for an infinite plate with a loaded hole derived by Bickley (24). Overall the results were basically in agreement with the work by Naik and Crews (66).

Work done by Eriksson (68) followed that of Hyer and Klang. In addition to the variables considered by Hyer and Klang, Eriksson also looked at the effects of the composite's elastic properties. The peak radial stress moved off the centre-line of the connection for laminates with high stiffness in the direction perpendicular to loading. Tangential stresses were also greatly affected by laminate properties although axial stress along the net section plane was less sensitive. Shear stress is also greatly affected. Eriksson's work confirmed the results of Hyer and Klang.
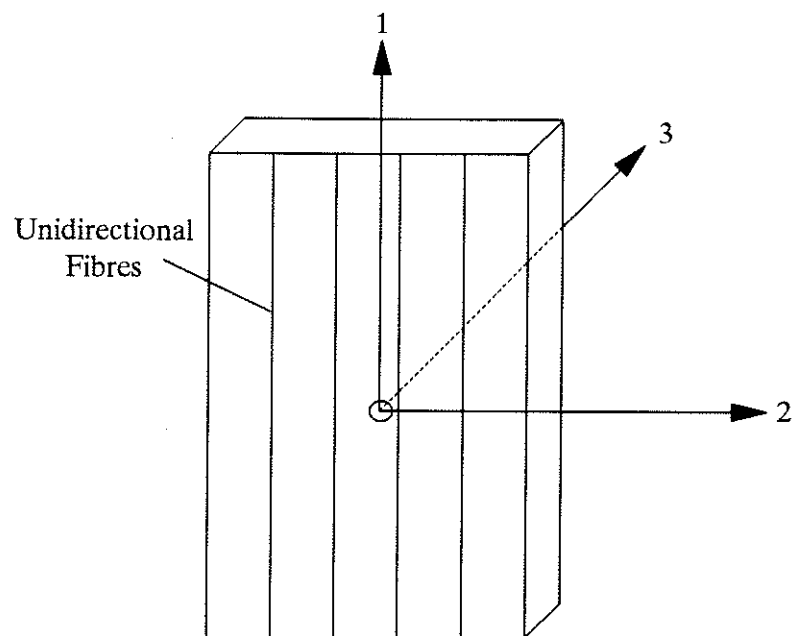
Figure 2.1 Principal Material Axes

Net Tension   Shear-out   Bearing   Cleavage
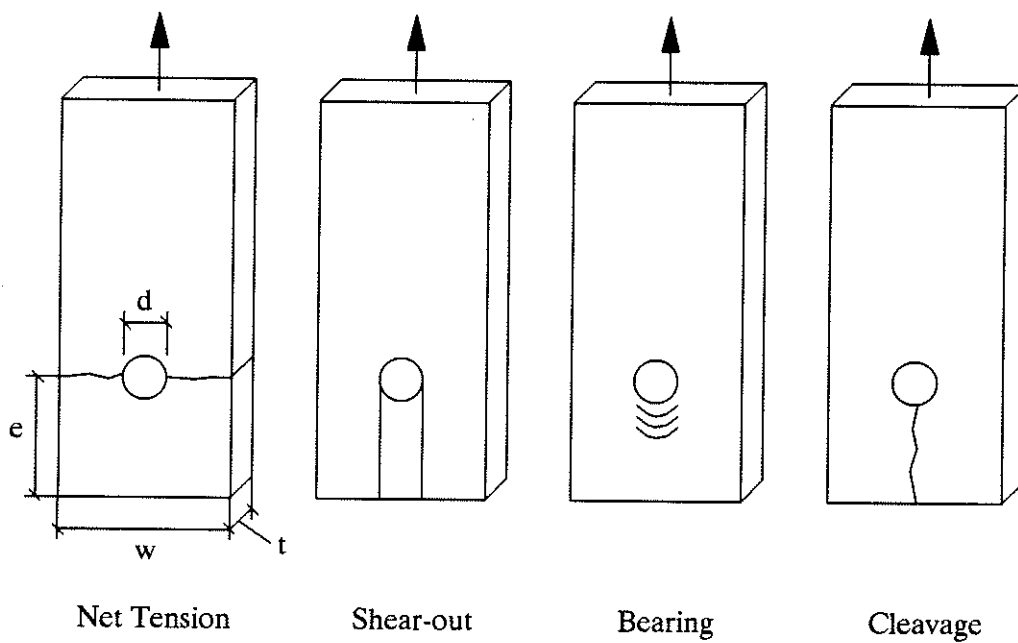
Figure 2.2 Basic Failure Modes

28
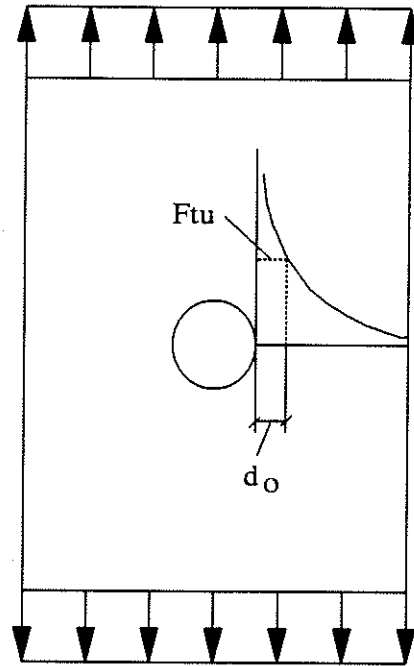
Figure 2.3 Point-Stress Failure Hypothesis
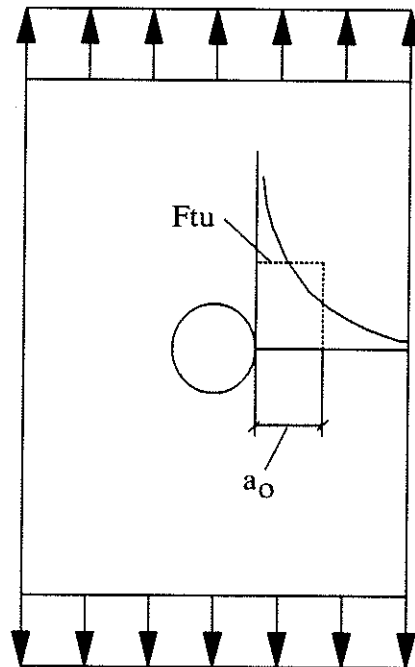
Figure 2.4 Average-Stress Failure Hypothesis

CHAPTER 3 EXPERIMENTAL PROGRAM

3.1 INTRODUCTION

This chapter presents an experimental program undertaken at the University of Manitoba to examine the behaviour of bolted connections fabricated from glass fibre-reinforced composite material members. Specimen configurations, test set-up, instrumentation and the various parameters considered in this program are presented in detail. Various coupon specimens used to determine the material properties are also described.

3.2 MATERIAL

The fibre-reinforced composite material used in this investigation is EXTREN Flat Sheet/ Series 500, a pultruded glass fibre sheet produced by the Morrison Molded Fibre Glass Company (MMFG). The composite material is orthotropic, consisting of symmetrically stacked, alternating layers of identically orientated unidirectional E-glass roving and randomly oriented E-glass continuous strand mat. The matrix consists of polyester plastic and the fibre content is approximately 40%. EXTREN Flat Sheet is produced in the form of 1.2 m x 2.4 m (4 x 8 ft.) sheets and is manufactured in several different thicknesses. Three thicknesses were used in this investigation: 9.525 mm (3/8 in.), 12.7 mm (1/2 in.), and 19.05 mm (3/4 in.).

3.2.1 Material Properties

To determine the material properties, 80 tension tests, 75 compression tests, and 95 shear tests were conducted. Each type of test was conducted for all of the material thicknesses used in this investigation and for various fibre orientations with respect to the applied load. As mentioned in Chapter 2, the principal directions of the material are designated as: axis-1, parallel to the unidirectional continuous fibres; axis-2, perpendicular to the unidirectional fibres; and axis-3, in the direction of the thickness. Several specimens were tested with the 1-axis having various angles, θ, with respect to the axis of the applied load, the X-axis, as shown in Fig. 3.1. The angle θ was varied between $0°$, where the direction of the unidirectional fibres coincides with the direction of the applied load, to $90°$ where the unidirectional fibres are perpendicular to the applied load.

The in-plane material properties of EXTREN Flat Sheet/ Series 500 are given in Table 3.1 to Table 3.8. The test results and the ranges of the coefficients of variation given for each of the material properties suggest large material variability.

In each case, the principal tensile moduli E_{11} and E_{22}, the major and minor Poisson's ratio v_{12} and v_{21}, the shear modulus G_{12}, are based on the data measured from the tension tests. The ultimate tensile strength F_{tu} and tensile moduli, E, were determined for several fibre orientations ranging from $0°$ to $90°$ with respect to the applied load. Compressive tests were used to determine the compressive strength F_{cu} at various fibre orientations with respect to the applied load. Shear tests were conducted to determine both "interlaminar" and "intralaminar" shear strengths F_{su}

at various fibre angles. Since the coupon testing program was extensive, each type of test will be discussed individually. Coupon dimensions for each test, measured loads, and statistical evaluations are given in detail in a separate technical report by the author, Rosner (69).

3.2.2 Tension Tests

Tension tests were conducted according to ASTM Standard D638. Dimensions of the tension coupons are given in Fig. 3.2(a). The tension coupons that were fabricated from the 9.525 mm (3/8 in.) and 12.7 mm (1/2 in.) thick sheets, were tested using a 130 kN (30,000 lb) Baldwin Testing Machine. Tension coupons fabricated from the 19.05 mm (3/4 in.) thick sheets exceeded the size of the T-grips of the Baldwin machine, and therefore, were tested using a 270 kN (60,000 lb) RIEHLE Testing Machine.

A MTS Extensometer Model 632.12C-20 with a 50 mm (2 in.) gauge length was used to measure the strain. Load was measured directly from the test machine. The load-displacement data were collected on a DATASCAN 7000 data acquisition system and recorded on a Hewlett-Packard Vectra 286 Computer. A JJ Instruments PL3 Plotter was used to plot the load-extension curve during each test. Copies of the load-extension plots for all tests are given in a separate technical report by the author, Rosner (69).

Typical stress-strain relationships for the tension coupons are shown in Fig 3.3 to Fig.3.5. The stress-strain behaviour for tension coupons fabricated from the 9.525

mm (3/8 in.) thick material with the fibre orientations at 0°, 45°, and 90° with respect to the applied load are shown in Fig. 3.3. As can be seen, the material behaves non-linearly up till fracture. The coupons with the 0° fibre orientation have the greatest tensile strength and stiffness. The coupons with the 90° fibre orientation have the lowest tensile strength but have a slightly higher stiffness, on average, than the coupons with the 45° fibre orientation. Results indicated that the tensile strength becomes lower as the fibre orientation changes from 0° to 90° with respect to the applied load, but the tensile modulus seems to be lowest at some intermediate fibre orientation angle and not at 90°. The stress-strain behaviour for the tension coupons fabricated from the 12.7 mm (1/2 in.) and the 19.05 mm (3/4 in.) material are shown in Fig. 3.4 and Fig. 3.5 respectively, for the various fibre orientations tested for these thicknesses. Again the behaviour is non-linear. The ultimate tensile strength is highest for the coupons with a 0° fibre orientation and lowest for those with a 90° fibre orientation. The tensile modulus for coupons with the fibre orientations ranging from 45° to 90° are fairly close as shown in Fig. 3.4 suggesting that the value for the lowest tensile modulus occurs in this range. The average tensile strengths, average elongations, and average tensile moduli are given in Table 3.1 to Table 3.3 respectively, including the number of tests for each material thickness and fibre orientation considered in the material testing program of this investigation. In addition, the standard deviations and coefficients of variation for each material property are also given. Details of the statistical evaluations of the material properties are given by Rosner (69).

The measured results indicate that all material properties are consistent among the three material thicknesses, as given in Table 3.1 to Table 3.3, with one exception; the average tensile strength and tensile modulus of the 9.525 mm (3/8 in.) thick material at the 0° fibre-orientation tends to be 1.2 times higher than that of the other two material thicknesses. This discrepancy could be attributed to the size of the tension coupons. Full size connection tests suggest the tensile strength and moduli for the 9.525 mm (3/8 in.) material is the same as those for the other two thicknesses. Therefore the tensile strength value of $F_{tu}=166$ MPa (24,100 psi) as given in Table 3.1, was used for all material thicknesses for the 0° fibre orientation.

It should be noted that the results for two connections, "A1" and "A2", which consist of members of 9.525 mm (3/8 in.) thick material and have a width of 25.4 mm (1 in.), show higher loads proportional to the higher strength value measured for the coupon tests for the 9.525 mm (3/8 in.) thick material. Since these two connections are very close in size to the tension coupons which have a width of 12.7 mm (1/2 in.), the tensile strength of $F_{tu}=198$ MPa (28700 psi) was used for the analysis of these two connections.

The influence of the fibre orientation is also shown in Table 3.1 to Table 3.3. The results indicate that the tensile strength decreases as the fibre orientation deviates from the direction of the applied load. This phenomenon is not applicable for the tensile moduli, since the lowest value does not occur at the 90° fibre orientation but at some intermediate angle between 0° and 90°. This is due to the fact that the material has a low shear modulus. Mallick (12) provides the range of

shear modulus values which determine if a material's tensile modulus will be a minimum at a 90° fibre orientation. These limits are:

$$\frac{E_{11}}{2(1+v_{12})} > G_{12} > \frac{E_{11}}{2(E_{11}/E_{22} + v_{12})} \tag{3.1}$$

Mallick, indicates that if the shear modulus is within these limits, the lowest tensile modulus will occur at a 90° fibre orientation, otherwise the lowest tensile modulus will occur at some intermediate angle. It was found that the upper and lower limits for EXTREN Flat Sheet material were 4.9 GPa (713,000 psi) and 4.3 GPa (623,000 psi). The shear modulus was determined to be 4.1 GPA (600,000 psi) and is below the lower limit. Therefore the lowest tensile modulus occurs between 0° and 90° fibre orientations as given in Table 3.3.

Seven of the 80 tension tests were instrumented with strain gauges to determine the major and minor Poisson Ratios as given in Table 3.4. The strain gauges used were Micro-Measurements type CEA-06-250UN-350 with a resistance of 350 ±0.3% ohms and a gauge factor of 2.070 ±0.5% at 24°C. The gauges were attached parallel and perpendicular to the applied tensile load on both front and back of the tension coupons as shown in Fig. 3.2(a). The arrangement of the strain gauges is documented in detail by the author, Rosner (69). The Poisson Ratios were determined directly from the strain gauge readings according to ASTM Standard E132. The strain gauge readings were plotted against the applied load and the slopes of the lines representing the front and back average of the longitudinal strains and the front and back average of the transverse strains were determined by

a regression analysis as shown in Fig. 3.6 and Fig. 3.7. The Poisson Ratio was taken as the ratio of the slope of the transverse readings to the slope of the longitudinal readings. Typical data obtained for the major and minor Poisson Ratios are shown in Fig. 3.6 and Fig. 3.7 respectively. The average Poisson Ratios as well as the standard deviations and coefficients of variation are given in Table 3.4. Graphs showing the strain gauge data for all seven "gauged" tests are given in the Appendix.

Given the elastic moduli in the two principal material directions E_{11}, E_{22}, and the major Poisson's Ratio v_{12}, the minor Poisson's Ratio can be calculated by:

$$v_{21} = v_{12} \frac{E_{22}}{E_{11}} \qquad (3.2)$$

Using the appropriate measured values given in Table 3.3 and Table 3.4, the minor Poisson's Ratio v_{21} was calculated to be 0.21 for the 9.525 mm (3/8 in.) material which confirms the experimentally determined value given in Table 3.4. Although the major Poisson's Ratio listed in Table 3.4 was determined for the 9.525 mm (3/8 in.) thick material, it is assumed to be valid for all thicknesses.

3.2.3 Shear Modulus Tests

Two methods were used in this investigation to determine the shear modulus G_{12} for EXTREN Flat Sheet/ Series 500. The first method utilizes the results of the tension coupons described in § 3.2.2 . The second method is based on testing of a special type of off-axis tension coupon designated in this thesis as a "shear modulus coupon" as given in Fig. 3.2(b).

The first method uses a stiffness transformation equation to calculate the shear modulus G_{12} based on the measured tensile moduli of the tension coupon tests. Given the basic elastic properties in the direction of the principal material axes 1 and 2, the tensile modulus, E_{xx} of an angle-ply lamina in which the unidirectional continuous fibres are at an angle θ with the positive direction of the applied load axis-X, as shown in Fig. 3.1, can be computed as follows:

$$\frac{1}{E_{xx}} = \frac{\cos^4\theta}{E_{11}} + \frac{\sin^4\theta}{E_{22}} + \frac{1}{4}(\frac{1}{G_{12}} - \frac{2v_{12}}{E_{11}})\sin^2 2\theta \qquad (3.3)$$

This equation is a rotational transformation of the basic stiffness matrix for an orthotropic elastic material. The elastic properties E_{11}, E_{22}, E_{xx}, and v_{12} are measured from the tension tests. For the 9.525 mm (3/8 in.) material it was found that the shear modulus G_{12} for the 45° fibre orientation case was 3.5 GPa (506,000 psi). For the 12.7 mm (1/2 in.) material, the shear moduli for the 30°, 45°, and 60° fibre orientation cases were 4.2 GPa (612,000 psi), 3.9 GPa (572,000 psi), and 4.4 GPa (631,000 psi) respectively. Therefore an average shear modulus for the 12.7 mm (1/2 in.) thick material of 4.2 GPa (605,000 psi), was used and assumed to be valid for all thicknesses. It should be noted that the magnitude of the shear modulus G_{12} is not sensitive to the value of Poisson's Ratio v_{12}.

In the second method the shear modulus was determined directly from the state of stress and strain of an off-axis tension test. The basic dimensions of the shear modulus coupon are shown in Fig. 3.2(b). In this test the direction of the unidirectional fibres was at an angle of 10° with respect to the direction of the

applied load axis-X. To determine the state of strain, a 45° strain gauge rosette was attached at the mid-length of the specimen. The measured strains were used to determine the state of strain at the principal axes of the material using the Mohr's Circle approach. Since both stress and strain states are known, the shear modulus was determined from the shear stress-strain graph.

In this investigation two shear-modulus coupons were tested to confirm the calculations from the tension coupon data. The coupons were fabricated from the 12.7 mm (1/2 in.) material and had a length of 254 mm (10 in.) and a width of 44.5 mm (1.75 in.). The length to width ratio was large enough to assume that the extension-shear coupling effect, which occurs for orthotropic materials loaded in a direction other than the principal axes, could be neglected. A strain gauge rosette was attached at the centre of the coupon as shown in Fig. 3.2 and the readings were recorded by the same data acquisition system that was used for the tension coupons. The states of stress and strain were determined for the principal directions of the material and the shear stress and strain curves were developed for each test as shown in Fig. 3.8 and Fig. 3.9. As shown in Fig. 3.8 and Fig. 3.9, the shear moduli were found to be 3.2 GPa (460,000 psi) and 3.0 GPa (430,000 psi) respectively. The average 3.1 GPa (445,000 psi) as given in Table 3.5, is somewhat lower than the average value calculated from the tension coupons. The discrepancy is attributed to the material variability.

3.2.4 Compression Tests

A total of 75 compression tests were conducted according to ASTM Standard D695. Figure 3.2(c) shows the typical dimensions of a compression coupon. The length of the coupon was small enough to insure that the compressive strength was not affected by buckling of the specimens. The average compressive strengths as well as the standard deviations and coefficients of variation for each material thickness at fibre orientations of 0° and 90° are given in Table 3.6. For the 12.7 mm (1/2 in.) thick material, the compressive strength is given for various fibre angles between 0° and 90°. It was found that the compressive strength of the 9.525 mm (3/8 in.) thick specimens for the 0° fibre orientation, was slightly higher those of the 12.7 mm (1/2 in.) and 19.05 mm (3/4 in.) thick specimens. The results confirm that the compressive strength is reduced as the fibre orientation increases from 0° to 90°.

3.2.5 Shear Tests

A total of 95 shear coupons were tested to determine shear strength. The basic dimensions of the shear coupons are shown in Fig. 3.2(d). Sixty tests were conducted according to ASTM Standard D3846 and thirty-five tests were conducted according to a modified version of this standard. According to ASTM Standards D3846, a compressive load is applied to the shear specimen to induce a shear failure in the plane between the notches. Shear tests were conducted for all material thicknesses and at 0° and 90° fiber orientations. The results are given in Table 3.7. Similarly, it was found that the shear strength of the 9.525 mm (3/8 in.) material was

higher than those for the 12.7 mm (1/2 in.) and 19.05 mm (3/4 in.) materials. Table 3.7 shows that the shear strength for the 0° fibre orientation F_{s13} and the shear strength in the 90° fibre orientation F_{s23} are fairly close in magnitude.

For bolted connections in composite materials, the material properties in the plane of the members, the 1-2 plane, is important for the analysis. According to ASTM Standard D3846 the notches are machined through the thickness of the material to produce a shear plane that lies in the 1-2 plane of the material. A stress analysis, as shown in Fig. 3.10(a), indicates that the measured shear strength is the interlaminar shear strength F_{s13} in the 1-3 plane, when the continuous fibres are at 0° to the applied load, and is the interlaminar shear strength F_{s23} in the 2-3 plane, when the fibres are at 90° to the applied load as shown in Fig. 3.10(b). Therefore, the desired intralaminar shear strength F_{s12} cannot be determined with the specimen notches machined in this fashion. This is normally not a problem for a transversely isotropic material, since $F_{s13}=F_{s12}$. However, for a material such as EXTREN Flat Sheet which consists of different layers in the thickness direction and hence has different properties in the "2" and "3" directions, the above equality is not valid. To solve this problem, 35 shear coupons were tested with the notches machined through the width-wise direction of the coupon as opposed to the thickness, as shown in Fig. 3.10(c). These "modified" shear coupons were tested in the same manner as the previous specimens. Machining the notches through the width-wise direction, produced a shear plane parallel to the 1-3 material plane. A stress analysis shows that by shearing through this plane, the strength that is measured is the desired

intralaminar shear strength F_{s12}. Table 3.8 lists the results of the "modified" shear tests. Comparing Table 3.7 and 3.8 it can be seen that the intralaminar shear strength F_{s12} is approximately 4 times higher than the interlaminar shear strength F_{s13}. The "modified" shear coupons that were tested at angles other than 0° did not fail through the shear plane and therefore their results are inconclusive as noted in Table 3.8.

A summary of the in-plane material properties for EXTREN Flat Sheet is given in Table 3.9 for the three thicknesses used in this investigation at fibre orientations of 0° and 90°.

3.3 CONNECTION SPECIMENS

3.3.1 Parameters

The four basic geometric parameters studied in this investigation, which influence the strength and failure mode of a connection, were the width of the member, the edge distance, the thickness of the member, and the orientation of the unidirectional fibres with respect to the applied load.

The effects of the width and the edge distance were effectively described in terms of dimensionless ratios with respect to the hole diameter. In this investigation the hole diameter was kept constant at 20.6 mm (13/16 in.) for all of the tested connections. The width and edge distance were varied to obtain different values for the width to hole diameter ratio (w/d) and the edge distance to hole diameter ratio (e/d). The values of the width and edge distance were selected so that different

failure modes could be induced. The dimensions of the various parameters and ratios are given in Table 3.10.

To determine the influence of the member's thickness on the behaviour of a connection, three different thicknesses were used: 9.525 mm (3/8 in.), 12.7 mm (1/2 in.), and 19.05 mm (3/4 in.) as given in Table 3.10. These thicknesses were selected as typical thicknesses applicable for structural members.

The fourth parameter, the angle of the unidirectional fibres with respect to the applied load, can be considered to be partly a geometric parameter and partly a material parameter. The structural shapes typically used in civil structures are usually long and slender and therefore are ideally suited to be manufactured by the pultrusion process. For this reason the principal load bearing fibres are usually continuous and unidirectional and are oriented in the lengthwise direction of the member. Random fibre mats are generally incorporated to provide transverse strength. Unlike aeronautical structural members which tend to be skins and plates and therefore can utilize multi-angle fibre lay-ups, pultruded structural shapes have the continuous unidirectional fibres usually oriented only in the lengthwise direction of the member. Since the bolt can bear at any angle with respect to the longitudinal direction of the member and the unidirectional fibres, it was critical to study the effects of this variable. In this investigation the 12.7 mm (1/2 in.) thick material was used to fabricate connections that were tested with the principal unidirectional fibre layers of the material at 0°, 45°, and 90° with respect to the applied load. The other two thicknesses, 9.525 mm (3/8 in.) and 19.05 mm (3/4 in.), were tested with the

unidirectional fibres at 0° to the applied load.

It should be noted that the above parameters are not the only factors that could influence the behaviour of bolted connections. Some of the more notable ones may include the amount of clearance between the bolt and hole, the amount of bolt torque or lateral pressure, the size of the washer, and bending effects caused by single-shear instead of double-shear connections. In this investigation standard washers with 19 mm (3/4 in.) high strength structural bolts were used. The hole diameter of the connections was 20.6 mm (13/16 in.) providing a 1.6 mm (1/16 in.) clearance for the bolt. This clearance was chosen as being typical of what is used in the field and was kept constant throughout this investigation. The amount of lateral pressure was also kept constant by tightening the bolt to a constant torque of 32.5 N-m (24 ft-lbs). This value is the recommended maximum installation torque for FIBREBOLT Studs and Nuts as given in the EXTREN Design Manual (70). Although the bolts used in this investigation were high strength steel bolts, the same installation torque as that recommended for FIBREBOLT was used so that a comparative study could be made with the different types of fasteners in a subsequent investigation.

The experimental program consisted of 5 series of tests as shown in Table 3.11. The first series, Series A, included all the connections fabricated from the 9.525 mm (3/8 in.) material with the fibre angle at 0° or parallel to the applied load. The next three series, B, C, and D consisted of the connections made from the 12.7 mm (1/2 in.) material with the fibre-load angle at 0°, 90°, and 45° respectively.

Series E consisted of the connections fabricated from the 19.05 mm (3/4 in.) material with the fibre-load angle at 0°. The width and edge distance were varied in an identical manner for each series producing 20 connection tests for each series except for Series A for which two tests were repeated giving a total of 22 tests. The test designations and various geometric dimensions are given for each connection test in Table 3.11. A total of 102 connections were tested in this experimental investigation.

3.3.2 Connection Fabrication

The connections tested in this investigation consisted of rectangular plates that were cut from the large 1.2 x 2.4 m (4 x 8 ft.) sheets on a table saw equipped with a carbide-tipped blade. The plates were cut to the desired width and to a length of 610 mm (24 inches) with an accuracy of ±1 mm (±1/32 inch). The length was selected to be long enough to avoid the influence of end effects on the behaviour of the connection and to produce a uniform applied stress at the mid-length.

To fabricate the connections that had the unidirectional fibres at 45° and 90° to the applied load, the plates were laid out and cut at 45° and 90° to the longitudinal or pultruded direction of the sheet.

At the end of the plate, a single bolt hole 20.6 mm (13/16 in.) in diameter was marked out and drilled in the centre of the plate and at the desired edge distance. At the far end of the plate, 19 mm (3/4 in.) diameter bolt holes were marked and drilled to match the hole patterns in the upper steel gripping plate. Since the basic

configuration of the connections consisted of two composite plates, namely Plate A and Plate B as described in § 3.4, both plates were clamped together and drilled simultaneously to ensure alignment of the holes. Although more accurate methods exist for fabricating these connections, such as reamed holes instead of drilled holes, the methods utilized in this investigation more closely resemble what would be used in the field.

3.4 TEST SET-UP

The connections were originally tested using a 270 kN (60,000 lb) RIEHLE testing machine. Many of the specimens failed catastrophically and would incur sudden load drops and displacement increases. It was found that the LVDT used to measure the load for this particular machine, had a large lag effect and could not accurately characterize the load drops which would normally occur in fractions of a second. For this reason, all subsequent tests were preformed using a 1000 kN (220,000 lb) MTS closed-loop servo-controlled loading system. In this system the loads were measured by a load cell which was more accurate in characterizing the load-displacement behaviour of the connections tested. Tensile load was applied at a constant stroke rate of 0.01 mm/sec (0.254 in/sec). The connections which were tested on the RIEHLE machine are marked with an "*" in Table 3.11.

The test set-up shown in Fig. 3.11 was used to fit the test specimen to the MTS loading system. The steel grips had a cup and cone shape which were machined into the bearing plate and bearing nut respectively to allow for self

alignment as shown in Fig. 3.11. The steel grips also had several hole patterns to allow for various sizes of the tested connections. For the tests performed on the REIHLE machine, the grips were attached through the crossheads in a slightly different manner.

An enlarged schematic of the connection set-up is shown in Fig. 3.12. Photographs of the set-up are given in Fig. 3.13. The actual connection consisted of two composites plates: Plate A and Plate B. The steel grips were placed between the composite plates as shown in Fig. 3.12. The connection under investigation, the "critical connection", was located at the lower end of the set-up and consisted of a single-bolt in double-shear. The upper grip consisted of two steel clamping plates that were used to "sandwich" the composite plates and the upper steel grip as shown in Fig. 3.12 . The applied tensile load was transferred from the upper grip assembly to the composite plates through the clamping force and bearing action of two or four bolts, depending on the width of the composite plates.

The two composite plate, double-shear configuration was selected to subject the composite members to concentrically applied loading and to eliminate bending effects. Most importantly, this type of "double specimen" arrangement simplified strain and displacement measurements and allowed direct observation of the various failure modes.

Throughout the connection set-up, 19 mm (3/4 in.) diameter ASTM A325 high strength structural bolts and washers were used. The specified tensile strength of the A325 bolts was 825 MPa (120,000 psi). For the larger connections 19 mm (3/4

in.) diameter SAE L9 high strength structural bolts were used. The specified tensile strength of the SAE L9 bolts was 1240 MPa (180,000 psi). These bolts were used on connections fabricated from the 19.05 mm (3/4 in.) thick material, where the connection's load capacity exceeded 180 kN (40,000 lb). During the assembly of each connection specimen, the bolts were carefully centred in the oversized holes. In all cases, the bolt lengths were selected to ensure that both composite plates in each connection intercepted the shank and not the threads of the bolt.

3.5 INSTRUMENTATION

To measure the relative displacement between the lower grip and the composite plates, one LVDT (Linearly Variable Differential Transducer) was used on each side of the connection as shown in Fig. 3.12. The LVDT's were mounted on the lower grip and metal T-shapes were individually clamped to each composite plate to align the LVDT's so as to measure the relative slip at the hole centre. The load was measured by the load cell of the testing machine. The load and the two displacement readings were recorded by a 40-channel Hewlett-Packard 3490A Multimeter data acquisition unit and a Hewlett-Packard Vectra 286 Computer. During each test, a Hewlett-Packard 7044A X-Y Recorder was used to produce an X-Y plot of the load versus the average displacement. The arrangement of the instrumentation as well as the loading system is shown in Fig. 3.14.

To measure the stress distribution at the net section, a total of 10 connections were instrumented with strain gauges and are identified in Table 3.11. The strain

gauges were attached to Member A for each connection. A typical arrangement of strain gauges is given in Fig. 3.15. The actual strain gauge arrangements for each connection are documented in a separate technical report by the author, Rosner (71). To measure strains close to the hole, a special washer was fabricated to provide spaces for the gauges adjacent to the hole. The strain gauges used were type CEA-06-250UN-350 manufactured by the Micro-Measurements Division of the Measurements Group Inc. The gauges had a resistance of 350.0 ±0.3% ohms and a gage factor of 2.070 ±0.5% at 24°C. The strain gauge readings were recorded by the same system used for the load and displacement data. Most of the connections selected to be instrumented with strain gauges had an edge distance equal to 101.6 mm (4 in.) and had widths varying from 101.6 mm (4 in.) to 254 mm (10 in.).

For connections that failed catastrophically, such as in net tension or cleavage failure, the load reduction and displacement increases took place in fractions of a second. To accurately characterize the load-displacement behaviour during such a sudden event, a Tektronix 2214 Digital Storage Oscilloscope was used to record the load and average displacement. Four connections, as listed in Table 3.11, were continuously monitored with the oscilloscope at a sampling rate of 16,000 readings per second. When a sudden failure occurred, the oscilloscope was manually triggered to "freeze" the load and average displacement information which was then downloaded to a personal computer for analysis.

Table 3.1 Tensile Strength

Thickness mm (in.)	Fibre Orientation (deg.)	Number of Tests	Tensile Strength				
			Average		Standard Deviation		Coeff. of Variation
			(MPa)	(psi)	(MPa)	(psi)	
9.525 (3/8)	0	10	198	28700	21.4	3100	0.108
	45	5	121	17600	6.2	900	0.051
	90	10	101	14700	6.7	976	0.066
12.7 (1/2)	0	10	166	24100	23.6	3430	0.142
	30	5	114	16600	3.3	485	0.029
	45	5	117	17000	4.0	581	0.034
	60	5	110	15900	4.1	593	0.037
	90	10	110	16000	8.3	1210	0.076
19.05 (3/4)	0	10	166	24100	27.2	3950	0.164
	90	10	103	14900	5.5	793	0.053

Total: 80

48

Table 3.2   Maximum Tensile Strain

Thickness mm (in.)	Fibre Orientation (deg.)	Number of Tests	Maximum Tensile Strain		
			Average (%)	Standard Deviation	Coeff. of Variation
9.525 (3/8)	0	10	1.6	0.06	0.04
	45	5	1.7	0.06	0.04
	90	10	1.2	0.17	0.14
12.7 (1/2)	0	10	1.6	0.16	0.10
	30	5	1.4	0.05	0.04
	45	5	1.6	0.08	0.05
	60	5	16	0.22	0.14
	90	10	1.4	0.11	0.08
19.05 (3/4)	0	10	1.6	0.16	0.10
	90	10	1.4	0.09	0.07

Total: 80

Table 3.3   Tensile Modulus

Thickness mm (in.)	Fibre Orientation (deg.)	Number of Tests	Elastic Moduli				Coeff. of Variation
			Average		Standard Deviation		
			(GPa)	(psi)	(GPa)	(psi)	
9.525	0	10	15.2	2.20E+06	3.1	4.51E+05	0.205
(3/8)	45	5	9.8	1.42E+06	0.4	6.10E+04	0.043
	90	10	10.8	1.56E+06	1.2	1.69E+05	0.108
12.7	0	10	12.7	1.84E+06	1.2	1.75E+05	0.095
(1/2)	30	5	11.6	1.68E+06	0.8	1.10E+05	0.066
	45	5	10.5	1.52E+06	0.6	9.32E+04	0.061
	60	5	10.8	1.57E+06	1.1	1.53E+05	0.098
	90	10	10.7	1.55E+06	1.1	1.54E+05	0.099
19.05	0	10	13.1	1.90E+06	2.4	3.41E+05	0.179
(3/4)	90	10	11.1	1.61E+06	1.3	1.91E+05	0.199

Total: 80

Table 3.4 Poisson's Ratios

Thickness mm (in.)	Fibre Orientation (deg.)	Number of Tests	Poisson's Ratios			
			Average (%)	Standard Deviation	Coeff. of Variation	
9.525	0	4	0.28	0.014	0.05	Major Poisson's Ratio
(3/8)	90	3	0.21	0.051	0.24	Minor Poisson's Ratio

Table 3.5   Shear Modulus

Tension Coupons			Shear Modulus (Calculated from Tension Coupon Results)				
			Calculated Average		Standard Deviation		Coeff. of Variation
			(GPa)	(psi)	(GPa)	(psi)	
Thickness=12.7 mm (1/2 in.) Fibre Orient.=30, 45, 60 deg.			4.2	605000	0.2	30100	0.05
Thickness	Fibre Orientation	Number of	Shear Modulus (Measured from Shear Modulus Coupons)				
			Average		Standard Deviation		Coeff. of Variation
mm (in.)	(deg.)	Tests	(GPa)	(psi)	(GPa)	(psi)	
12.7 (1/2)	10	2	3.1	445000	0.15	21200	0.048

Table 3.6 Compression Strength

Thickness mm (in.)	Fibre Orientation (deg.)	Number of Tests	Compression Strength				
			Average		Standard Deviation		Coeff. of Variation
			(MPa)	(psi)	(MPa)	(psi)	
9.525	0	10	213	30900	13.6	1970	0.0638
(3/8)	90	10	145	21100	14.1	2040	0.0967
12.7	0	10	175	25400	12.2	1770	0.0697
(1/2)	30	5	159	23000	6.4	926	0.0403
	45	5	159	23000	7.4	1070	0.0465
	60	5	148	21500	7.4	1070	0.0498
	90	10	145	21000	5.8	834	0.0397
19.05	0	10	157	22700	7.2	1050	0.0463
(3/4)	90	10	139	20200	8.6	1250	0.0619

Total: 75

Table 3.7 Interlaminar Shear Strength

Thickness mm (in.)	Fibre Orientation (deg.)	Number of Tests	Interlaminar Shear Strength				
			Average		Standard Deviation		Coeff. of Variation
			(MPa)	(psi)	(MPa)	(psi)	
9.525	0	10	32.3	4690	6.4	926	0.1970
(3/8)	90	10	37.2	5390	2.7	398	0.0738
12.7	0	10	27.8	4030	3.8	553	0.1370
(1/2)	90	10	24	3480	6.3	908	0.2610
19.05	0	10	27.6	4000	3.6	522	0.1310
(3/4)	90	10	27.9	4050	2.4	351	0.0867

Total: 60

Table 3.8 Intralaminar Shear Strength

Thickness mm (in.)	Fibre Orientation (deg.)	Number of Tests	Intralaminar Shear Strength				
			Average		Standard Deviation		Coeff. of Variation
			(MPa)	(psi)	(MPa)	(psi)	
9.525 (3/8)	0	5	116	16800	6.4	930	0.0554
12.7 (1/2)	0	5	104	15100	5.7	826	0.0547
	30	5	115	16700	5.3	764	0.0457
	45	5	120	17400	15.9	2300	0.1320
	60	5	117	17000	2.5	358	0.0211
	90	5	120	17400	7.4	1070	0.0615
19.05 (3/4)	0	5	114	16600	8.1	1180	0.0711

Total: 35

Table 3.9 Summary of Material Properties

Thickness mm (in.)	Fibre Orientation deg.	Tensile Modulus GPa (Msi)	Tensile Strain %	Tensile Strength MPa (psi)	Comp. Strength MPa (psi)	Inter-Shear Strength MPa (psi)	Intra-Shear Strength MPa (psi)
9.525 (3/8)	0	15.2 (2.20)	1.6	198 (28700)	213 (30900)	32.3 (4690)	116.0 (16800)
	90	10.8 (1.56)	1.2	101 (14700)	145 (21100)	37.2 (5390)	---
12.7 (1/2)	0	12.7 (1.84)	1.6	166 (24100)	175 (25400)	27.8 (4030)	104.0 (15100)
	90	10.7 (1.55)	1.4	110 (16000)	145 (21000)	24.0 (3480)	120.0 (17400)
19.05 (3/4)	0	13.1 (1.90)	1.6	166 (24100)	157 (22700)	27.6 (4000)	114.0 (16600)
	90	11.1 (1.61)	1.4	103 (14900)	139 (20200)	27.9 (4050)	---

Shear Modulus = 4.2 GPa
Major Poisson's Ratio = 0.28

Table 3.10 Experimental Parameters

Parameter:		Dimensions:					
Hole Diameter "d":	mm	20.6					
	(in)	(13/16)					
Thickness "t":	mm	9.525	12.7	19.05			
	(in)	(3/8)	(1/2)	(3/4)			
Width "w":	mm	25.4	38.1	50.8	101.6	152.4	254
	(in)	(1)	(1.5)	(2)	(4)	(6)	(10)
Edge Distance "e":	mm	19.05	38.1	63.5	101.6	203.2	
	(in)	(0.75)	(1.5)	(2.5)	(4)	(8)	
Fibre Orientation:	deg.	0	45	90			
Ratios:							
Width / Hole Dia. (w/d):		1.23	1.85	2.46	4.92	7.38	12.31
Edge Distance / Hole Dia. (e/d):		1.23	1.85	3.08	4.92	9.85	

58

Table 3.11 Experimental Program

Test Designation	thickness "t" & fibre angle	width "w" mm	(in)	edge distance "e" mm	(in)	RIEHLE Machine	Strain Gauges	Oscilli-scope
Series A								
A1		25.4	(1)	19.05	(0.75)	*		
A2				203.2	(8)	*		
A3				38.1	(1.5)	*		
A4		38.1	(1.5)	63.5	(2.5)	*		
A5				101.6	(4)	*		
A6				38.1	(1.5)	*		
A7		50.8	(2)	63.5	(2.5)			Yes
A8				101.6	(4)	*		
A9				38.1	(1.5)	*		
A10	9.525 (3/8) @ 0 deg.	101.6	(4)	63.5	(2.5)	*		
A11				101.6	(4)	*		
A12				203.2	(8)	*		
A13				38.1	(1.5)	*		
A14		152.4	(6)	63.5	(2.5)	*		
A15				101.6	(4)	*		
A16				19.05	(0.75)	*		
A17				38.1	(1.5)	*		
A18		254	(10)	63.5	(2.5)	*		
A19				101.6	(4)	*	Yes	
A20				203.2	(8)			
A21		101.6	(4)	101.6	(4)		Yes	Yes
A22		152.4	(6)	101.6	(4)	*	Yes	
Series B								
B1		25.4	(1)	19.05	(0.75)	*		
B2				203.2	(8)	*		
B3				38.1	(1.5)	*		
B4		38.1	(1.5)	63.5	(2.5)	*		
B5				101.6	(4)	*		
B6				38.1	(1.5)	*		
B7		50.8	(2)	63.5	(2.5)	*		
B8				101.6	(4)	*		
B9	12.7 (1/2) @ 0 deg.			38.1	(1.5)	*		
B10		101.6	(4)	63.5	(2.5)			Yes
B11				101.6	(4)	*		
B12				203.2	(8)			
B13				38.1	(1.5)	*		
B14		152.4	(6)	63.5	(2.5)	*		
B15				101.6	(4)	*		
B16				19.05	(0.75)			
B17				38.1	(1.5)			
B18		254	(10)	63.5	(2.5)			Yes
B19				101.6	(4)		Yes	
B20				203.2	(8)			

Table 3.11 Experimental Program (cont'd)

Test Designation	thickness "t" & fibre angle	width "w" mm	(in)	edge distance "e" mm	(in)	RIEHLE Machine	Strain Gauges	Oscilli-scope
Series C								
C1		25.4	(1)	19.05	(0.75)			
C2				203.2	(8)			
C3		38.1	(1.5)	38.1	(1.5)			
C4				63.5	(2.5)	*		
C5				101.6	(4)			
C6		50.8	(2)	38.1	(1.5)			
C7				63.5	(2.5)	*		
C8				101.6	(4)			
C9	12.7	101.6	(4)	38.1	(1.5)			
C10	(1/2)			63.5	(2.5)	*		
C11	@ 90 deg.			101.6	(4)			
C12				203.2	(8)			
C13		152.4	(6)	38.1	(1.5)			
C14				63.5	(2.5)	*		
C15				101.6	(4)		Yes	
C16		254	(10)	19.05	(0.75)			
C17				38.1	(1.5)			
C18				63.5	(2.5)			
C19				101.6	(4)		Yes	
C20				203.2	(8)			
Series D								
D1		25.4	(1)	19.05	(0.75)			
D2				203.2	(8)			
D3		38.1	(1.5)	38.1	(1.5)			
D4				63.5	(2.5)	*		
D5				101.6	(4)			
D6		50.8	(2)	38.1	(1.5)			
D7				63.5	(2.5)	*		
D8				101.6	(4)			
D9	12.7	101.6	(4)	38.1	(1.5)			
D10	(1/2)			63.5	(2.5)	*		
D11	@ 45 deg.			101.6	(4)			
D12				203.2	(8)			
D13		152.4	(6)	38.1	(1.5)			
D14				63.5	(2.5)	*		
D15				101.6	(4)			
D16		254	(10)	19.05	(0.75)			
D17				38.1	(1.5)			
D18				63.5	(2.5)			
D19				101.6	(4)			
D20				203.2	(8)			

Table 3.11 Experimental Program (cont'd)

Test Designation	Parameter Dimensions mm (in.): thickness "t" & fibre angle	width "w" mm	(in)	edge distance "e" mm	(in)	RIEHLE Machine	Strain Gauges	Oscilli-scope
Series E								
E1		25.4	(1)	19.05	(0.75)			
E2				203.2	(8)			
E3				38.1	(1.5)			
E4		38.1	(1.5)	63.5	(2.5)			
E5				101.6	(4)			
E6				38.1	(1.5)			
E7		50.8	(2)	63.5	(2.5)			
E8				101.6	(4)			
E9	19.05			38.1	(1.5)			
E10	(3/4)	101.6	(4)	63.5	(2.5)			
E11	@ 0 deg.			101.6	(4)		Yes	
E12				203.2	(8)			
E13				38.1	(1.5)			
E14		152.4	(6)	63.5	(2.5)			
E15				101.6	(4)		Yes	
E16				19.05	(0.75)			
E17				38.1	(1.5)			
E18		254	(10)	63.5	(2.5)			
E19				101.6	(4)		Yes	
E20				203.2	(8)		Yes	

Total=102 Connection Tests
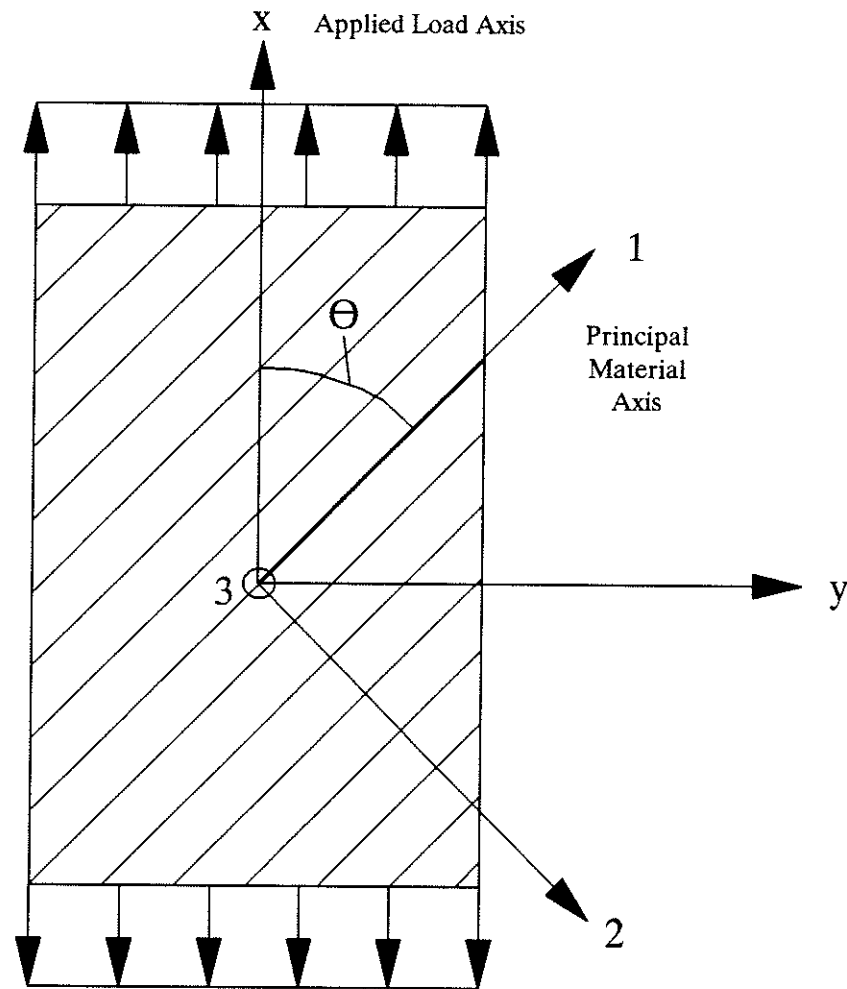
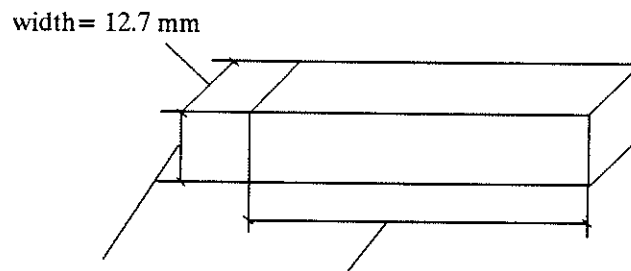Figure 3.1 Load Axes and Principal Material Axes

Gauge Length=50 mm

t=9.525, 12.7, 19.05 mm

width=12.7 mm

Strain Gauges

radius=76 mm
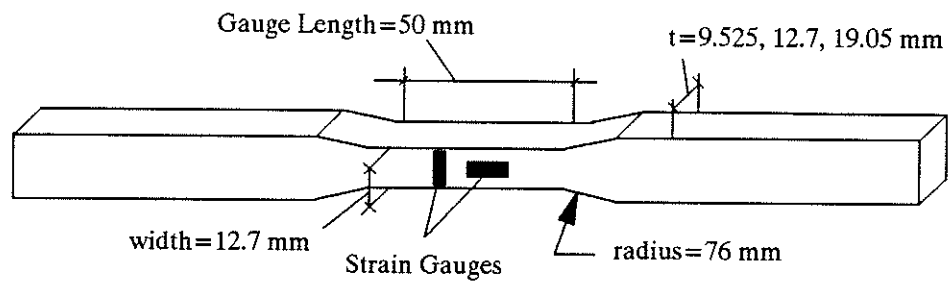
(a) Tension Coupon Dimensions (ASTM D638)

t=12.7 mm

Fibre Angle =10 deg

Rosette

Width=44.5 mm
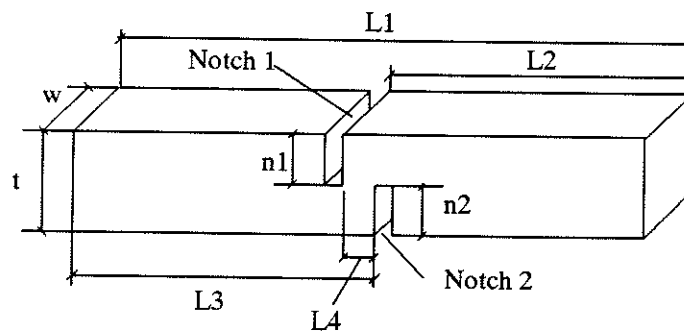
x

1

y

2

Length=254 mm
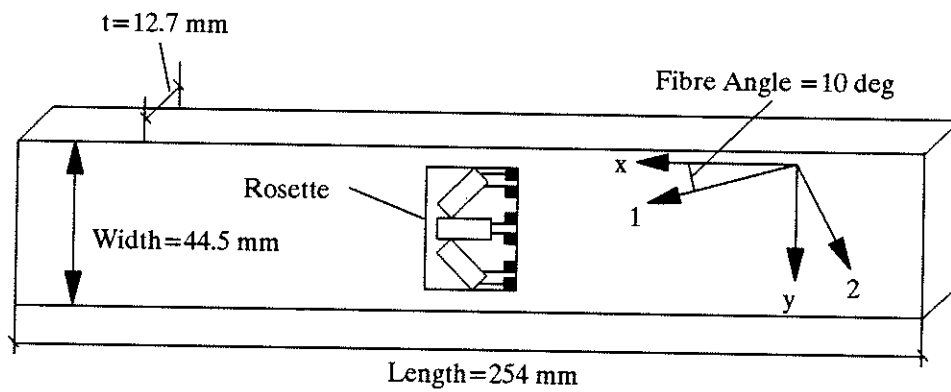
(b) Shear Modulus Coupon Dimensions

Figure 3.2 Material Coupon Dimensions

width= 12.7 mm

Thickness: Length:
9.525 mm............38.1 mm
12.7 mm............. 50 mm
19.05 mm............ 50 mm

(c) Compression Coupon Dimensions (ASTM D695)

Coupon Dimensions:
width=12.7 mm   thickness=9.525, 12.7, 19.05 mm
L1=79.5 mm   n1=n2=t /2
L2=L3=36.3 mm   Notch width=1.02 to 1.65 mm
L4=6.4 mm

(d) Shear Coupon Dimensions (ASTM D3846)

Figure 3.2 Material Coupon Dimensions (cont'd)
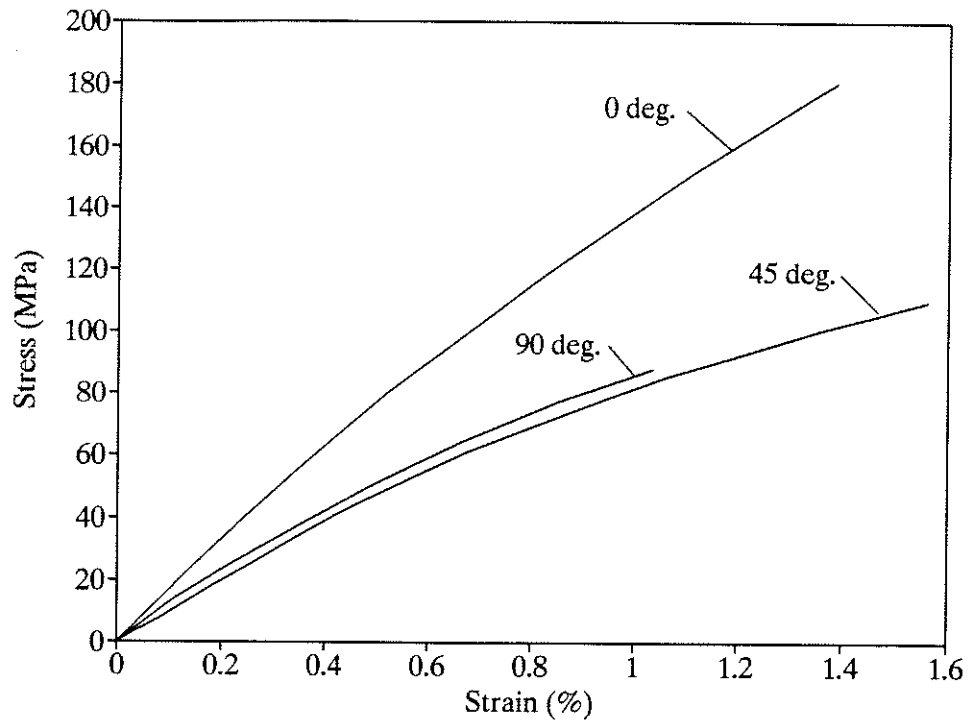
Figure 3.3 Stress-Strain Curves for Material Thickness t=9.525 mm
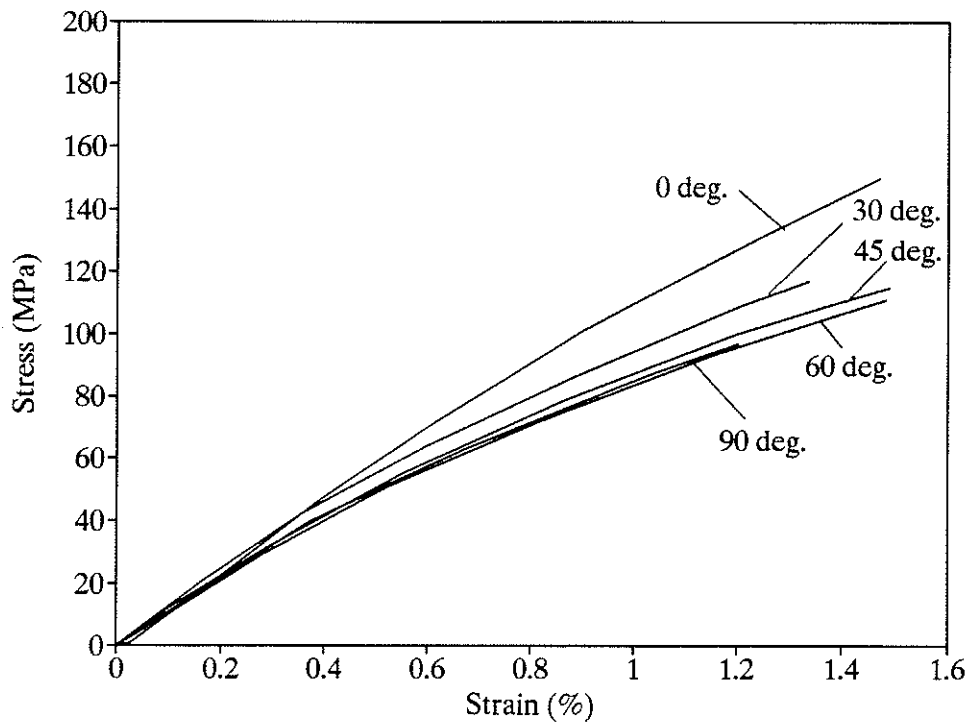
Figure 3.4 Stress-Strain Curves for Material Thickness t=12.7 mm
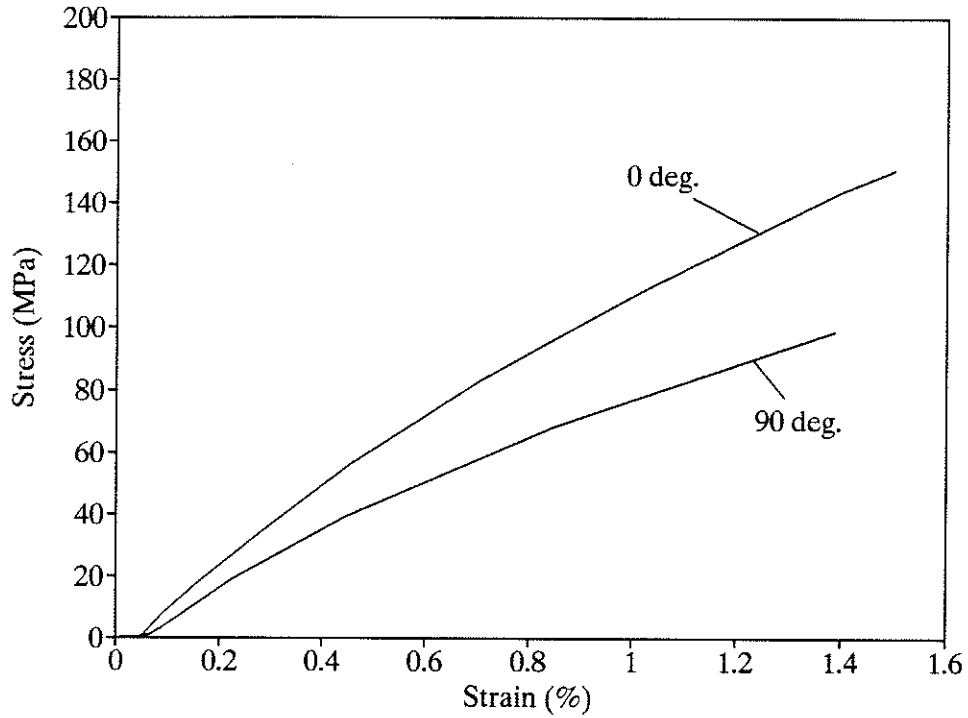
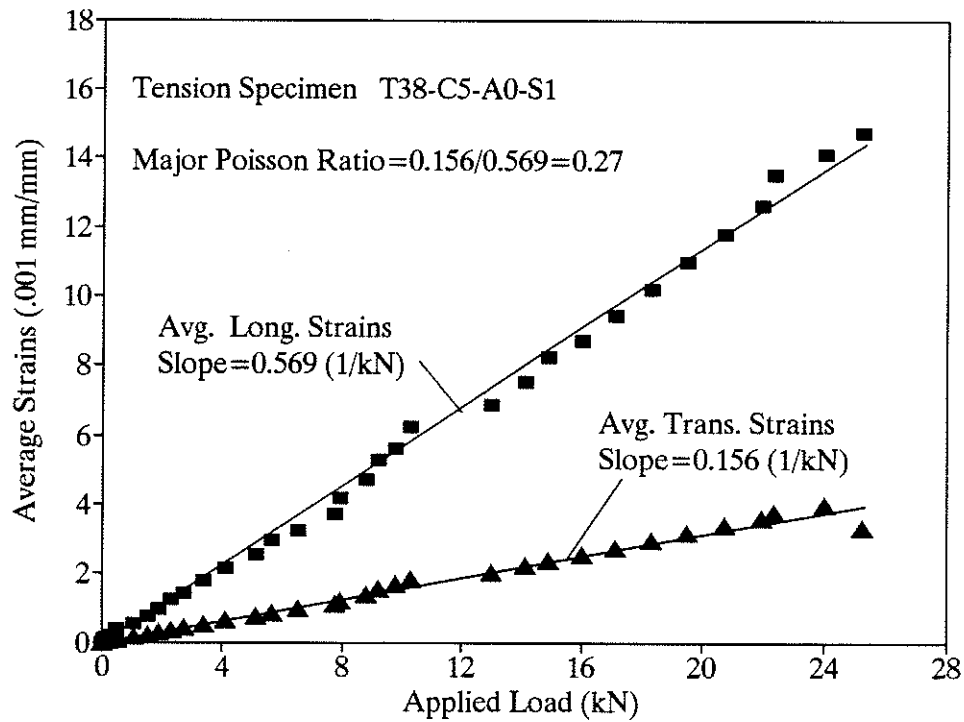Figure 3.5 Stress-Strain Curves for Material Thickness t=19.05 mm

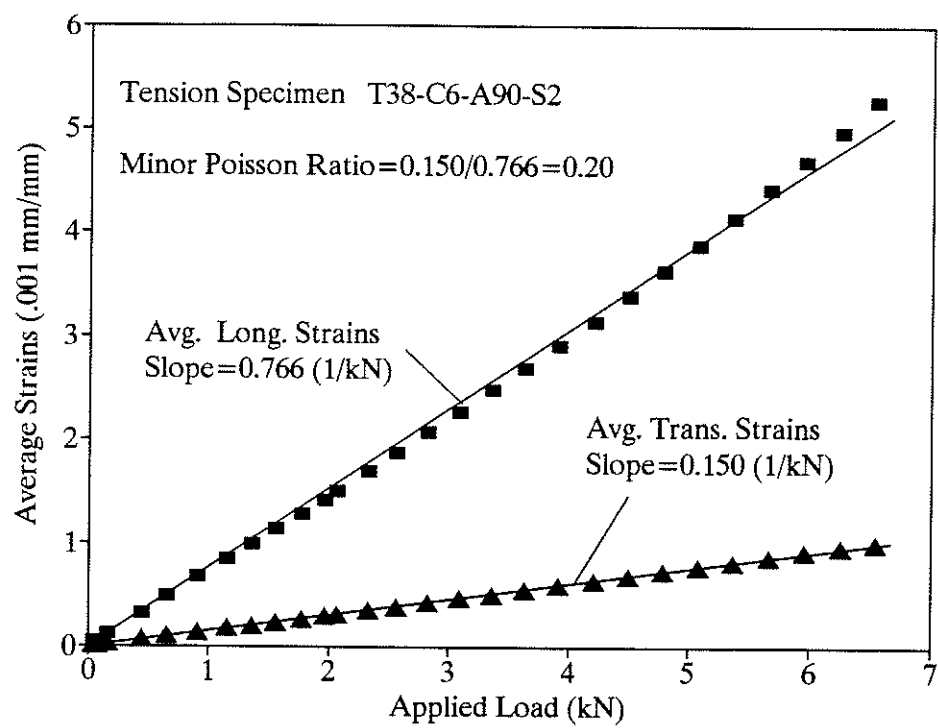Figure 3.6 Determination of Major Poisson's Ratio

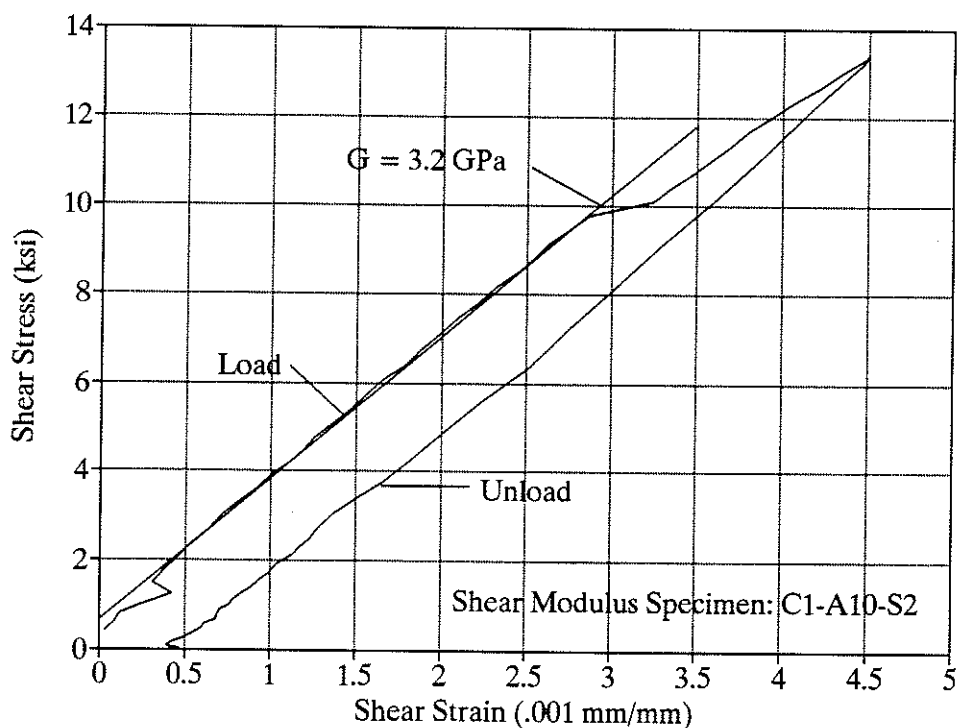Figure 3.7 Determination of Minor Poisson's Ratio

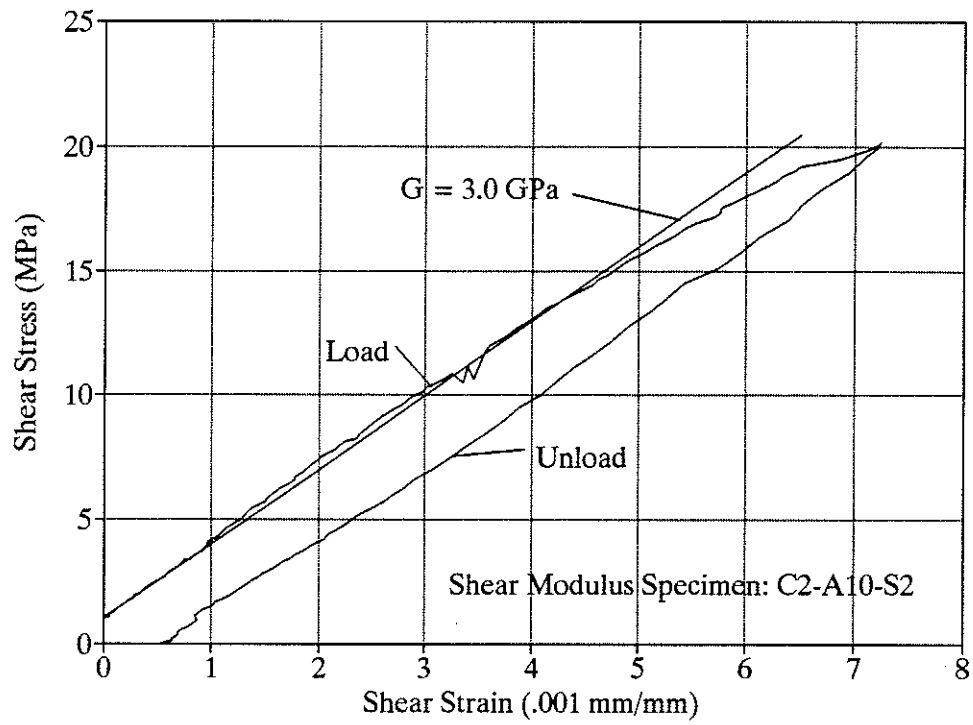Figure 3.8 Shear Stress-Strain Graph for Shear Modulus Specimen #1

Figure 3.9 Shear Stress-Strain Graph for Shear Modulus Specimen #2

Shear Coupon ASTM D3846
Fibre Orientation = 0 deg.
Measured Shear Strength Fs(13).

(a)

Shear Coupon ASTM D3846
Fibre Orientation = 90 deg.
Measured Shear Strength Fs(23).

(b)

Modified Shear Coupon
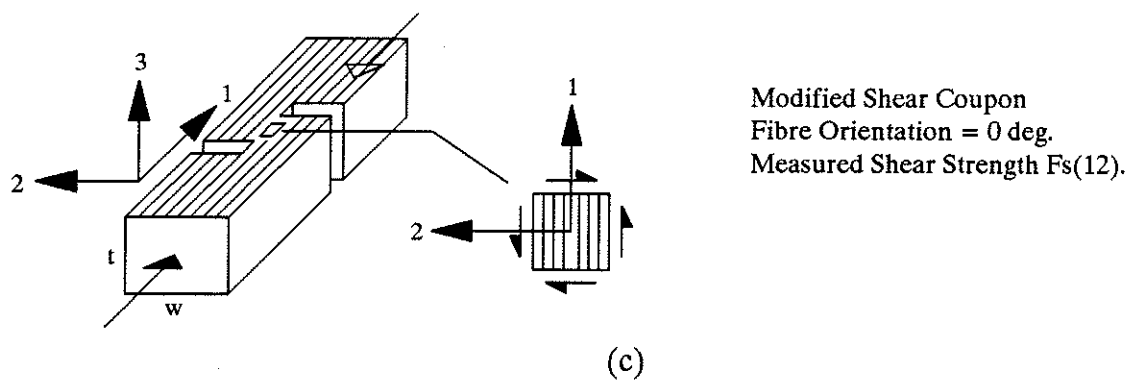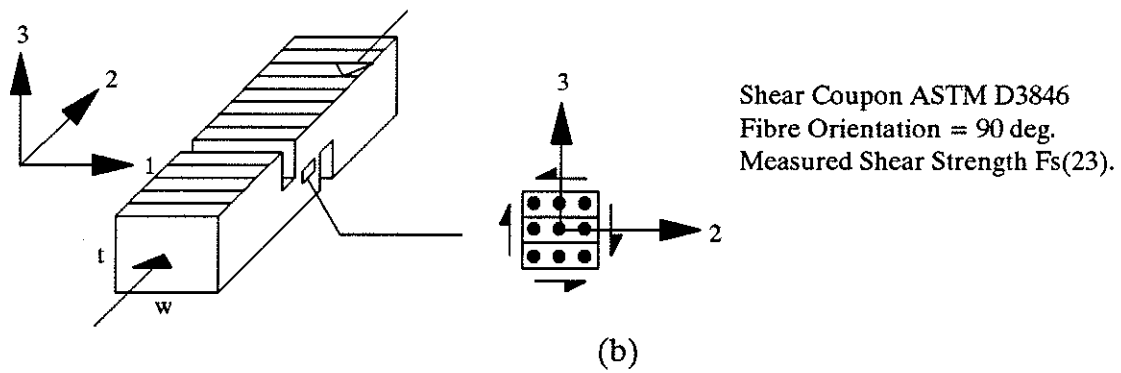Fibre Orientation = 0 deg.
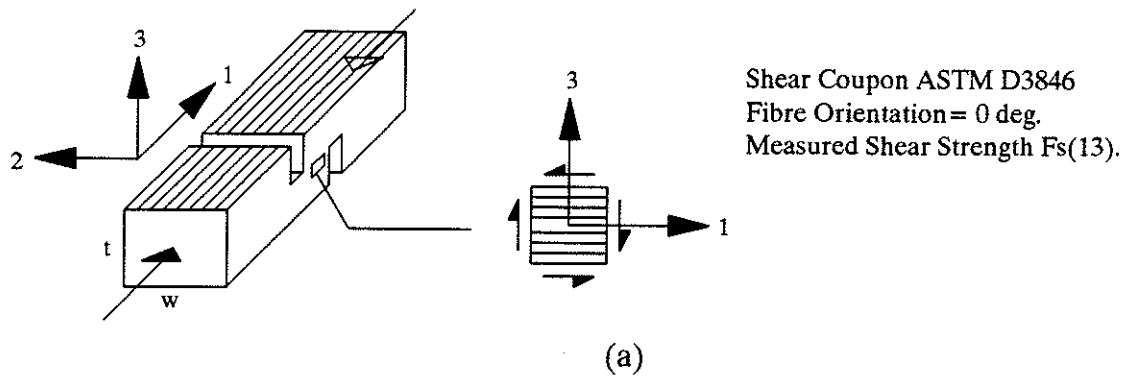Measured Shear Strength Fs(12).

(c)

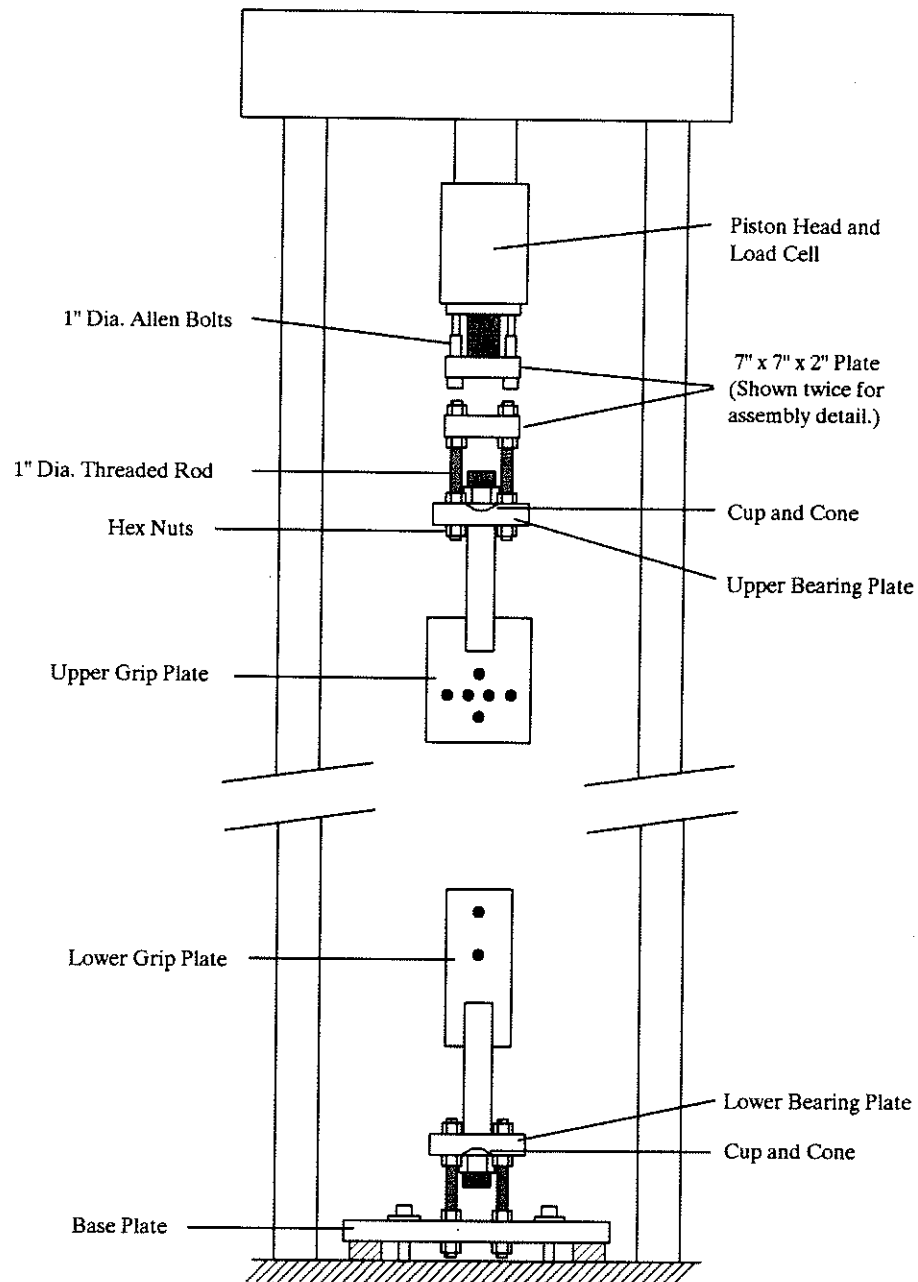Figure 3.10 Stress Analysis of Shear Coupons

Figure 3.11 Load Frame and Gripping System
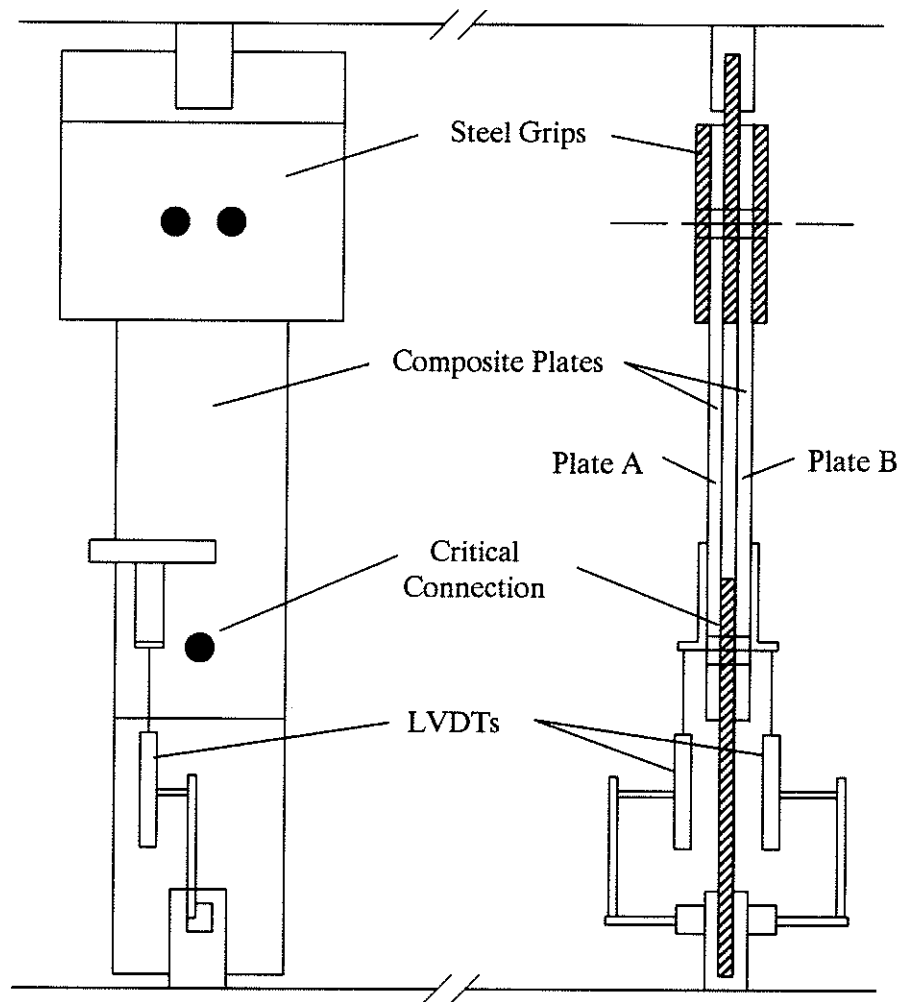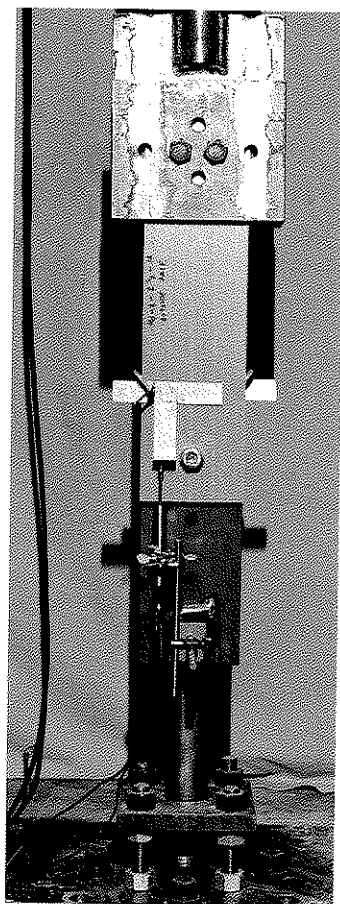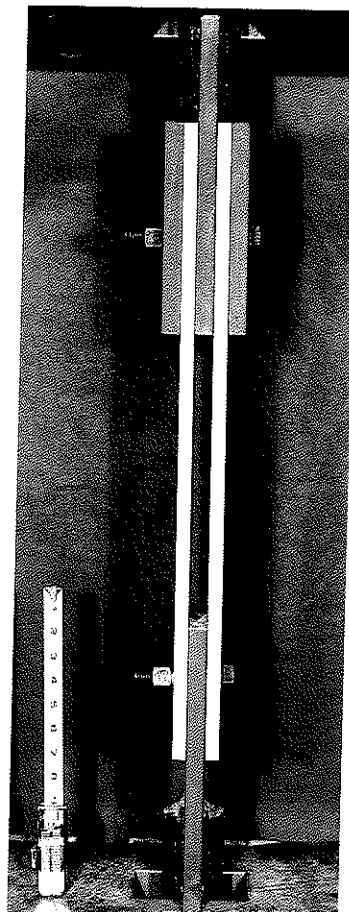
Figure 3.12 Test Set-up

Front   Side
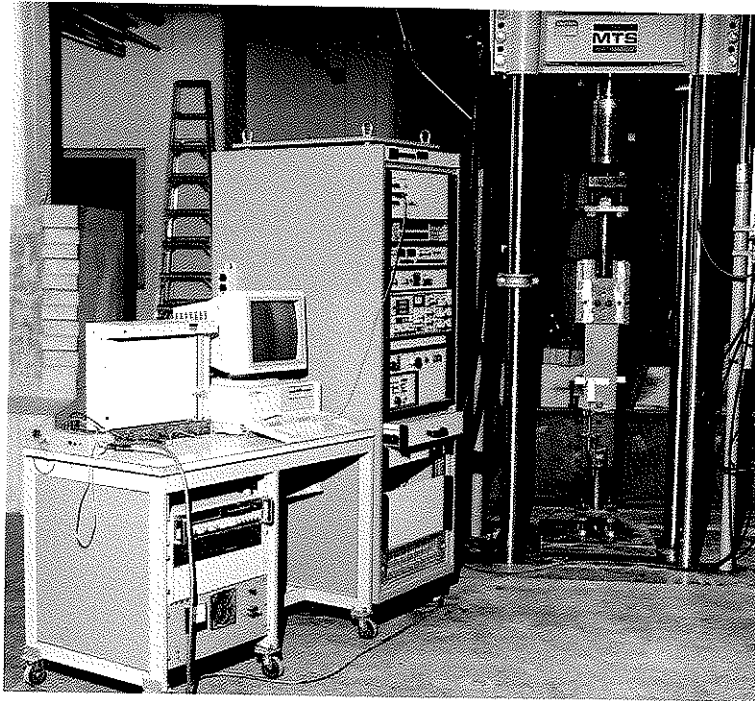
Figure 3.13 Connection Configuration
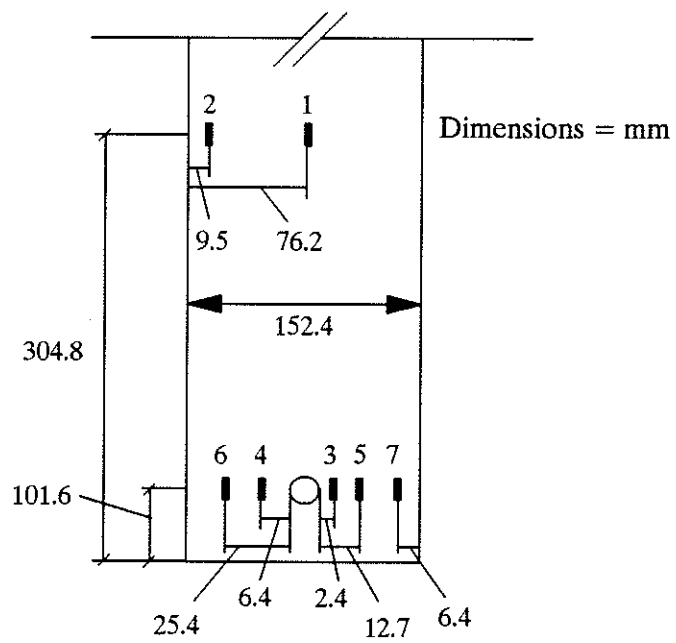
Figure 3.14 Instrumentation and Loading System

Figure 3.15 Typical Strain Gauge Arrangement

CHAPTER 4 TEST RESULTS AND DISCUSSION

4.1 TEST RESULTS

This chapter presents the test results of a total of 102 single-bolted connections tested in this investigation. The measured ultimate load and mode of failure for all of the connections tested are summarized in Table 4.1. The ultimate load is the total capacity of the connection based on the two composite plate members it is comprised of. The failure mode is also given for each plate member in the connection.

In Series A, two connections, A11 and A15 were repeated and marked A21 and A22 respectively to determine the variability of the results. In general the failure modes corresponded for both pairs of tests. As given in Table 4.1, the ultimate load of connections A11 and A21 varied approximately 10% and the ultimate load of connections A15 and A22 varied by only 5%. The variability of the test results is acceptable, since it is within the range of material variability. The ultimate strengths of connections, when normalized with respect to the thickness of the material, generally corresponded with one another and confirmed that the variability of the connection test results was within the variability range of the material properties.

4.2 FAILURE MODES

Three of the four basic failure modes were observed in this investigation as shown in Fig. 4.1. The three modes were net-tension failure as shown in Fig. 4.1(a), cleavage failure as shown in Fig. 4.1(b), and bearing failure as shown in Fig. 4.1(c). Net tension failure was characterized by typical fracture through the net section. Cleavage failure was characterized by a crack parallel to the applied load propagating from the end of the plate towards the bolt hole leading to the initiation of other cracks near the net section due to the formation of in-plane bending stresses. Bearing failure was characterized by crushing of the material in the vicinity of the bolt-to-hole interface.

Combinations of the three basic failure modes were also observed. Combined bearing-net tension failure, bearing-cleavage failure, and cleavage-net tension failure are shown in Fig. 4.2(a), (b), and (c) respectively.

Due to the high percentage of random fibres in the material used in this investigation, the shearout mode of failure was not observed. This failure mode required very small edge distances that were impractical.

4.3 LOAD-DISPLACEMENT CHARACTERISTICS

A comparison of typical load-displacement relationships for the three basic modes of failure are shown in Fig. 4.3. The displacement is the average reading of the two LVDT's mounted on either side of the connection. The load is the total resistance of the two plate members comprising each connection.

The behaviour shown in Fig. 4.3, reflects a small initial friction resistance capacity of the connection due to the applied bolt torque of 32.5 N-m (24 ft-lb). Slipping of the connections occurred at the initial loading stage. Once the bolt slipped into bearing, all of the connections behaved linearly. Fig. 4.3 illustrates a step-function behaviour characterizing the sudden drop in load carrying capacity for the net tension and cleavage failure modes. The load drops typically occurred in two distinct "events" as the two composite plates comprising each connection would not fracture at the same time. For connections that failed in bearing, the load reduction occurred gradually as the bolt pulled through the composite plates simultaneously and the overall behaviour was much more ductile than the other modes of failure.

Load-displacement curves for the combined failure modes are shown in Fig. 4.4 to Fig. 4.6. The behaviour of a connection that failed in combined bearing-cleavage is compared to the behaviour of a similar connection that failed in bearing as shown in Fig. 4.4. The behaviours of the two connections are essentially the same with the only difference occurring in the post-failure stages where cleavage failure occurs for the combined mode reducing the overall ductility.

The load-displacement behaviour for a connection that failed in combined bearing-net tension failure is compared to a connection that failed in net tension as shown in Fig. 4.5. The behaviour is almost identical, however, the larger width of the members used for specimen B12 allowed the connection to gain additional capacity through bearing before the net tension failure occurred.

The behaviour of a connection that failed in combined cleavage-net tension is shown in Fig. 4.6. As shown in Table 4.1, this combined mode was only observed for the connections with members having a fibre orientation of 45° with respect to the applied load. The behaviour is compared to both a pure net tension failure case and a cleavage failure case for similar connections with the same fibre orientation. The behaviour of the combined case is located between that of the two basic failure modes. The increase in the load capacity in comparison to the cleavage case is due to an increase in the edge distance. The higher load for the net tension case is again due to an increase in the edge distance.

In most cases, the slippage, which occurred as a result of the bolt being centred in an oversized bolt hole, had progressed in one step. The load increased until the friction forces between the composite plates and the washers and the lower steel grip were overcome, causing the load to plateau and the displacement to increase as the slippage took place. The slippage was approximately equal to half the clearance between the bolt and the oversized hole.

In some connection tests the slippage had occurred in two steps as shown in Fig. 4.7. The first step occurred when the composite plate members, along with the bolt, slipped with respect to the lower grip plate. Therefore, the slip distance of the first step was normally equivalent to the small clearance that existed between the bolt and the hole of the lower steel grip. The second slippage step occurred as the composite plates slipped with respect to both the lower grip and the bolt, leading to a larger slip distance approximately equal to half the clearance between the bolt

and the holes in the composite plates.

Catastrophic failure modes, such as net tension and cleavage, usually took place in fractions of a second. This usually meant that the load-displacement behaviour between the time that the failure was initiated and the time that it stopped could not be recorded unless a very fast data acquisition system was used. To accurately characterize such a sudden event, a storage oscilloscope was used to monitor the signals from the load and displacement transducers. Figure 4.8 represents the data recorded on the oscilloscope screen. Both the load resistance and the average displacement readings were recorded in the same figure with respect to time. In this case the selected time interval "frozen time" was 1 second. The vertical axis in Fig. 4.8 represents the resolution of the oscilloscope as the number of oscilloscope divisions. For the load signal, one level is equal to 1 kN (224.8 lb) and for the displacement signal, one level equals 0.508 mm (.002 in.). The failure event is enlarged using a larger time scale as shown in Fig 4.9 where the load and displacement data are given for a time interval of 0.1 seconds. The oscillations in the displacement signal are the result of electronic noise from the displacement transducers and should be ignored. The damped oscillations in the load signal right after the drop in load are a result of the physical response of the load cell to the fracture impulse and should also be ignored. The failure event occurs as the load instantly drops a certain amount and the displacement increases over a certain time interval. These signals can be modelled using linear segments as shown in Fig. 4.10. Using the modelled curves and the conversion factors, the load and displacement

readings during the failure event can be plotted on a load-displacement graph. This curve can then be superimposed onto the load-displacement graph recorded by the slower data acquisition system as shown in Fig. 4.11. The L-shaped load-displacement curve recorded by the oscilloscope is the correct behaviour of a connection during a catastrophic failure event and is typical of all the connections tested in this investigation which failed in a sudden manner.

4.4 ULTIMATE STRENGTHS

To analyze the results of the connection tests, the following average ultimate strengths are defined as:

$$Ultimate\ Bearing\ Strength\ =\ \frac{P_{ult}}{d_{bolt}(2t)} \tag{4.1}$$

$$Ultimate\ Net\ Tension\ Strength\ =\ \frac{P_{ult}}{(w-d)(2t)} \tag{4.2}$$

In Eq.(4.1) and (4.2), P_{ult} is the ultimate failure load, taken as the maximum load attained during a connection test. The variables w, d, d_{bolt} and t are the member width, the hole diameter, the bolt diameter and the material thickness of a connection respectively. Since each connection is comprised of two composite plates, the thickness is multiplied by two in Eq.(4.1) and (4.2).

4.5 EFFECT OF WIDTH

Variation of the width of the members in a connection predominantly influences the capacity of a connection as well as the corresponding mode of failure. For connections comprised of members with a 0° fibre orientation, the ultimate bearing strength with respect to the width-to-hole-diameter ratio (w/d) is given in Fig. 4.12 to Fig. 4.14 for Series A, B, and E respectively. For comparative purposes the same results are given in Fig. 4.15 for all of the above series. The various failure modes are represented as "NT" for net tension, "C" for cleavage, and "B" for bearing with the combined modes represented by hyphenated letters. The lines in Fig. 4.12 to Fig. 4.15 are given for connections with the same edge distance. For connections with relatively small edge distances, the mode of failure changes from net tension failure to cleavage failure as the (w/d) ratio increases. For connections with relatively large edge distances, the mode of failure changes from net tension failure to bearing failure. Associated with the change in failure mode is an increase in bearing strength as the (w/d) ratio increases. The strength increases tend to level off past (w/d)=5 which is within the range of typical values for composite materials given in Chapter 2. The transition between failure modes is not sharply defined as shown in Fig. 4.12 to Fig. 4.15, since the connections within the transition zones are influenced by combined modes of failure.

The ultimate net tension strengths for connections with various edge distances of Series A, B, and E are plotted with respect to the (w/d) ratio in Fig. 4.16 . The lines in Fig. 4.16 represent connections with the same edge distance. The net

tension strengths of connections with large (w/d) ratios are relatively small compared to the net tension strengths of connections with small (w/d) ratios. This behaviour is mainly due to the high magnitude of stress concentrations for members with large widths. These stress concentrations can be in the order of 4 to 6 as will be discussed. For the narrow connections, with relatively small (w/d) ratios, the net stress concentrations are more moderate, in the order of 2 to 3, thereby allowing higher net tension strengths to be achieved.

4.6 EFFECT OF EDGE DISTANCE

To illustrate the effects of variation in edge distance, the ultimate bearing strengths of the connections are plotted with respect to the edge-distance-to-hole-diameter ratio (e/d) in Fig. 4.17 to Fig. 4.19 for Series A, B, and E respectively. The results for all three series are combined and shown in Fig. 4.20. The lines in Fig. 4.17 to Fig. 4.20 are given for connections with the same width. For narrow connections, the variation of edge distance has little effect on the failure mode or ultimate strength as shown in Fig. 4.17 to Fig. 4.20, where the predominant failure mode is net tension regardless of the size of the edge distance. However, for wider connections, the failure mode changes from cleavage failure to bearing failure with increasing (e/d) ratios. The results indicate that the ultimate bearing strength increases with an increase in the (e/d) ratio up to a value of (e/d)=5. This value is within the range of typical values for composite materials. Again the transition between failure modes is not sharply defined.

The ultimate net tension strengths for the connections of Series A, B, and E are plotted with respect to the (e/d) ratio in Fig. 4.21. The lines in Fig. 4.21 are given for connections with the same width. With an increasing (e/d) ratio, the ultimate net tension strengths tend to increase up till a value of (e/d)=5. This suggests that increasing edge-distances tend to reduce the stress concentrations associated with net stresses and therefore increase the net tension strength capacity.

4.7 EFFECT OF THICKNESS

For the three material thicknesses used in this investigation, the results indicate that the member thickness had little effect on the overall behaviour of the connections. This is demonstrated in Figures 4.15, 4.16, 4.20, and 4.21, which show the results of 0° connections for all three material thicknesses. The ultimate strengths of the connections for different thicknesses tend to match within the range of material variability. The failure modes of connections with the same geometry but different thicknesses also correspond.

The lateral constraint applied by the washers reduces the influence of the member thickness on the connection behaviour. It seems that high strength structural bolts tightened to a torque of 32.5 N-m (24 ft-lbs) as used in this investigation, are adequate to remove most of the influence of the material thickness.

4.8 EFFECT OF FIBRE ORIENTATION

The influence of fibre orientation on the modes of failure is shown in Fig. 4.22 for connections of the same dimensions. Due to the presence of the unidirectional fibres at 45° and 90° to the applied load, the typical cleavage failure that had occurred in connections with a 0° fibre orientation as shown in Fig. 4.22(a), was suppressed for the corresponding connections that had a fibre orientations of 45° and 90° to the applied load as shown in Fig. 4.22(b) and (c).

The load-displacement behaviours of the connections in Fig. 4.22 are given in Fig. 4.23. Although the ultimate loads of the 45° and 90° connections were lower than their 0° counterparts, the general shape of the load-displacement curves remained unchanged.

The ultimate bearing strengths of connections with a fibre orientation of 45° and 90° are plotted with respect to the (w/d) ratio in Fig. 4.24 and Fig. 4.25 respectively. The lines represent connections with the same edge distance. As shown in the figures and in Table 4.1, the predominate mode of failure is net tension regardless of the connection geometry. Only in the extreme ranges of the geometrical dimensions do the failure modes change to cleavage and bearing. For large widths and very small edge distances, cleavage failure occurred and for large widths and large edge distances, bearing failure occurred as shown in Fig. 4.24 and 4.25. The 45° case seems to be more susceptible to combined failure modes suggesting that at this fibre orientation there is a larger interaction between the stresses corresponding to each basic failure mode.

The ultimate bearing strengths with respect to the (w/d) ratio of the 45° and 90° fibre orientation connections are compared to the results for the 0° connections of the same thickness in Fig. 4.26. The increases in bearing strength with increasing (w/d) ratio, begin to level off past (w/d)=5. However, the results suggest that to achieve bearing failure the (w/d) value must be larger. Figure 4.26 illustrates the reduction in bearing strength with the change in fibre orientation from 0° to 90°. The results in Fig. 4.26 are given for those edge distances which best reflect the effects of the fibre orientation. From the ultimate loads given in Table 4.1 it can be shown that a change in fibre orientation from 0° to 90°, reduces the bearing strength approximately 18% for the 45° case and 24% for the 90° case. For the connections with small (w/d) ratios the predominant failure mode was net tension for all fibre orientations. At higher (w/d) ratios, the predominant failure mode was either bearing or cleavage failure for the 0° case but remained net tension failure for the 45° and 90° cases due to their high susceptibility to net tension fracture, as shown in Fig. 4.26.

The ultimate bearing strengths for the 45° and 90° connections are plotted with respect to the (e/d) ratio in Fig. 4.27 and 4.28 respectively. The lines in Fig. 4.27 and 4.28 are given for connections with constant width. As with the 0° connections, the bearing strengths of the 45° and 90° connections tended to increase with increasing (e/d) ratios up till a value of (e/d)=5. Again the results suggest that to achieve bearing failure in the 45° and 90° cases the (e/d) ratio must be larger.

The bearing strengths with respect to the (e/d) ratios for the three fibre

orientations are compared in Fig. 4.29 and Fig. 4.30. The results in Fig. 4.29 and 4.30 are given for connection widths that best represent the influence of the fibre orientation. These figures illustrate the difference in failure mode between the 0° connections and the 45° and 90° connections. Figure 4.29 illustrates that for intermediate widths, the net tension failure mode is more predominant in the 45° and 90° cases than the 0° cases which tended to fail in a combined bearing-net tension mode. Even for very wide connections as shown in Fig. 4.30, the 45° and 90° connections still tended to fail in net tension instead of cleavage or bearing.

4.9 STRESS CONCENTRATION FACTORS

Selected specimens, as given in Table 3.11, were instrumented with strain gauges to determine the effect of the various parameters on the strain and stress distributions in the directions of the applied load along the net section of the connections. Since the material behaves nonlinearly, the stress distributions will be similar but not equal to the strain distributions. For purposes of this investigation this difference is insignificant. The strain distributions for the various connection specimens are compared in Fig. 4.31 to Fig. 4.35. The strain concentration factor is equivalent to the ratio of the measured strain at the bolt hole to the strain of the member measured at the gross section away from the hole. All of the strain distributions given in these figures represent the maximum strains recorded before any strain redistribution along the net section had taken place.

The influence of the connection width on the distribution of strain is shown

in Fig. 4.31 and Fig. 4.32 for member thicknesses of 9.252 mm (3/8 in.) and 19.05 mm (3/4 in.) respectively. The figures illustrate that in general, increases in member width increase the strain concentration factors. This is obvious in the case of the 254 mm (10 in.) wide connections where the strain concentration factor adjacent to the hole approaches a value of 6, in comparison to the 101.6 mm (4 in.) wide connections where the strain concentration factor approaches the value of 2. These results are in agreement with the theoretical deductions of Hart-Smith (39). Since the applied stress at the gross section away from the hole must be reacted by the bolt, most of the load is resisted by the material in the vicinity of the hole. This is shown in the 254 mm (10 in.) wide connections, where the strain distributions are well below unity near the sides of the plate and are essentially zero at the free edge. The strain distributions confirm that the structural efficiency of a connection is highly dependent on the width of the plate.

The influence of the edge distance on the strain distribution is shown in Fig. 4.33. The connections shown are identical except for the edge distances. The connection with the 203.2 mm (8 in.) edge distance has lower strain concentrations than the one with the 101.6 mm (4 in.) edge distance. The larger edge distance seems to allow the material at the net section to be used more efficiently as the stresses are not forced to "flow" as close to the bolt hole as in the case of small edge distance. Overall it seems that the edge distance does not have as great an influence on the strain distributions as the width does.

The effect of the material thickness on the strain distribution seems to be

negligible as shown in Fig. 3.34. The connections shown are identical except for the material thickness. The maximum strain concentration factor is in the range of 5 to 6 for the three thicknesses.

Fibre orientation has a marked effect on the strains as shown in Fig. 4.35 which gives the distributions for 0° and 90° connections. The strain distribution away from the hole does not seem to be influenced as much as the strain concentrations near the hole. For connections with the same geometry, the maximum strain concentration factor adjacent to the hole is approximately 6 for the 0° fibre orientation connection and approximately 7.5 for the 90° fibre orientation connection. The higher strain concentrations coupled with the lower tensile strength in the direction of the applied load both contribute to the lower ultimate loads experienced by the "angled" connections.

88

Table 4.1 Test Results

Test Designation	thickness "t" & fibre angle	width "w" mm	(in)	edge distance "e" mm	(in)	Ultimate Load kN	(lbs)	Failure Mode Plate A	Plate B
Series A									
A1		25.4	(1)	19.05	(0.75)	12.2	2750	NT	NT
A2				203.2	(8)	14.5	3250	NT	NT
A3				38.1	(1.5)	44.0	9900	NT	NT
A4		38.1	(1.5)	63.5	(2.5)	43.8	9850	NT	NT
A5				101.6	(4)	39.4	8850	NT	NT
A6				38.1	(1.5)	55.3	12425	NT	NT
A7		50.8	(2)	63.5	(2.5)	57.8	12990	NT	NT
A8				101.6	(4)	61.3	13775	NT	NT
A9				38.1	(1.5)	69.2	15550	C	C
A10	9.525	101.6	(4)	63.5	(2.5)	95.3	21425	B-NT	B-NT
A11	(3/8)			101.6	(4)	103.0	23150	B-NT	B-NT
A12	@ 0 deg.			203.2	(8)	100.5	22600	B-NT	B-NT
A13				38.1	(1.5)	67.6	15200	C	C
A14		152.4	(6)	63.5	(2.5)	109.4	24600	C	C
A15				101.6	(4)	129.0	29000	B-NT	B
A16				19.05	(0.75)	28.9	6500	C	C
A17				38.1	(1.5)	66.7	15000	C	C
A18		254	(10)	63.5	(2.5)	113.0	25400	C	C
A19				101.6	(4)	116.8	26250	B	B
A20				203.2	(8)	113.9	25600	B	B
A21		101.6	(4)	101.6	(4)	92.1	20700	B	B-NT
A22		152.4	(6)	101.6	(4)	122.8	27600	B	B
Series B									
B1		25.4	(1)	19.05	(0.75)	13.3	3000	NT	NT
B2				203.2	(8)	14.9	3350	NT	NT
B3				38.1	(1.5)	52.3	11750	NT	NT
B4		38.1	(1.5)	63.5	(2.5)	60.5	13600	NT	NT
B5				101.6	(4)	54.9	12350	NT	NT
B6				38.1	(1.5)	72.9	16400	NT	NT
B7		50.8	(2)	63.5	(2.5)	75.4	16950	NT	NT
B8				101.6	(4)	83.4	18750	NT	NT
B9	12.7			38.1	(1.5)	97.5	21925	C	C
B10	(1/2)	101.6	(4)	63.5	(2.5)	115.1	25870	B-NT	B-NT
B11	@ 0 deg.			101.6	(4)	145.0	32600	B-NT	B-NT
B12				203.2	(8)	137.9	31010	B-NT	B-NT
B13				38.1	(1.5)	95.2	21400	C	C
B14		152.4	(6)	63.5	(2.5)	152.6	34300	C	C
B15				101.6	(4)	167.2	37600	B	B
B16				19.05	(0.75)	36.6	8225	C	C
B17				38.1	(1.5)	101.1	22740	C	C
B18		254	(10)	63.5	(2.5)	133.9	30100	C	C
B19				101.6	(4)	184.1	41400	B-NT	B
B20				203.2	(8)	186.0	41810	B	B

Failure Modes: NT=Net Tension C=Cleavage B=Bearing B-NT=Combined Bearing-Net Tension
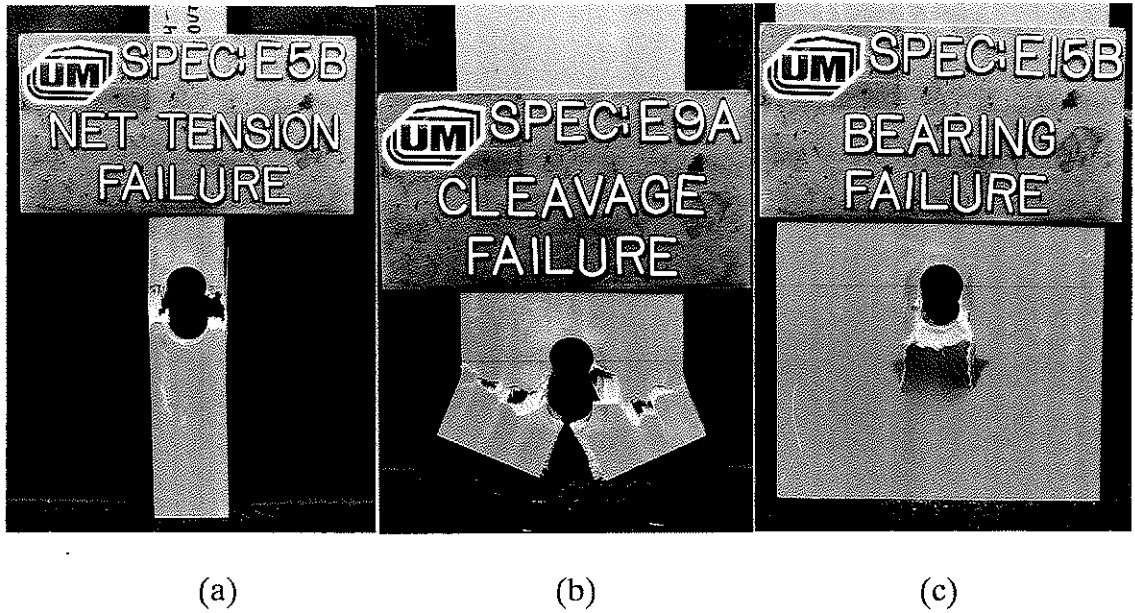B-C=Combined Bearing-Cleavage   C-NT=Combined Cleavage-Net Tension

Table 4.1 Test Results (cont'd)

Test Designation	Parameter Dimensions mm (in.): thickness "t" & fibre angle	width "w" mm	(in)	edge distance "e" mm	(in)	Ultimate Load kN	(lbs)	Failure Mode Plate A	Plate B
Series C									
C1		25.4	(1)	19.05	(0.75)	11.8	2650	NT	NT
C2				203.2	(8)	11.7	2630	NT	NT
C3				38.1	(1.5)	34.9	7840	NT	NT
C4		38.1	(1.5)	63.5	(2.5)	28.7	6450	NT	NT
C5				101.6	(4)	32.1	7210	NT	NT
C6				38.1	(1.5)	57.8	12990	NT	NT
C7		50.8	(2)	63.5	(2.5)	51.2	11500	NT	NT
C8				101.6	(4)	60.9	13690	NT	NT
C9	12.7			38.1	(1.5)	78.8	17720	NT	NT
C10	(1/2)	101.6	(4)	63.5	(2.5)	81.2	18250	NT	NT
C11	@ 90 deg.			101.6	(4)	106.3	23890	NT	NT
C12				203.2	(8)	107.7	24210	NT	NT
C13				38.1	(1.5)	82.8	18620	NT	NT
C14		152.4	(6)	63.5	(2.5)	90.3	20300	NT	NT
C15				101.6	(4)	120.4	27070	NT	NT
C16				19.05	(0.75)	39.9	8970	C	C
C17				38.1	(1.5)	84.2	18940	NT	NT
C18		254	(10)	63.5	(2.5)	114.2	25670	NT	NT
C19				101.6	(4)	135.8	30530	NT	NT
C20				203.2	(8)	165.1	37120	B	B
Series D									
D1		25.4	(1)	19.05	(0.75)	11.4	2570	NT	NT
D2				203.2	(8)	11.6	2600	NT	NT
D3				38.1	(1.5)	40.2	9040	NT	NT
D4		38.1	(1.5)	63.5	(2.5)	31.0	6975	NT	NT
D5				101.6	(4)	43.4	9750	NT	NT
D6				38.1	(1.5)	64.9	14590	NT	NT
D7		50.8	(2)	63.5	(2.5)	47.8	10750	NT	NT
D8				101.6	(4)	64.0	14390	NT	NT
D9	12.7			38.1	(1.5)	79.8	17930	NT	NT
D10	(1/2)	101.6	(4)	63.5	(2.5)	96.5	21700	NT	NT
D11	@ 45 deg.			101.6	(4)	116.9	26280	NT	NT
D12				203.2	(8)	109.7	24670	NT	NT
D13				38.1	(1.5)	88.9	19990	NT	NT
D14		152.4	(6)	63.5	(2.5)	93.9	21100	NT	NT
D15				101.6	(4)	143.2	32190	NT	NT
D16				19.05	(0.75)	36.3	8150	C	C
D17				38.1	(1.5)	89.3	20070	NT	C-NT
D18		254	(10)	63.5	(2.5)	126.8	28510	NT	NT
D19				101.6	(4)	157.6	35440	NT	B-NT
D20				203.2	(8)	185.6	41730	B	B

Failure Modes: NT=Net Tension C=Cleavage B=Bearing B-NT=Combined Bearing-Net Tension
B-C=Combined Bearing-Cleavage   C-NT=Combined Cleavage-Net Tension

Table 4.1 Test Results (cont'd)

Test Designation	thickness "t" & fibre angle	width "w" mm	(in)	edge distance "e" mm	(in)	Ultimate Load kN	(lbs)	Failure Mode Plate A	Plate B
Series E									
E1		25.4	(1)	19.05	(0.75)	20.4	4580	NT	NT
E2				203.2	(8)	23.4	5270	NT	NT
E3				38.1	(1.5)	76.7	17240	NT	NT
E4		38.1	(1.5)	63.5	(2.5)	83.9	18870	NT	NT
E5				101.6	(4)	84.0	18890	NT	NT
E6				38.1	(1.5)	106.0	23830	NT	NT
E7		50.8	(2)	63.5	(2.5)	117.1	26330	NT	NT
E8				101.6	(4)	129.7	29150	NT	NT
E9	19.05			38.1	(1.5)	133.5	30020	C	C
E10	(3/4)	101.6	(4)	63.5	(2.5)	206.9	46520	B-NT	B-C
E11	@ 0 deg.			101.6	(4)	228.3	51330	B-NT	B-NT
E12				203.2	(8)	236.1	53080	B	B
E13				38.1	(1.5)	135.7	30500	C	C
E14		152.4	(6)	63.5	(2.5)	224.4	50460	B-C	B-C
E15				101.6	(4)	233.4	52480	B	B
E16				19.05	(0.75)	45.5	10240	C	C
E17				38.1	(1.5)	129.1	29030	C	C
E18		254	(10)	63.5	(2.5)	233.1	52400	B-C	B-C
E19				101.6	(4)	266.6	59940	B	B
E20				203.2	(8)	254.1	57130	B	B

Total=102 Connection Tests

Failure Modes: NT=Net Tension C=Cleavage B=Bearing B-NT=Combined Bearing-Net Tension
B-C=Combined Bearing-Cleavage   C-NT=Combined Cleavage-Net Tension

(a)   (b)   (c)

Figure 4.1 Basic Failure Modes

(a)   (b)   (c)
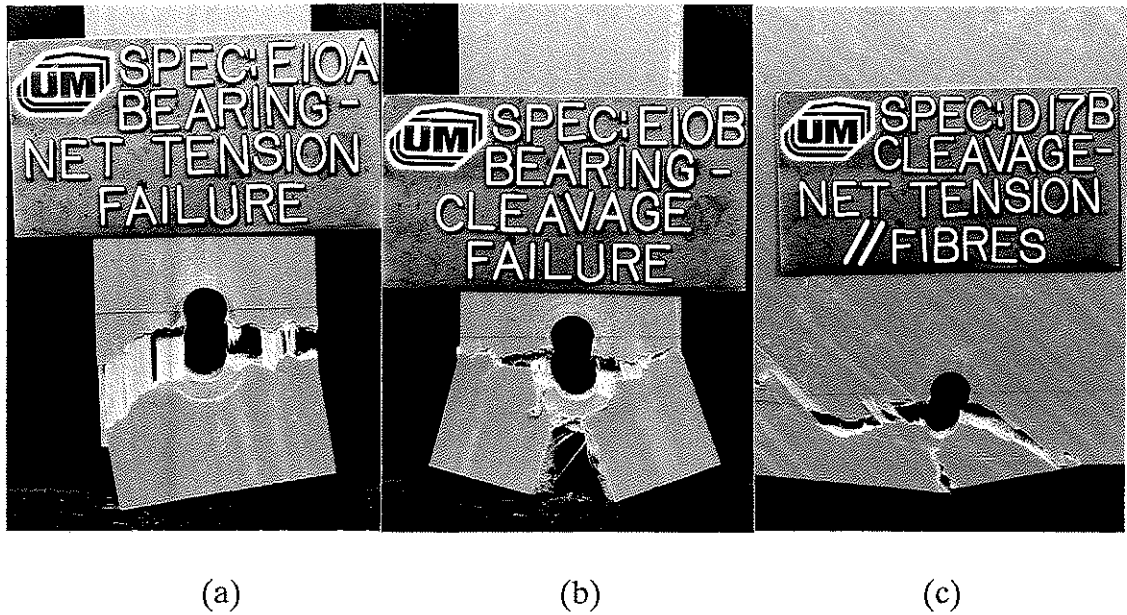
Figure 4.2 Combined Failure Modes
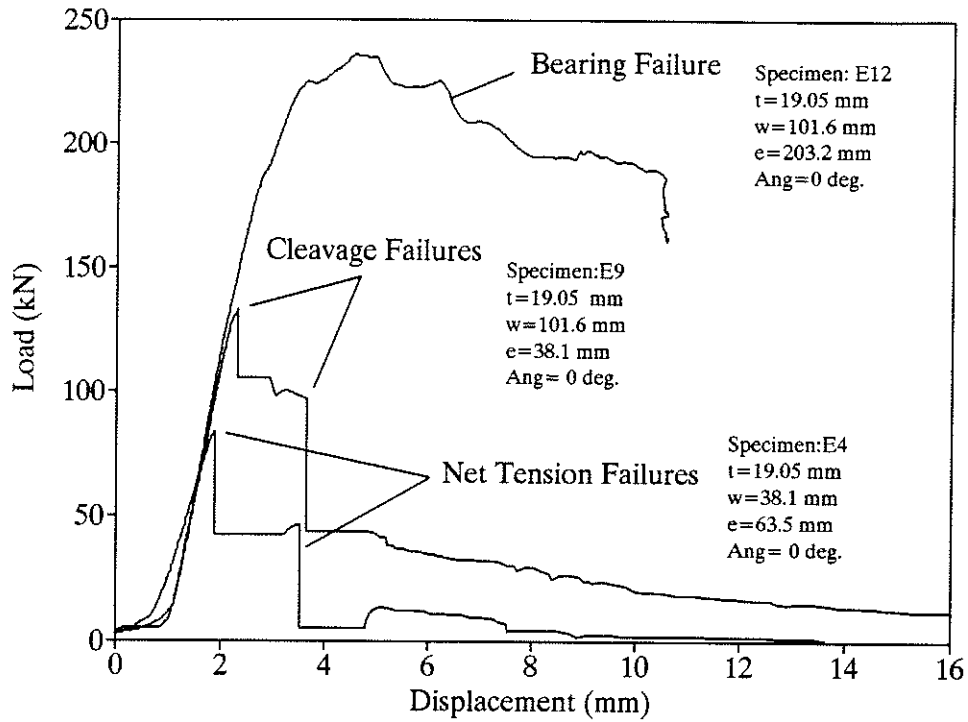
Figure 4.3 Typical Load-Displacement Curves
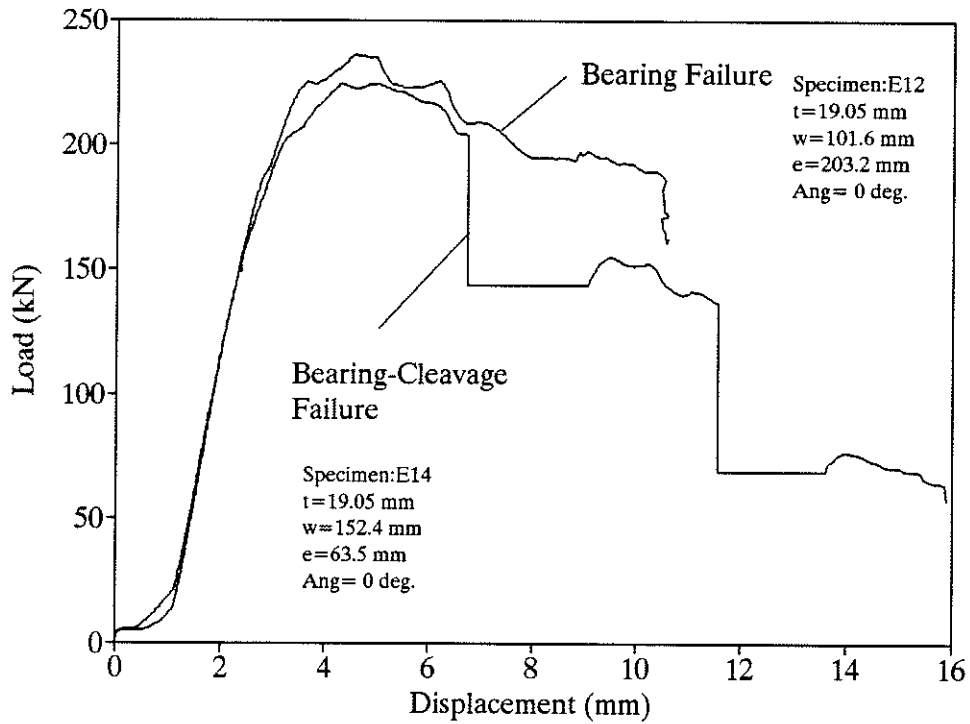
Figure 4.4 Load-Displacement Curve for Bearing-Cleavage Failure
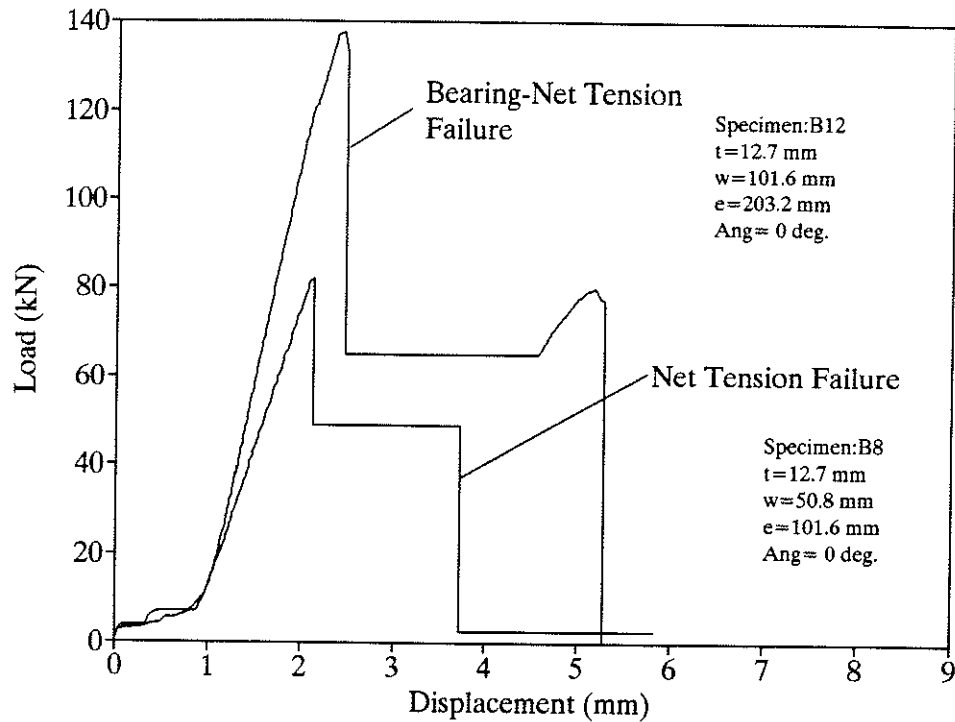
Figure 4.5 Load-Displacement Curve for Bearing-Net Tension Failure
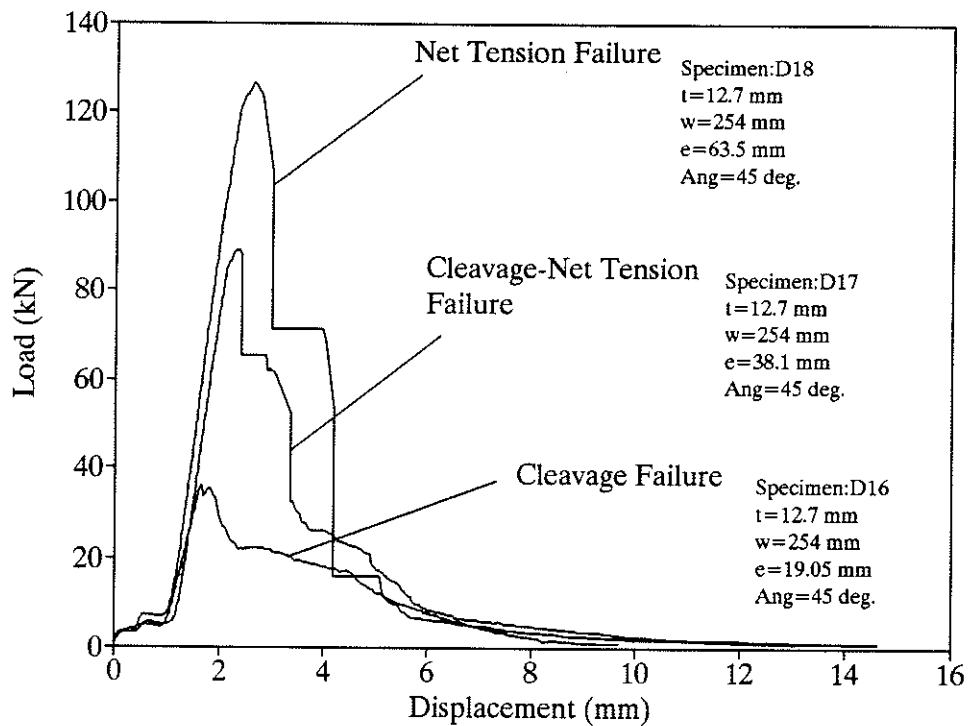
Figure 4.6 Load-Displacement Curve for Cleavage-Net Tension Failure
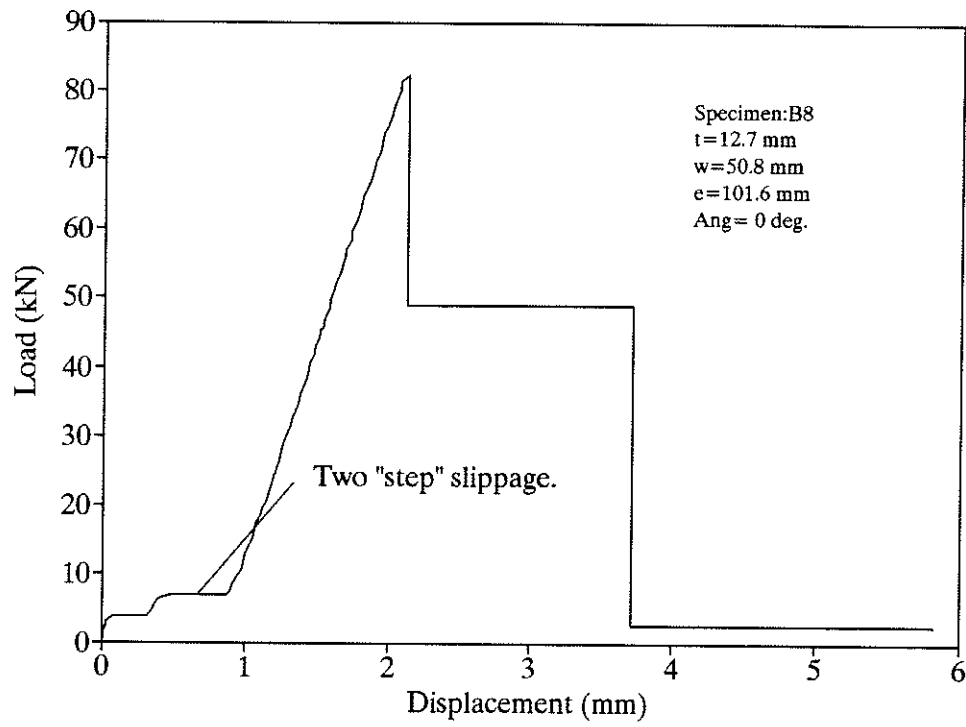
Figure 4.7 Two "Step" Slippage
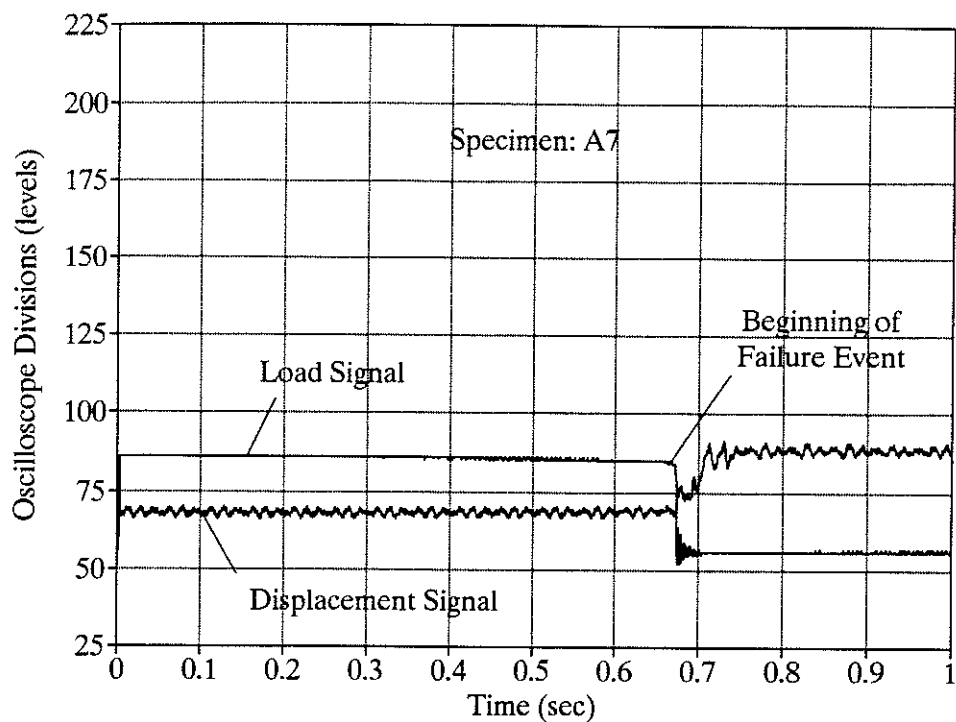
Figure 4.8 Oscilloscope Data
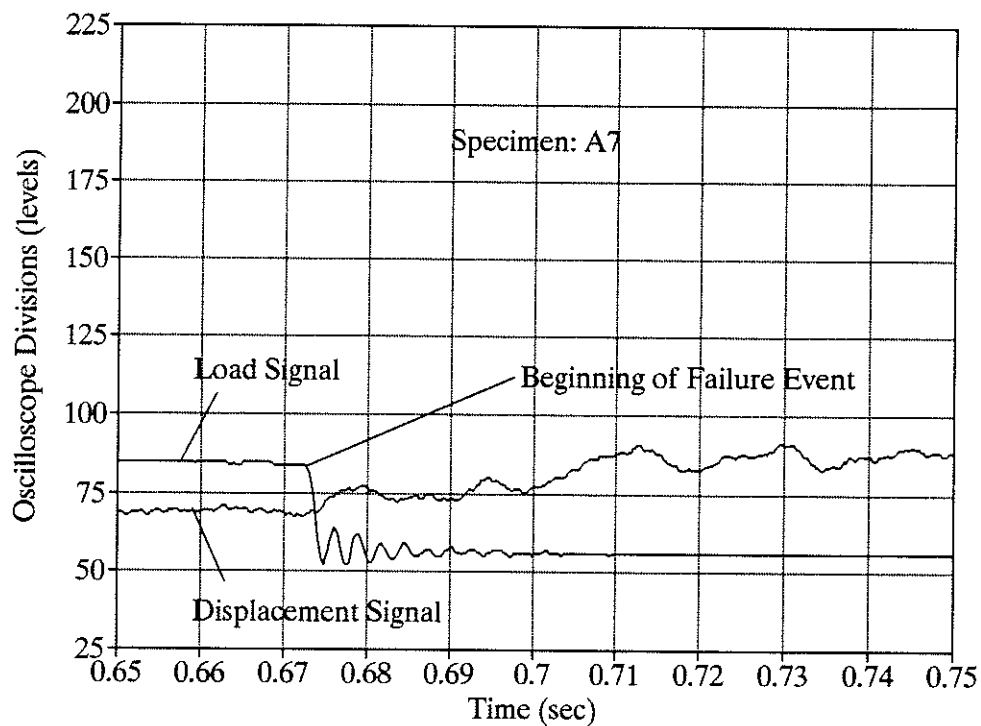
Figure 4.9 Oscilloscope Data (Expanded Time Scale)
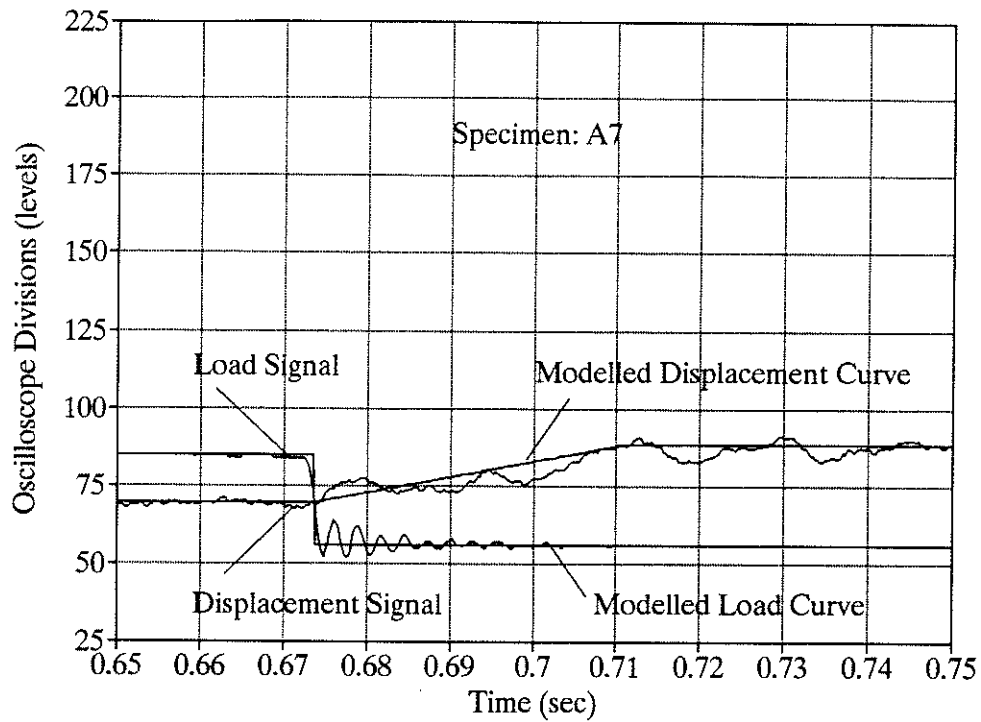
Figure 4.10 Modelled Load & Displacement Curves
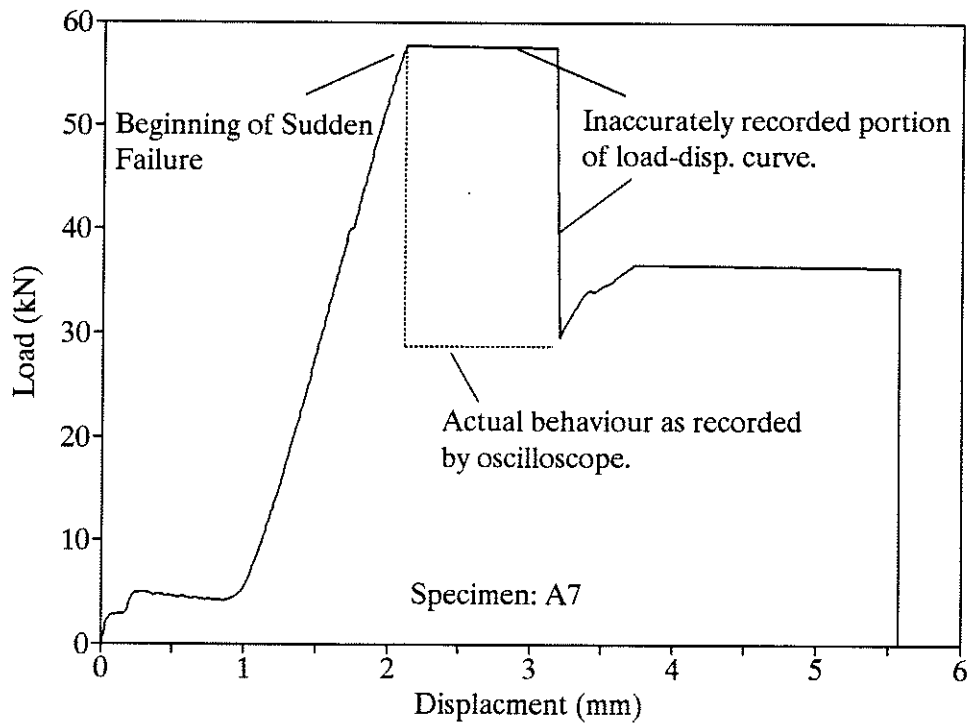
Figure 4.11 Corrected Load-Displacement Curve
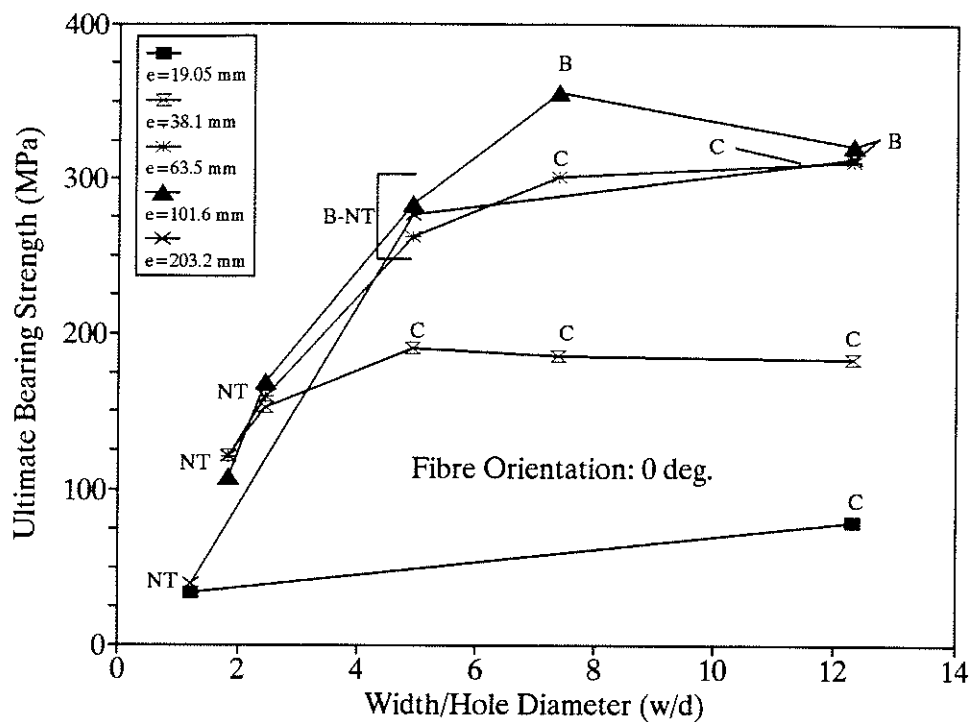
Figure 4.12 Bearing Strength vs (w/d) Ratio for Test Series A
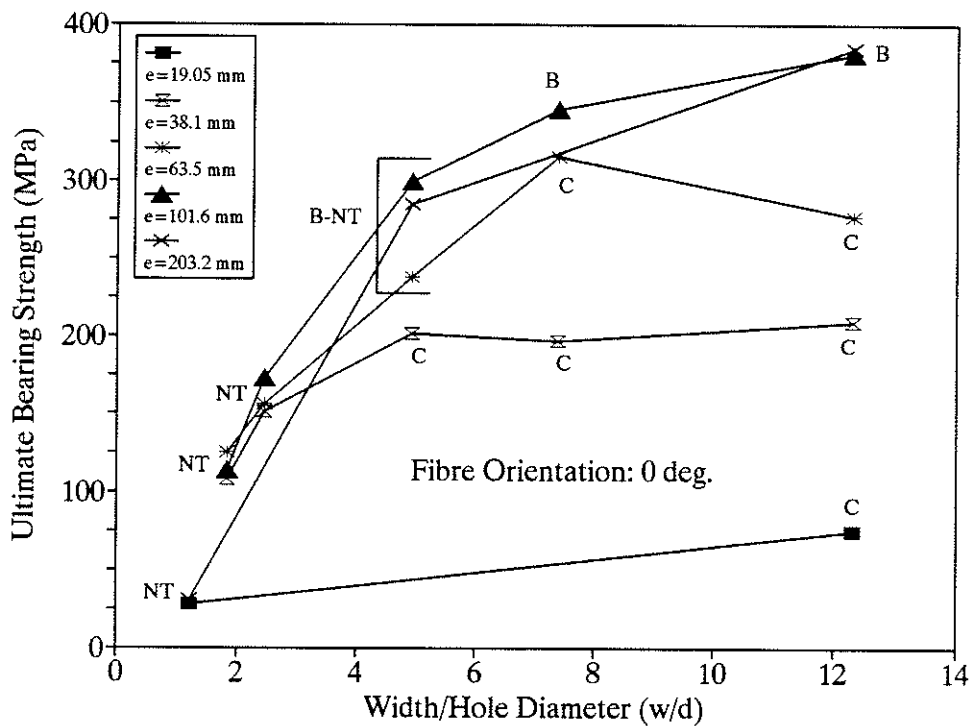
Figure 4.13 Bearing Strength vs (w/d) Ratio for Test Series B
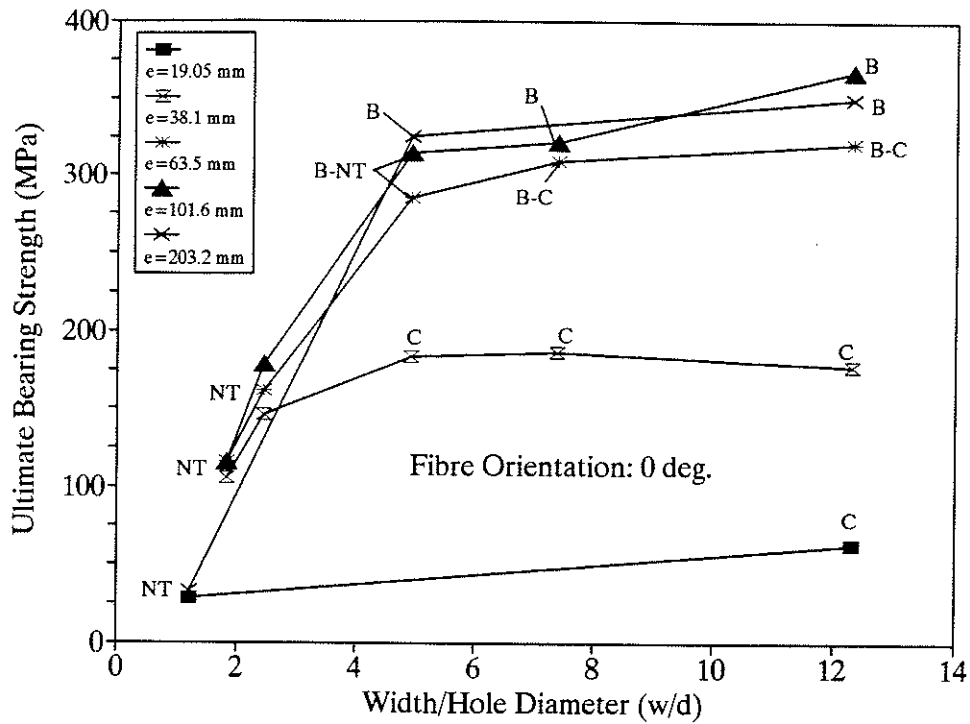
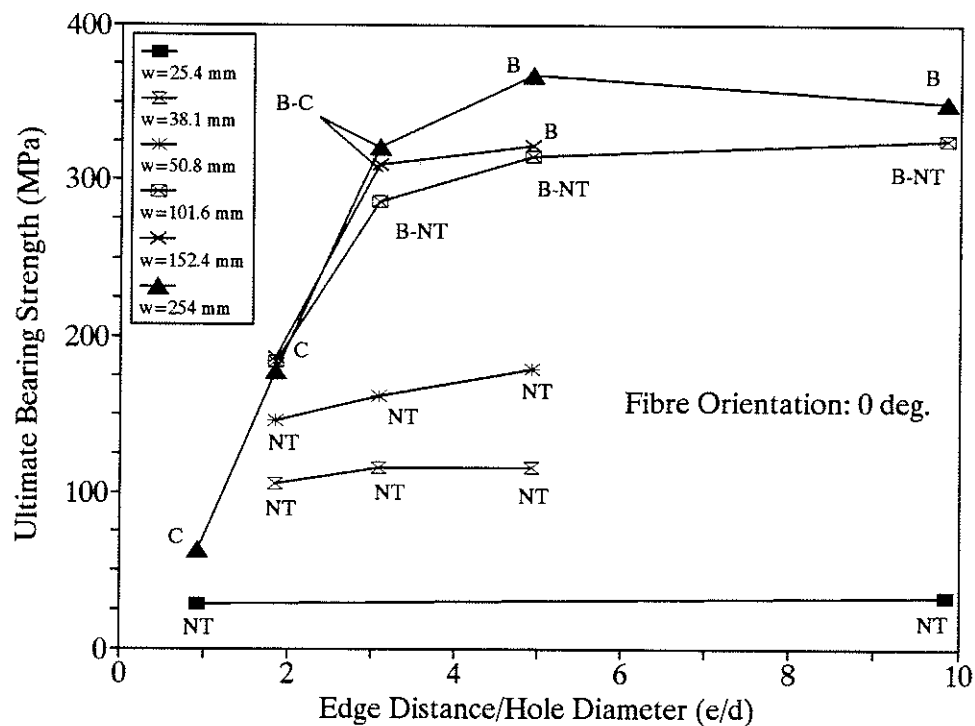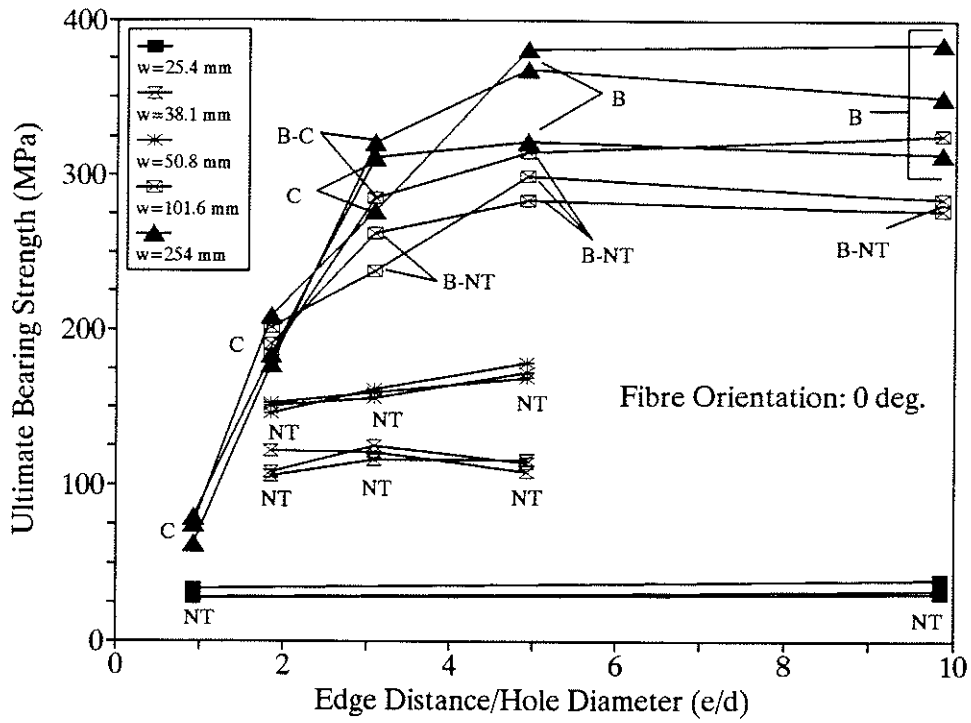Figure 4.14 Bearing Strength vs (w/d) Ratio for Test Series E
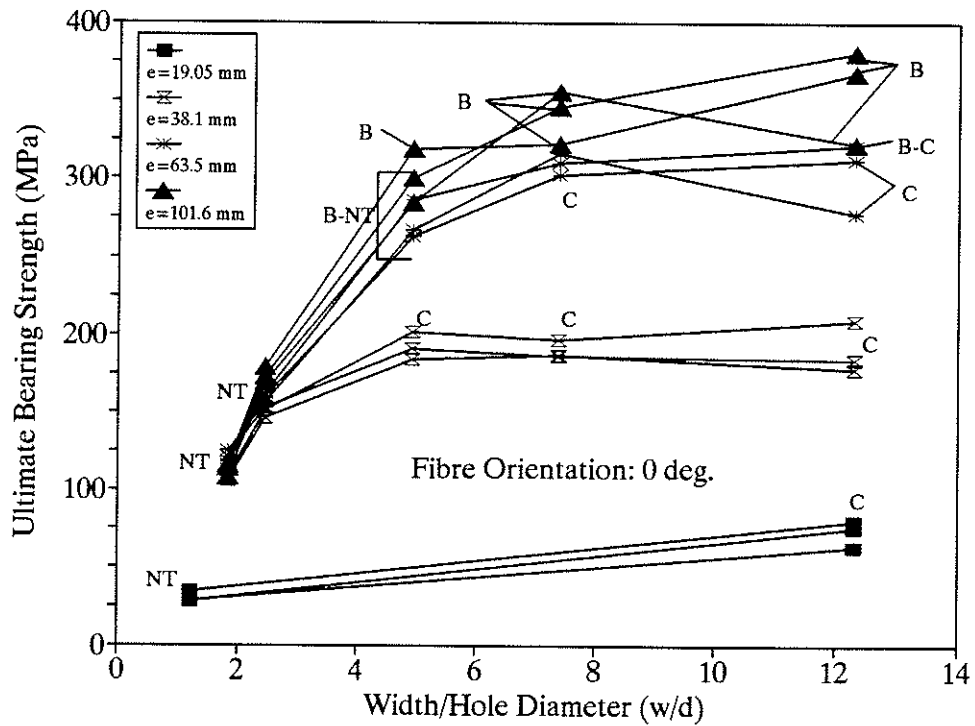
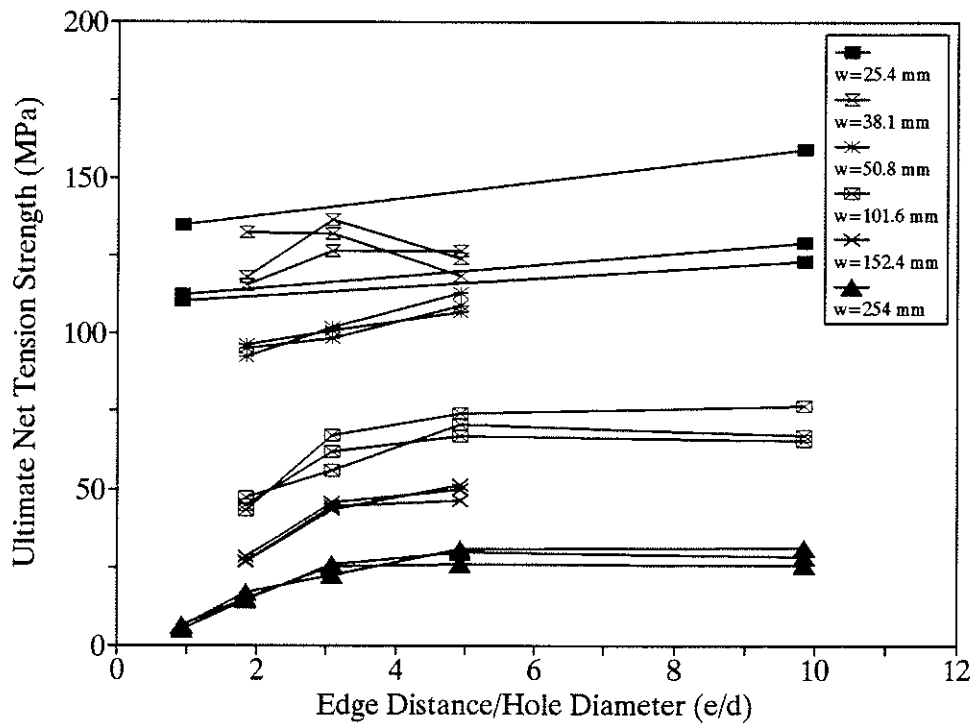Figure 4.15 Bearing Strength vs (w/d) Ratio for Test Series A, B, and E
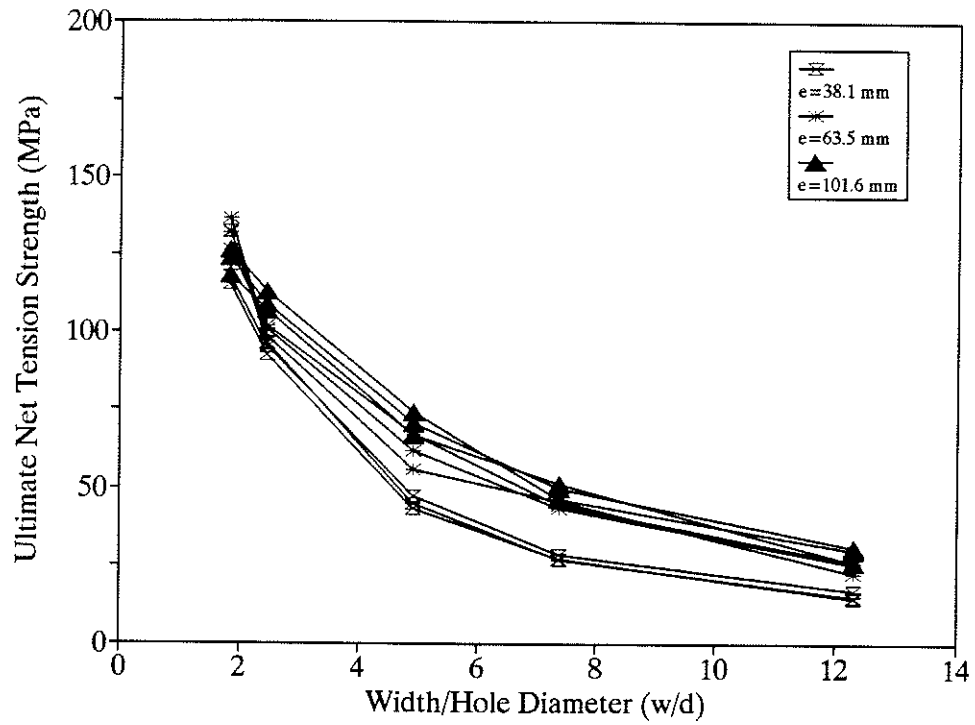
Figure 4.16 Net Tension Strength vs (w/d) Ratio for Test Series A, B and E
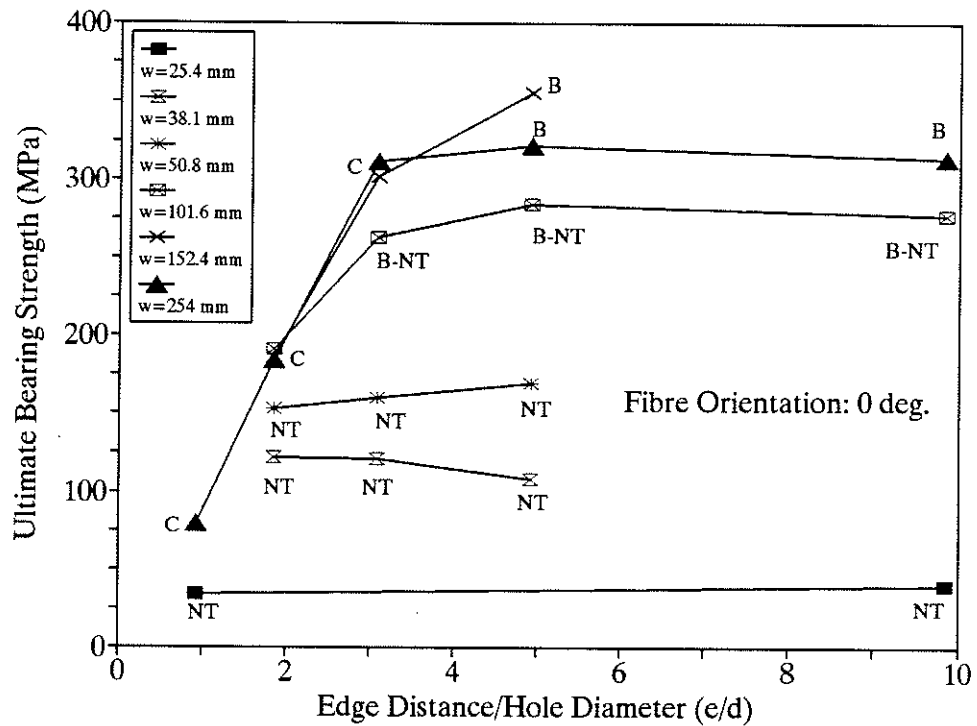
Figure 4.17 Bearing Strength vs (e/d) Ratio for Test Series A
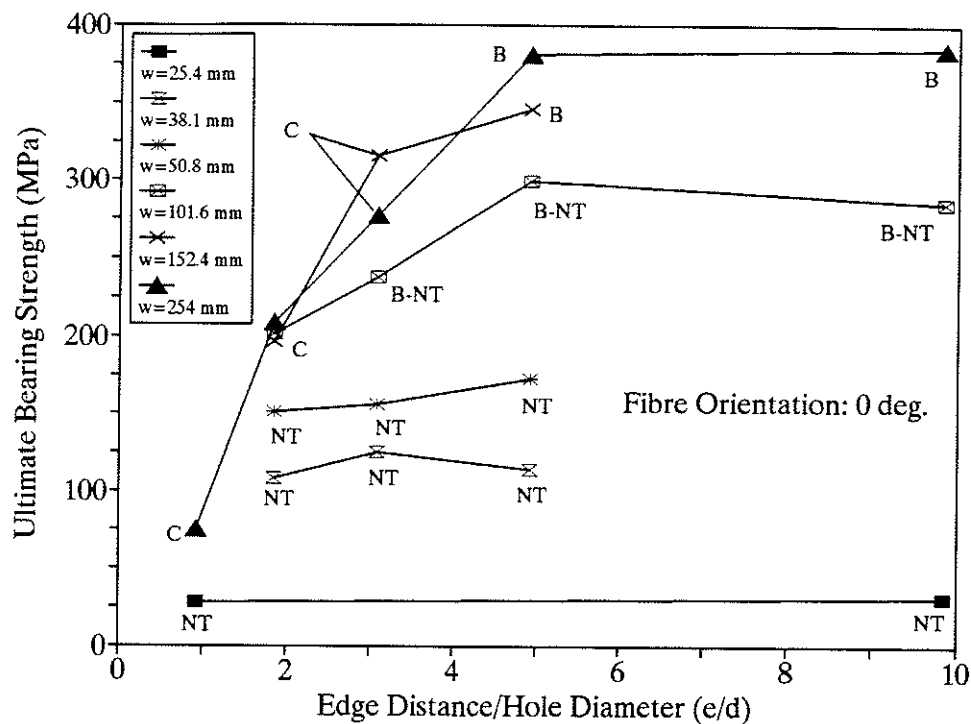
Figure 4.18 Bearing Strength vs (e/d) Ratio for Test Series B

Figure 4.19 Bearing Strength vs (e/d) Ratio for Test Series E

Figure 4.20 Bearing Strength vs (e/d) Ratio for Test Series A, B, and E

Figure 4.21 Net Tension Strength vs (e/d) Ratio for Test Series A, B, and E

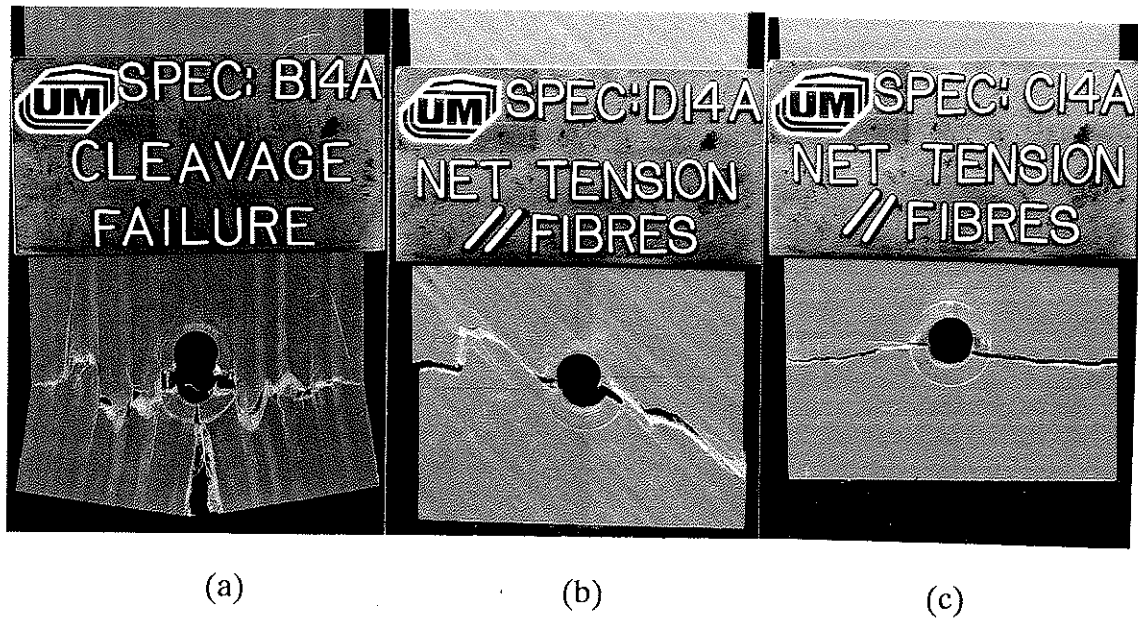(a)   (b)   (c)

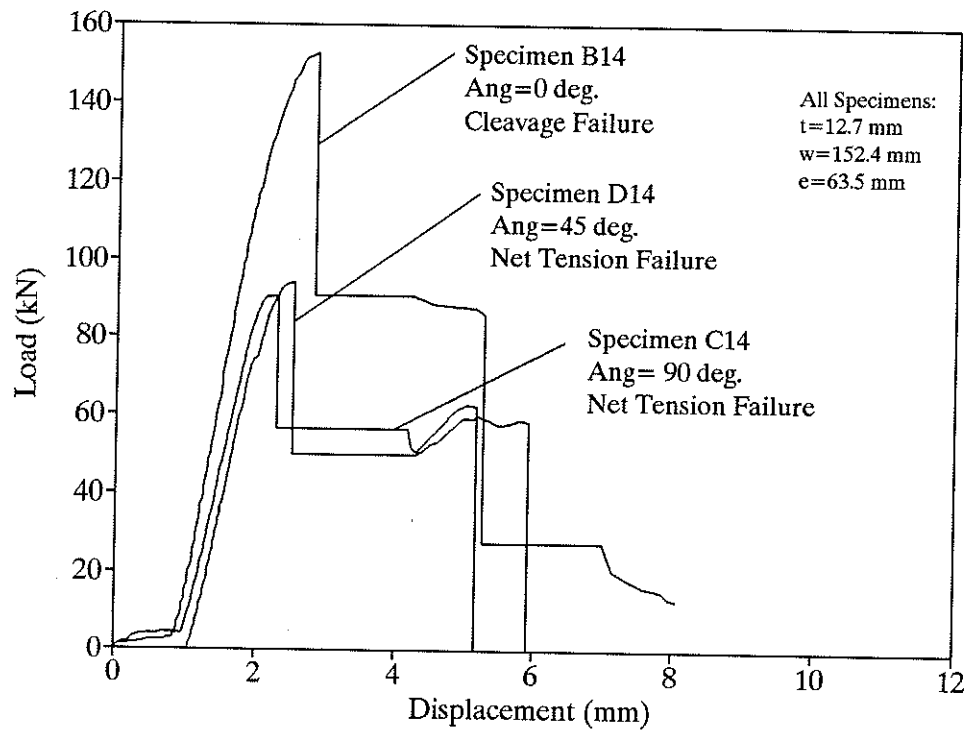Figure 4.22 Effect of Fibre Orientation on Failure Mode

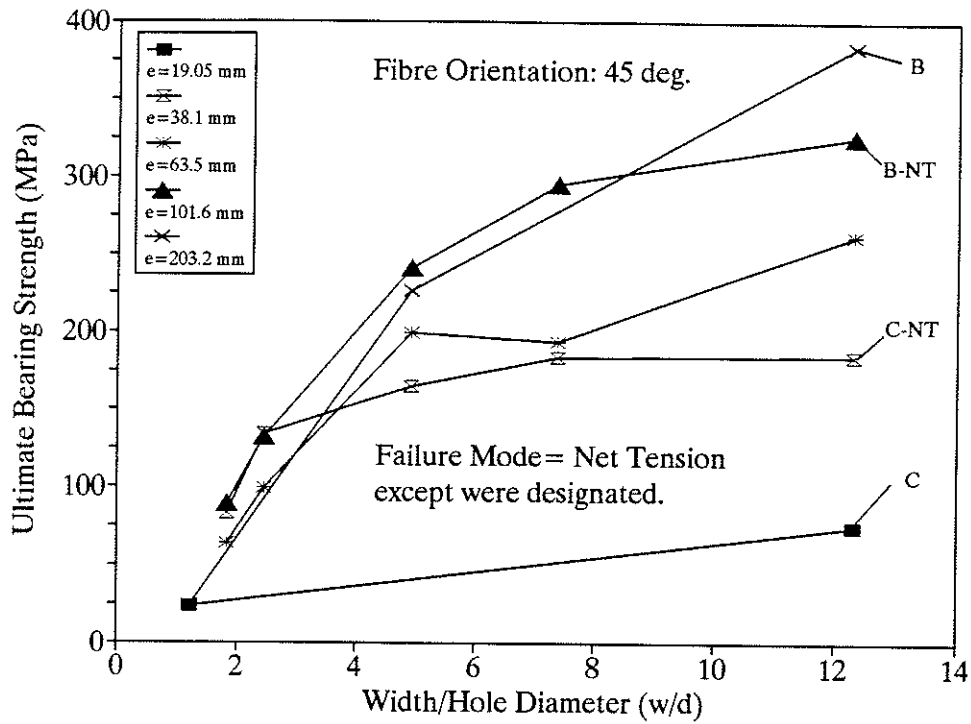Figure 4.23 Effect of Fibre Angle on Load-Displacement Behaviour

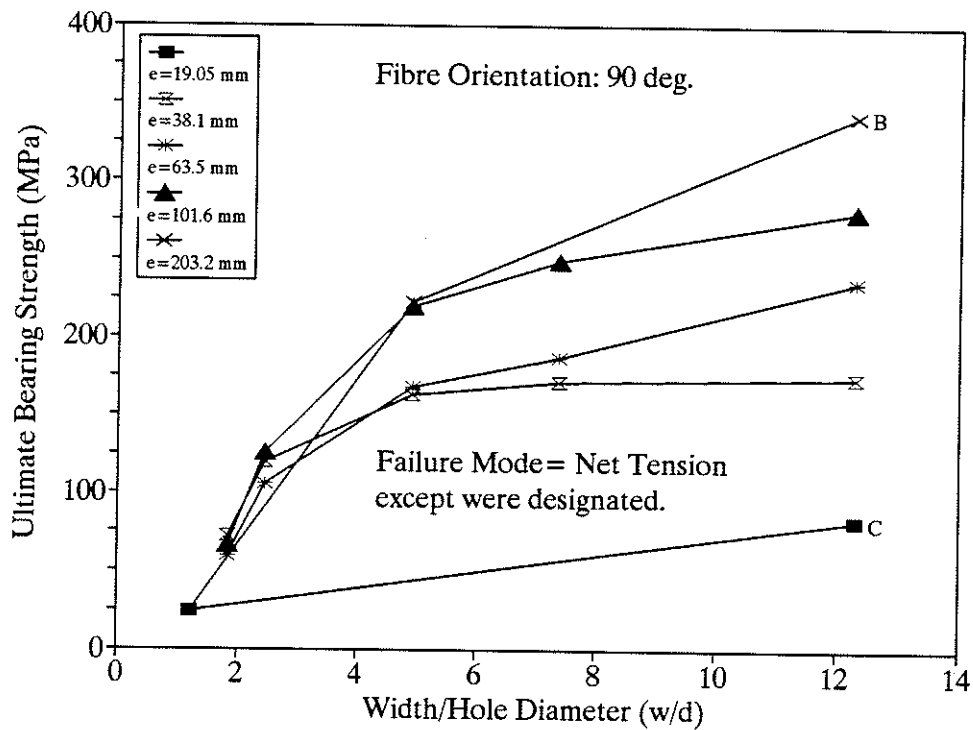Figure 4.24 Bearing Strength vs (w/d) Ratio for Test Series D

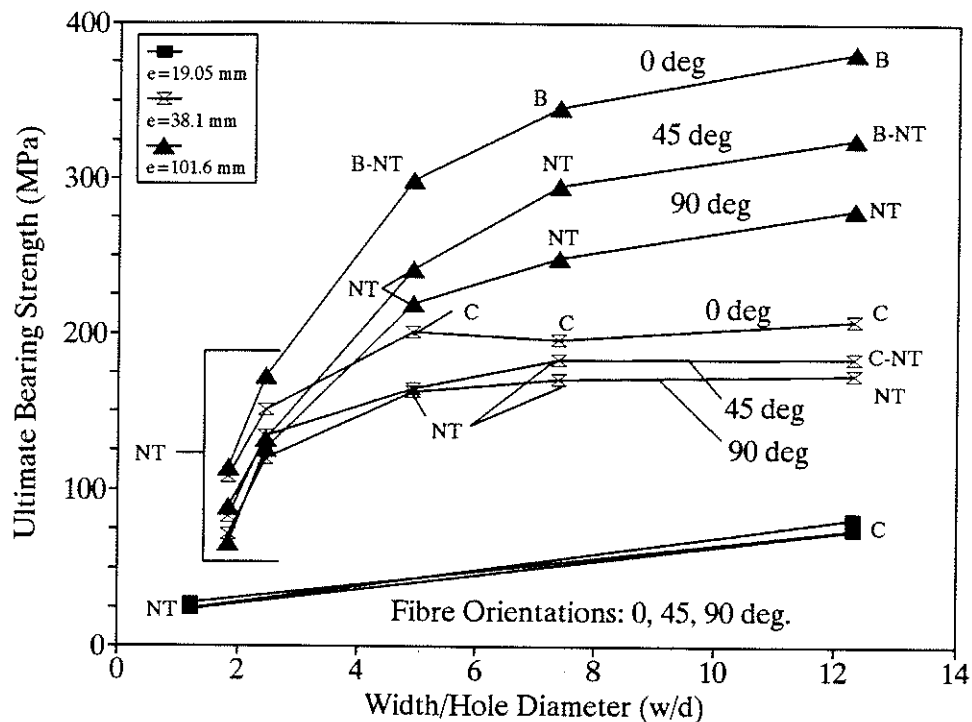Figure 4.25 Bearing Strength vs (w/d) Ratio for Test Series C

Figure 4.26 Bearing Strength vs (w/d) Ratio for Test Series B, C, and D
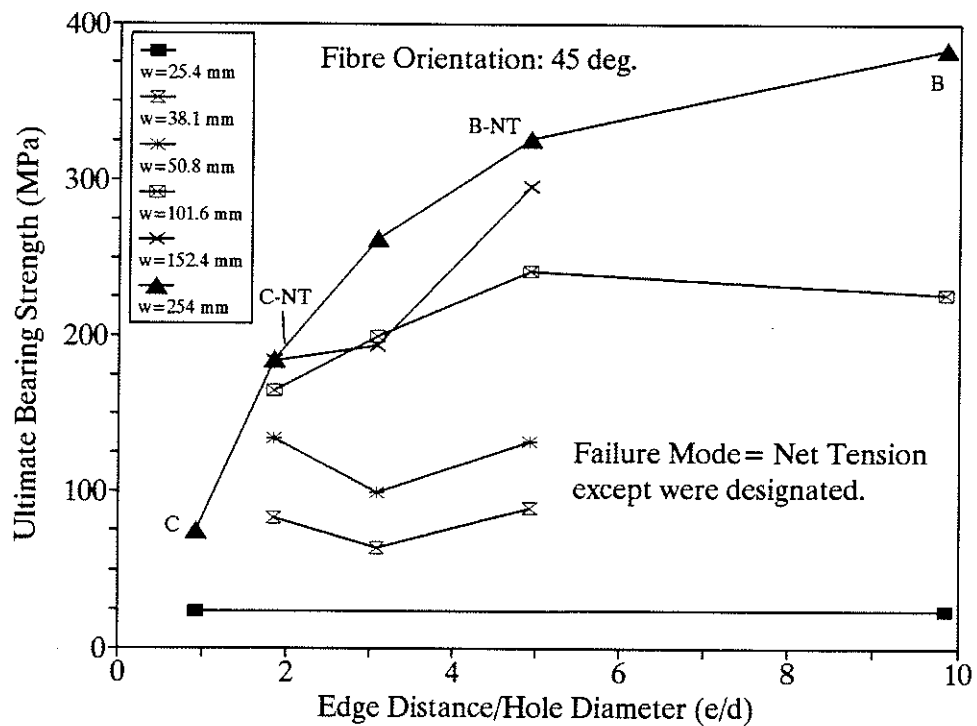

Figure 4.27 Bearing Strength vs (e/d) Ratio for Test Series D
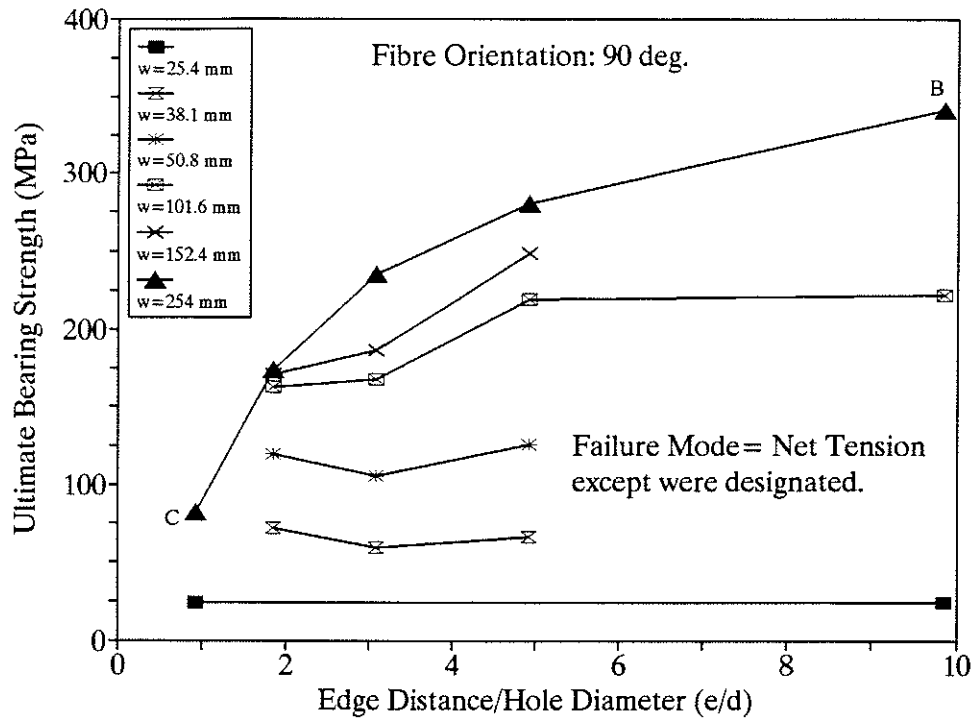
Figure 4.28 Bearing Strength vs (e/d) Ratio for Test Series C
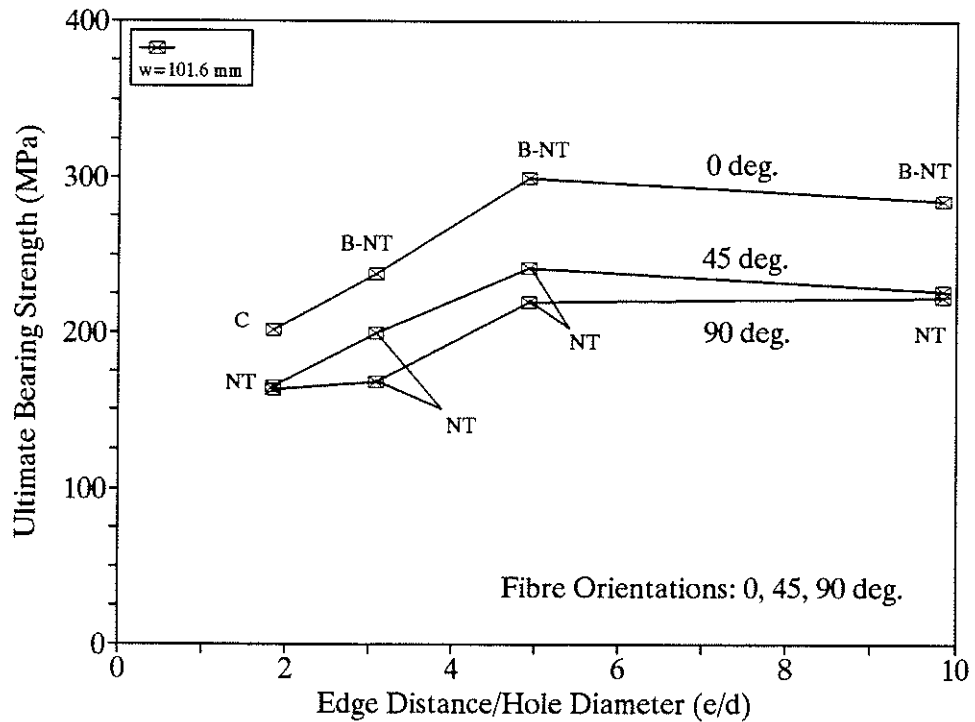
Figure 4.29 Bearing Strength vs (e/d) Ratio for Test Series B, C, and D
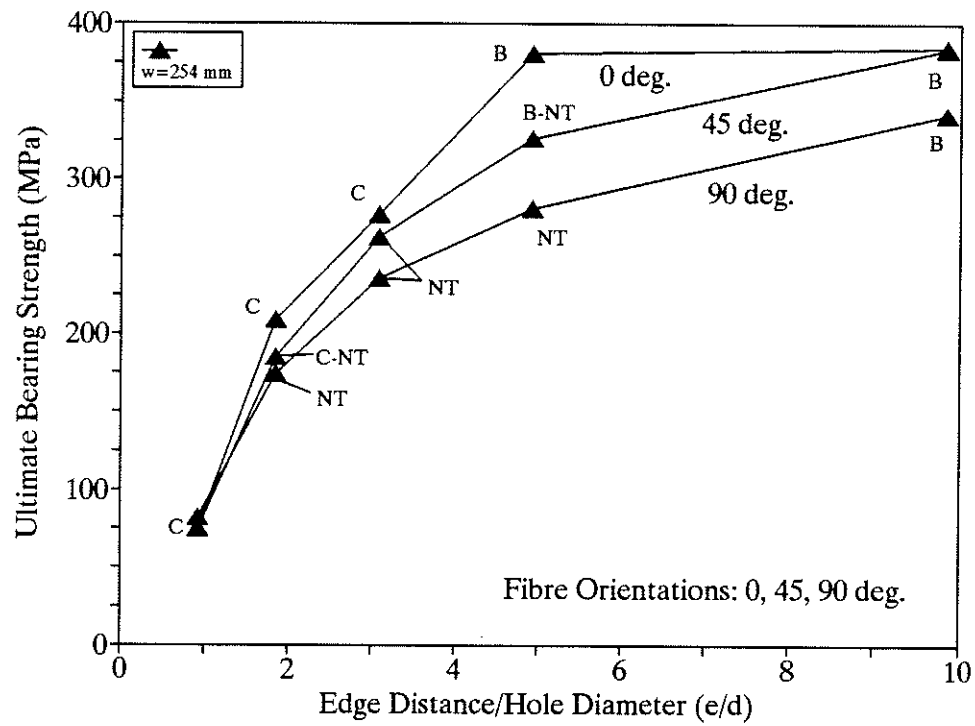for (w=101.6 mm)

Figure 4.30 Bearing Strength vs (e/d) Ratio for Test Series B, C, and D
for (w=254 mm)
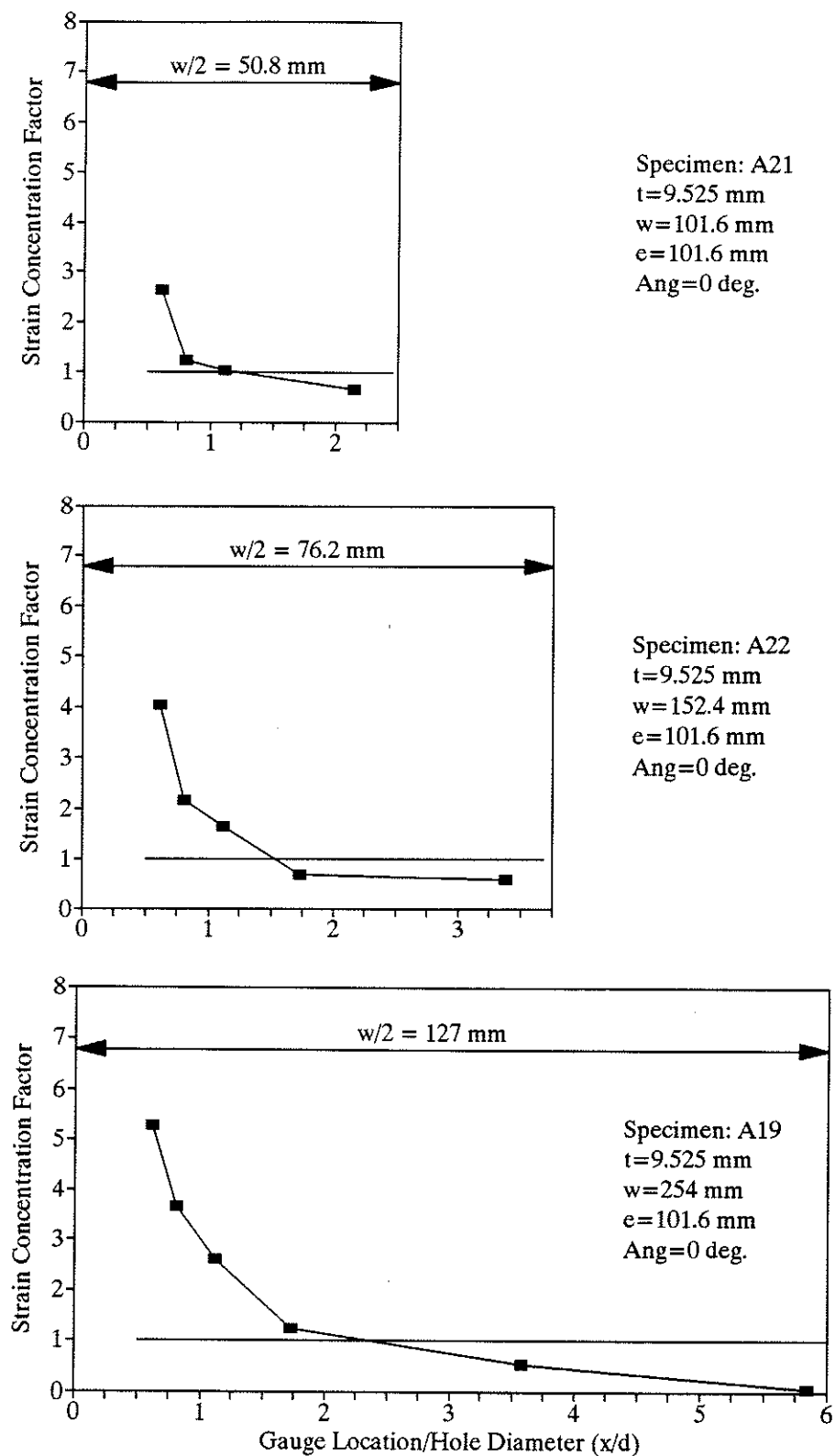
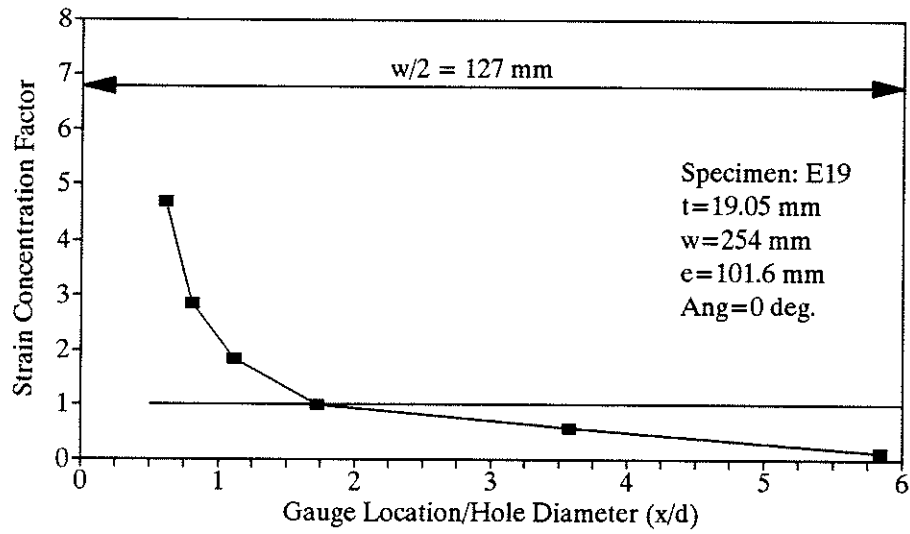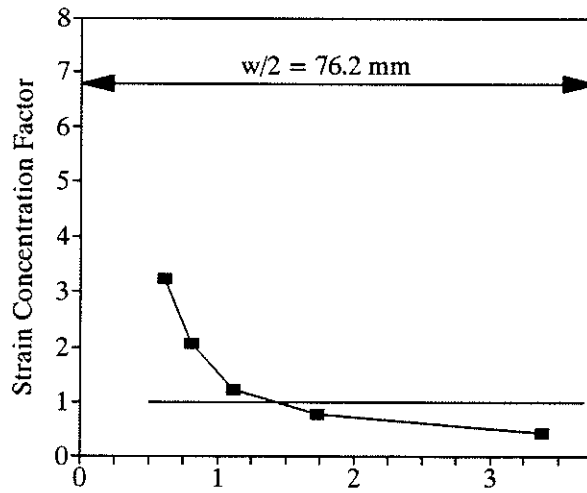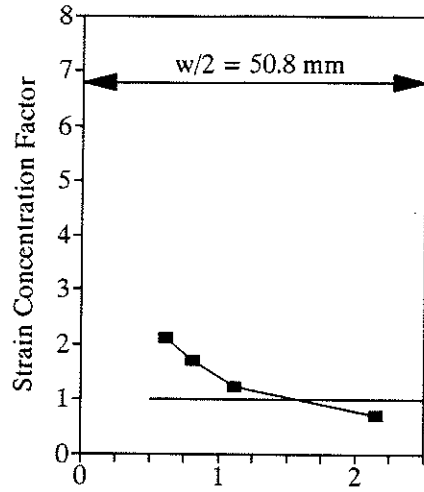Figure 4.31 Effect of Width on SCF for Material Thickness t=9.525 mm

Figure 4.32 Effect of Width on SCF for Material Thickness t=19.05 mm
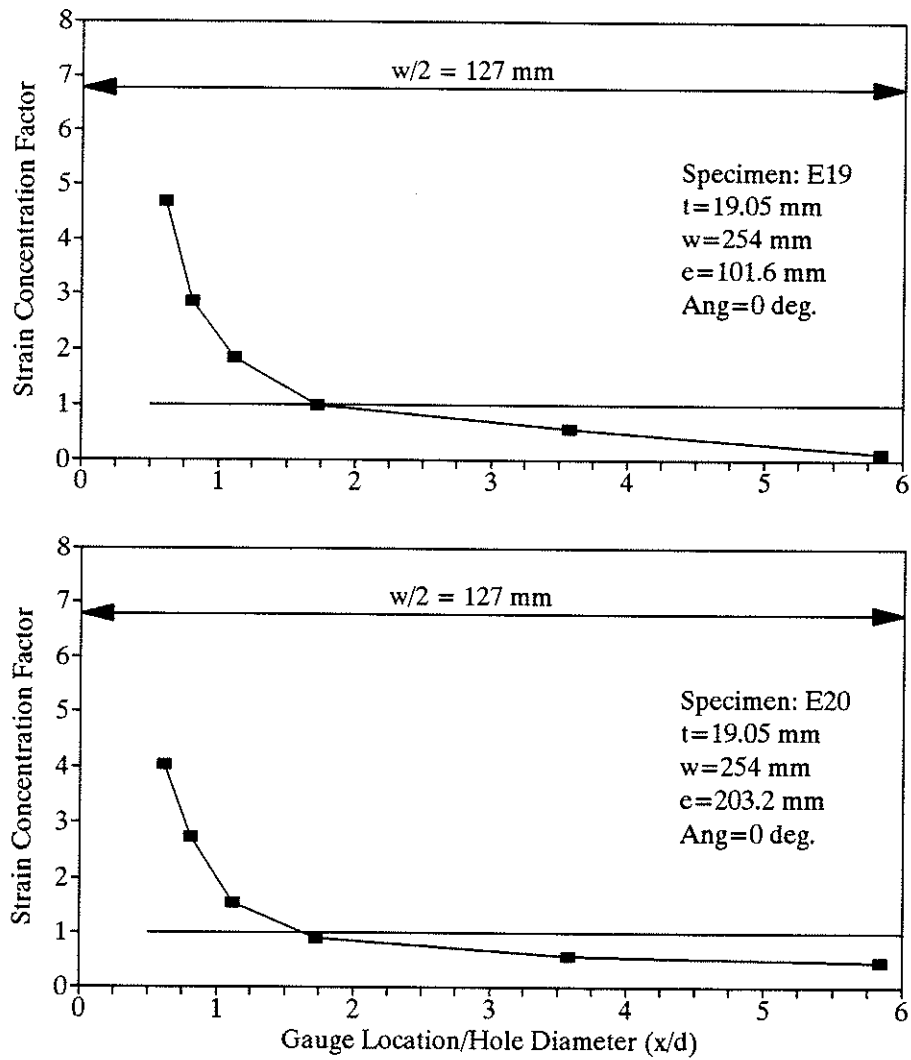
Figure 4.33 Effect of Edge Distance on SCF
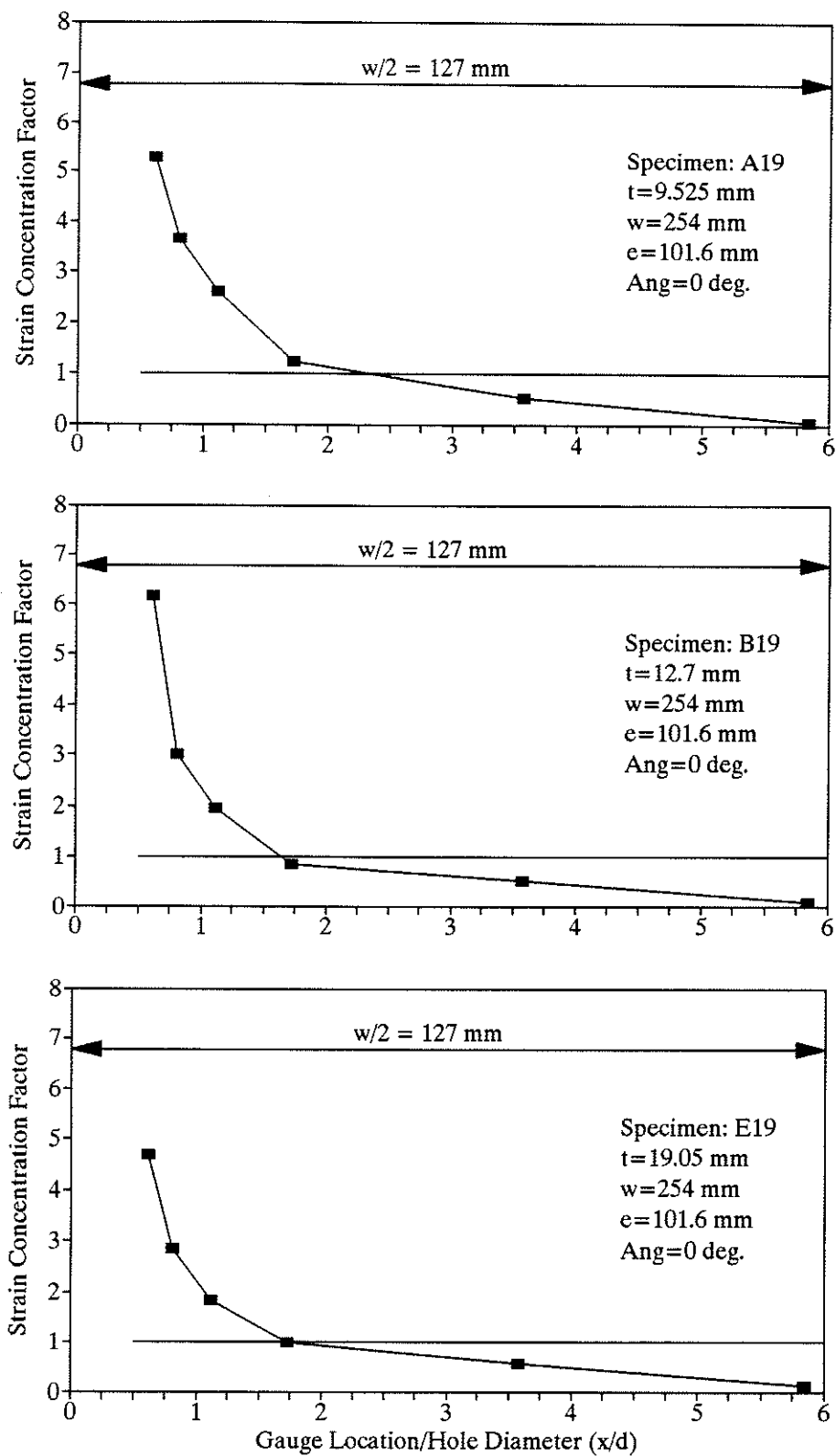
Figure 4.34 Effect of Thickness on SCF
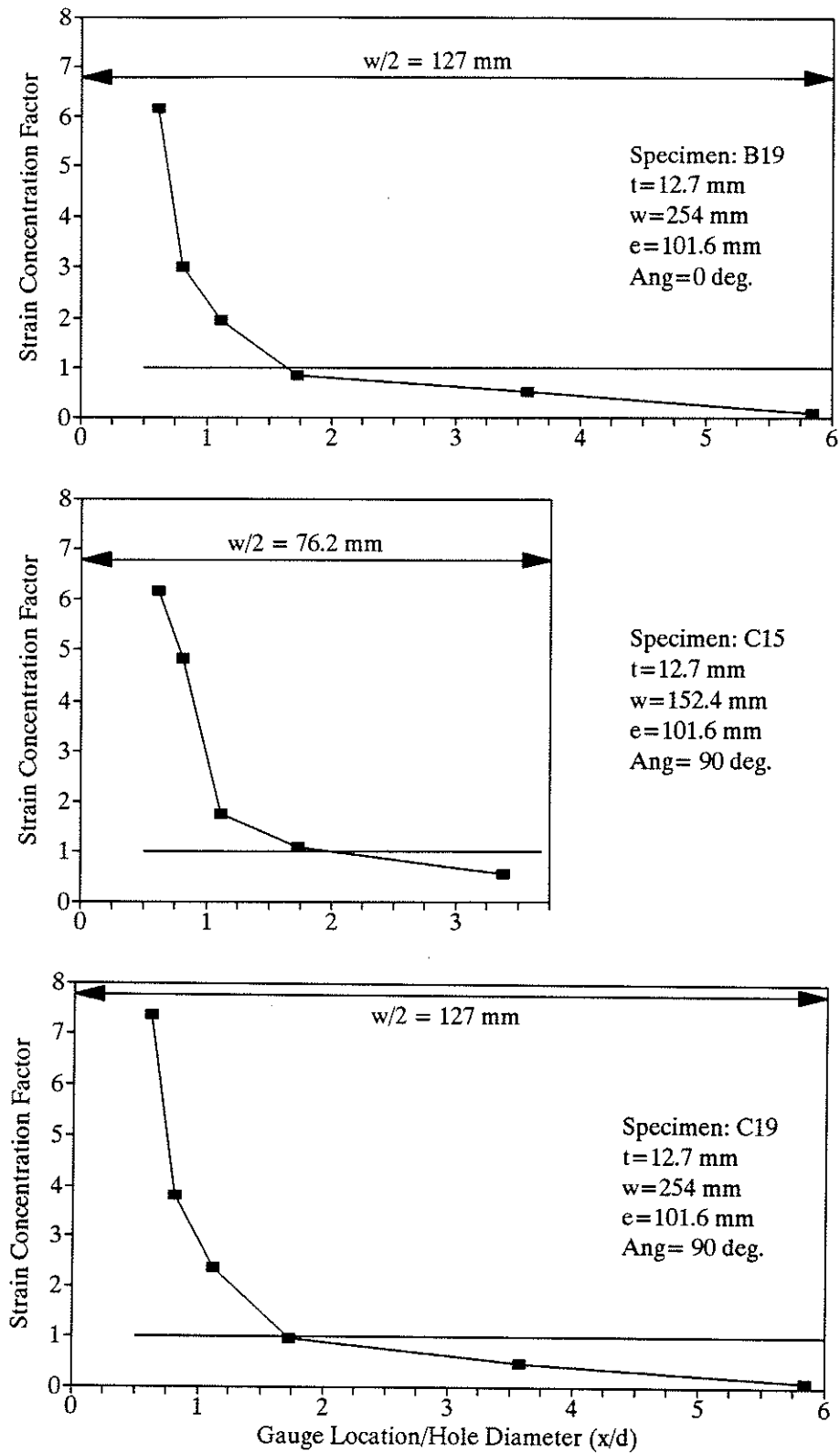
Figure 4.35 Effect of Fibre Orientation on SCF

CHAPTER 5 DESIGN PROCEDURE

5.1 INTRODUCTION

This chapter discusses an analytical model proposed to describe the behaviour of double-shear single-bolted connections in a fibre-reinforced composite material in terms of the ultimate load capacity and the mode of failure. The model is semi-empirical, consisting of two basic failure criteria to determine the ultimate capacity and failure mode of a connection.

The first criterion used in the model describes the net tension failure mode of the connection. Prediction of the ultimate tensile strength is based on a modified version of the theory presented by Hart-Smith (39). The theory accounts for the elastic stress concentrations at a loaded hole in an elastic, isotropic material. For fibre-reinforced composite material, Hart-Smith introduced a correlation coefficient which can be derived from experimental tests. This correlation coefficient relates the elastic stress concentration factor which occurs in elastic materials to that which occurs in fibre-reinforced composite materials for a connection of the same geometry. The correlation coefficient accounts for the composite's orthotropy, pseudo-yielding capability, heterogeneity, and other factors which influence the behaviour of a bolted connection. Since the theory is based on elastic isotropic materials, it can be applied to many material systems and fibre patterns using only limited test data for the specific composite material. Once the correlation

112

coefficient for a specific system is established, the ultimate net tension load can be predicted for any geometry.

The second criterion used in the model describes the bearing failure mode of a bolted connection. Prediction of the ultimate bearing capacity of a connection is based on the bearing strength of the material which can be determined from experimental results. In the proposed model, cleavage failure is treated as a special type of bearing failure with an inadequate edge distance. Since the shearout mode of failure was not obtained in the experimental part of this investigation, it will not be extensively discussed and will be considered in future research work.

5.2 EFFICIENCY OF THE CONNECTION

The structural efficiency of a bolted connection can be defined as:

$$Efficiency = \frac{P_{ult}}{t \cdot w \cdot F_{tu}}$$

(5.1)

where P_{ult} is the ultimate load of the connection and t and w are the thickness and width respectively. F_{tu} is the unnotched tensile strength of the material. Due to the presence of the hole, the ultimate strength of a member in a bolted connection will obviously be less than that of a similar member without a hole, and therefore the range of the efficiency will always be between 0 and 1.

5.3 NET TENSION FAILURE

The maximum stress, σ_{max}, adjacent to a bolt hole along a net section of a member subjected to an applied load, P, perpendicular to the net section, can be determined as follows:

$$\sigma_{max} = k_{te} \frac{P}{t(w-d)} \tag{5.2}$$

where t, w, and d are the thickness, width and hole diameter of the connection respectively, as shown in Fig. 5.1. The elastic stress concentration factor, k_{te}, corresponds to the maximum stress adjacent to the hole.

The elastic stress concentration factor, k_{te}, for an isotropic, perfectly elastic material, can be determined using an expression proposed by Hart-Smith (39) as follows:

$$k_{te} = 2+(w/d-1)-1.5\frac{(w/d-1)}{(w/d+1)} \theta \tag{5.3}$$

where θ is a non-dimensional factor and is a function of the edge distance to width ratio (e/w) as given by:

$$\begin{array}{ll} \theta = 1.5 - \dfrac{0.5}{e/w} & \textit{for } e/w \le 1 \\ \theta = 1 & \textit{for } e/w \ge 1 \end{array} \tag{5.4}$$

Equations (5.3) and (5.4) were developed based on experimental data and theoretical deductions from several sources as described in detail by Hart-Smith (39). Equations (5.3) and (5.4) were derived so as to produce a monotonic function in terms of the ratios (d/w) and (e/w).

Based on the limited number of specimens tested in this program, the test results suggest that the limiting value of $\theta = 1$ when $(e/w) \geq 1$ in Eq.(5.4) may not be valid for the material used in this investigation. This is evident from the fact that the ultimate average net stress of the connections tend to increase with an increasing (e/w) ratio even past the value of $(e/w) = 1$ as shown in Fig. 5.2. Therefore Eq.(5.4) originally proposed by Hart-Smith is modified for the proposed model in this investigation to:

$$\theta = 1.5 - \frac{0.5}{e/w} \qquad for \ 0 \leq e/w \qquad (5.5)$$

For a perfectly elastic material, when the maximum induced stress σ_{max} reaches the tensile strength of the material F_{tu}, net tension failure occurs as the crack catastrophically propagates through the net section. The failure mode in this case is brittle and sudden. Therefore by rearranging Eq.(5.2) and replacing the maximum stress σ_{max} by the ultimate tensile strength of the elastic material F_{tu}, the ultimate load of the connection can be determined as follows:

$$P = \frac{F_{tu}}{k_{te}} \, t \cdot (w - d) \qquad (5.6)$$

From Eq.(5.1) and (5.6), the efficiency of the connection can be shown to be:

$$Efficiency = \frac{1}{k_{te}} \, (1 - d/w) \qquad (5.7)$$

For a perfectly plastic material where the material can yield extensively before failure, the stress concentration factor k_{te} could eventually reach unity and Eq.(5.7) will be reduced to:

$$Efficiency \; = \; (1-d/w) \qquad\qquad (5.8)$$

Equations (5.7) and (5.8) are plotted versus the ratio (d/w) in Fig. 5.3 for a constant value of (e/w)=1. It should be noted that values of (d/w) outside the interval 0 to 1 are not possible.

In Fig. 5.3 as (d/w) approaches 1, the member width approaches the size of the hole diameter, and therefore, the efficiency of the connections will certainly approach zero for both elastic and plastic materials. By increasing the member width with respect to the hole diameter, that is, by decreasing the (d/w) ratio, the efficiencies increase for both types of material. For a perfectly plastic material, which can yield extensively before failure, the stresses will be uniform at the net section as shown in Fig. 5.4(a). The stress concentration factor k_{te} is unity and therefore the efficiency will approach one as the (d/w) ratio approaches zero as shown in Fig. 5.3. For a perfectly elastic material, the stress concentration factor at the bolt hole k_{te}, as described by Eq.(5.7), will approach infinity as shown in Fig. 5.4(b). Therefore for a perfectly elastic material the efficiency will approach zero as the (d/w) ratio approaches zero. The maximum efficiency that could be achieved for a connection of a perfectly elastic material is 0.21 at (d/w)=0.4 as reported by Hart-Smith (39).

Fibre-reinforced composites do not have the yielding capability of a ductile

metal, and therefore do not behave like a perfectly plastic material. However, since composite materials still exhibit some stress concentration relief in the form of matrix cracking, fibre-matrix debonding, fibre breakage and fibre pull-out, they do not behave like a perfectly elastic material either. Therefore, the behaviour of bolted connections in fibre-reinforced composite materials is neither fully plastic nor fully elastic but somewhere in between as shown in Fig 5.3.

Since bolted connections in fibre-reinforced composites exhibit some stress redistribution before ultimate failure, the stress concentration factor k_{te}, for isotropic perfectly elastic materials, is too high for fibre-reinforced composites, and therefore it predicts an efficiency that is too low. To correlate the two materials, it has been reasonably shown that the stress concentration factor in isotropic elastic materials k_{te}, and those in fibre-reinforced composites k_{tc} are linearly related and can be expressed in terms of a correlation coefficient, C, by the following equation given by Hart-Smith (39):

$$(k_{tc}-1) = C(k_{te}-1) \qquad (5.9)$$

where:

$$k_{tc} = F_{tu} \frac{t(w-d)}{P_{ult}} \qquad (5.10)$$

F_{tu} is the ultimate tensile strength of the composite material in the loaded direction, and P_{ult} is the ultimate load of a composite connection. The term k_{tc} is the average stress concentration factor observed at failure of a bolted connection using composite material members and k_{te} is the corresponding elastic stress concentration

factor of a connection with the same geometry using a perfectly elastic isotropic material. Computing k_{te} for perfectly elastic isotropic materials, and k_{tc} from Eq.(5.10) based on measured experimental values, the correlation coefficient C can be determined for any fibre-reinforced composite material using a limited number of experimental observations. The correlation coefficient, C, accounts for the composite's orthotropy, pseudo-yielding capability, heterogeneity, clearance effects, and other factors which affect the behaviour of bolted connections. It should be noted that the linear relationship in Eq.(5.9) is valid only for the net tension mode of failure and therefore only experimental results for connections that failed in net tension should be used to determine the correlation coefficient.

In this investigation three different fibre orientations were used. The connections were tested with the applied load at 0°, 45°, and 90° to the unidirectional fibre layers. The measured results were used to determine the correlation coefficient for the 0°, 45°, and 90° fibre orientations, based on a least squares regression analysis as shown in Fig. 5.5, Fig. 5.6, and Fig. 5.7 respectively. For this analysis, values of the composite stress concentration factor k_{tc} were based on Eq.(5.10) and the values of k_{te} were based on Eq.(5.3) for the same connection geometry. In these figures the correlation coefficient C represents the slope of the best-fit-straight line. Due to the nature of Eq.(5.9) the best-fit-curve is constrained by the point (1,1). The correlation coefficients for the fibre orientations of 0°, 45°, and 90° to the applied load were found to be 0.33, 0.21 and 0.25 respectively for EXTREN Flat Sheet/ Series 500. The standard errors of the correlation coefficients

as determined from the regression analysis were 0.0153, 0.096, and 0.0307 respectively. The correlation coefficient for the 45° fibre orientation connections is the lower than the 90° case, since the lowest tensile modulus occurs approximately at 45° to the unidirectional fibres as discussed in Chapter 3.

Using the stress concentration factor k_{tc} and Eq.(5.7), the efficiency of a single-bolted connection in a fibre-reinforced composite can be expressed as:

$$Efficiency = \frac{1}{k_{tc}} \ (1-d/w) \tag{5.11}$$

Equation (5.11) can be expressed in terms of C and k_{te} as:

$$Efficiency = \frac{1}{C(k_{te}-1)+1} \ (1-d/w) \tag{5.12}$$

Consequently, the ultimate load of a single-bolted connection in a composite material can be determined using Eq.(5.1) as follows:

$$P_{ult} = Efficiency \cdot (t \cdot w \cdot F_{tu}) \tag{5.13}$$

Therefore, for a given correlation coefficient C and the tensile strength of a composite material, the design engineer can predict the ultimate "net tension failure" load of a single-bolt connection, of any geometry using Eq.(5.13).

Equation (5.12) was used to produce a family of failure envelopes in terms of the connection's efficiency and the ratio (d/w) as shown in Fig. 5.8 to Fig. 5.10 for the three fibre orientations used in this investigation. Each envelope in Fig. 5.8 to 5.10 is given for a constant (e/d) ratio. As can be seen, the failure envelopes predict the test results extremely well. The experimental results indicated in general that

connection strengths increased by increasing the edge-distance up to a maximum value of (e/d)=5. Therefore, the failure envelope corresponding to (e/d)=5 is set as the outermost failure envelope.

5.4 BEARING/CLEAVAGE FAILURE

As (d/w) approaches zero, the connection becomes infinitely wide with respect to the hole diameter and net tension failure is preceded by bearing failure for connections with large edge distances and by cleavage or shearout failure for connections with small edge distances. The ultimate bearing capacity of a connection is obviously dependent on the bearing strength of the material. Using the results of a full size connections, the bearing strength of a material F_{br} can be determined as:

$$F_{br} = \frac{P_{ult}}{t \cdot d_{bolt}}$$

(5.14)

where d_{bolt} is the diameter of the bolt. The hole diameter, d, used in this investigation was 20.6 mm (13/16 in.) and the bolt diameter, d_{bolt}, was 19 mm (3/4 in.).

The bearing strength of fibre-reinforced composite materials can be determined using a standard test, ASTM Standard D953. However, measured results could be very conservative compared to the bearing strength of actual full size connections. Therefore, it is recommended to use full size connections to determine the actual bearing strength.

The efficiency of a connection that fails in bearing, can be expressed in terms of the ratios F_{br}/F_{tu} and d_{bolt}/d as:

$$Efficiency = \frac{F_{br}}{F_{tu}} \frac{d_{bolt}}{d} \frac{d}{w} \tag{5.15}$$

Equation (5.15) is presented in Fig. 5.11 for the case of $d = d_{bolt}$ and various F_{br}/F_{tu} ratios. The term $(F_{br}/F_{tu})(d_{bolt}/d)$ is equivalent to the slope of the lines shown in Fig. 5.11.

In this investigation it was found that increasing (e/d) ratios did not increase the bearing stresses appreciably for (e/d)$\geq$5 as shown in Fig 4.20 and repeated in Fig. 5.12. The failure for these connections was predominantly bearing failure, therefore all connections that had (e/d)$\geq$5 were used to determine the material bearing strength, F_{br}, for the three fibre orientations used in this investigation. Using Eq.(5.15), Fig. 5.13 to Fig. 5.15 illustrate the best-fit lines for the three fibre orientations considered using a least squares regression analysis. From the test results of the connections with the specified bolt diameter to hole diameter ratio, the bearing strength to tensile strength ratios, F_{br}/F_{tu}, were found to be 1.84, 2.20, and 2.13 for the 0°, 45°, and 90° fibre orientations respectively. The numerical values are given for the three fibre orientations in Table 5.1. Using Eq.(5.14), the average value and standard deviation of the F_{br}/F_{tu} ratios of the specimens with (e/d)$\geq$5 are given in Fig. 5.16 to Fig. 5.18 for the three fiber orientations. The average F_{br}/F_{tu} values are 1.95, 2.51, and 2.38 for the 0°, 45°, and 90° fibre orientations respectively. As can be seen from Table 5.1 the average value of F_{br} as

determined from Eq.(5.14) is slightly higher than the least squares value of F_{br} as determined from Eq.(5.15). The large standard deviations as given in Table 5.1 are possibly due to the large material variability as well as the influence of combined modes of failure for those connections near the transition zones of the failure modes. The values obtained by the least squares method based on Eq.(5.15) were used in this investigation.

It should be noted that for a given (d/w) ratio and for adequate edge distances, the predominant mode of failure is bearing. With a decreasing (e/d) ratio the mode of failure tends to change from bearing failure to cleavage failure. In this investigation it was found that cleavage failure is related to bearing failure by a simple quadratic expression in terms of the ratio (d/2e). This expression is a reduction factor that relates the efficiency of a connection that would tend to fail in bearing to the efficiency of a similar connection with a smaller edge distance that would tend to fail in cleavage and is expressed as:

$$Cleavage\ Reduction\ Factor\ =\ (1-\frac{d}{2e})^2 \qquad (5.16)$$

The quadratic expression was found to be the simplest and fit the measured data the best. By introducing this reduction factor into Eq.(5.15) an expression that characterizes both bearing and cleavage failure can be defined as follows:

$$Efficiency\ =\ \frac{F_{br}}{F_{tu}}\ \frac{d_{bolt}}{d}\ (1-\frac{d}{2e})^2\ \frac{d}{w} \qquad (5.17)$$

Equation (5.17) satisfies the limiting case as (e/d) approaches ∞, as the quadratic term in Eq.(5.17) becomes unity and the efficiency reduces to Eq.(5.15) given before for bearing failure. Equation (5.17) satisfies the other limiting case which occurs when (e/d) approaches 1/2, and the expression predicts zero capacity of the connection. This is due to the fact that "e", which is measured to the centre of the bolt hole, cannot be less than half the hole diameter.

The results of this investigation show that for connections with (e/d)≥5 the failure mode is predominantly bearing. Therefore to satisfy this new practical limit, the cleavage reduction factor should reduce to 1 when (e/d)=5. To accomplish this, the constants in the cleavage reduction factor must be computed based on the practical boundary conditions. Equation (5.17) can be rewritten in terms of constant coefficients "a" and "b" as follows:

$$Efficiency = \frac{F_{br}}{F_{tu}} \frac{d_{bolt}}{d} (a-b\frac{d}{e})^2 \frac{d}{w} \tag{5.18}$$

Therefore to satisfy the upper limit when (e/d)=5:

$$(a-\frac{b}{5}) = 1 \tag{5.19}$$

and to satisfy the lower limit when (e/d)=1/2:

$$(a-2b) = 0 \tag{5.20}$$

Solving Eq.(5.19) and (5.20) simultaneously, the two constant coefficients were found to be: a=10/9 and b=5/9.

Therefore, for (e/d)≤5 Eq.(5.18) becomes as follows for cleavage failure:

$$Efficiency = \frac{F_{br}}{F_{tu}} \frac{d_{bolt}}{d} (\frac{10}{9} - \frac{5}{9}\frac{d}{e})^2 \frac{d}{w} \quad for(e/d) \leq 5 \quad Cleavage \quad (5.21)$$

For (e/d)≥5 Eq.(5.18) reduces to Eq.(5.15) for bearing failure:

$$Efficiency = \frac{F_{br}}{F_{tu}} \frac{d_{bolt}}{d} \frac{d}{w} \quad\quad for(e/d) \geq 5 \quad Bearing \quad (5.22)$$

Using the least efficiency, the ultimate load of a connection can be determined as:

$$P_{ult} = Efficiency \ (t \cdot w \cdot F_{tu}) \quad\quad (5.23)$$

Equations (5.21) and (5.22) were used to produce a family of failure envelopes in terms of the efficiency and the ratio (d/w) as shown in Fig. 5.19 to Fig. 5.21 for the three orientations used in this investigation. The various envelopes are given for constant (e/d) ratios. The curves are in excellent agreement with the measured experimental values for both bearing and cleavage modes of failure.

The shear-out mode of failure was not observed in this experimental investigation due to the presence of a high volume of random fibres in the material used. However, since shearout and cleavage can be considered types of bearing failures with inadequate edge distances, it is reasonable to assume that the behaviour for cleavage failure discussed here could be applicable to shearout failure which could occur in other types of composite materials.

5.5 DESIGN PROCEDURE

Superimposing the failure envelopes of the two failure criteria described before, one set of design envelopes was developed for each fibre orientation as shown in Fig. 5.22 to Fig. 5.24. Given a particular connection geometry t, w, e, d, and d_{bolt} the efficiency and mode of failure of the connection can be predicted using the proposed failure envelopes for the corresponding (d/w) and (e/d) ratios and the given fibre orientation. The efficiency can also be determined using Eq.(5.12) for net tension failure and Eq.(5.21) or Eq.(5.22) for cleavage/bearing failure with the lowest value of the two failure criteria determining the connection's efficiency and its corresponding failure mode.

It can be seen that for fibre reinforced composites an optimum value of (d/w) exists which will produce a maximum connection efficiency. For EXTREN Flat Sheet/ Series 500 this maximum connection efficiency is approximately 0.4 for (d/w)$\approx$0.3 and (e/d)=5. To prevent a catastrophic failure mode such as net tension, it may be necessary to increase the width to induce bearing failure and accept a loss in connection efficiency.

In general for any composite material, the proposed design procedure can be used by determining the material properties and correlation coefficient experimentally and by developing failure envelopes similar to the one used in this investigation to predict the load capacity and the mode of failure.

The measured ultimate loads of the connections tested in this program for the three fibre orientations are compared to the predicted values obtained from the

proposed design procedure in Fig. 5.25 to Fig. 5.27. The comparison indicates that most of the data fall close to the 1:1 correspondence line or are on the conservative side.

Table 5.2 lists the percent difference between the measured and predicted ultimate loads and compares the predicted mode of failure to the observed modes. As the results indicate, the proposed design procedure predicted the ultimate load and failure mode of the tested connections with an adequate degree of accuracy. On average, the predicted loads were within 10% of the experimentally determined values. For the 0° connections the correspondence between the predicted and experimental failure modes was excellent with only a few discrepancies occurring for those connections that had failed in a combined failure mode. Since the model is based on the 0° connections, in terms of failure modes, it could not predict the suppression of the cleavage failure mode for the 45° and 90° connections as shown in Table 5.2. Although it had predicted the net tension and bearing failure modes for those "angled" connections that had the same failure mode as their 0° counterparts, it had predicted typical bearing and cleavage failure modes for those connections in which the "angled" fibre orientation induced a net tension failure. This is not a major problem as the prediction of failure modes can be empirically corrected for the 45° and 90° cases.

Obviously connections that were tested with the principal fibre direction at 45° and 90° to the applied load had lower ultimate loads than their 0° counterparts. However, due to the lower values of F_{tu} in these directions, their efficiencies were

actually higher than their 0° counterparts as shown in Fig. 5.22 to Fig. 5.24. This means that the failure envelopes for the 0° case can also be used to predict conservatively the loads of connections of all fibre orientations considered in this investigation. This suggests that only one set of design envelopes needs to be used to predict the connection behaviour regardless of the direction in which the bolt is bearing with respect to the fibre orientation.

Because the procedure is based on isotropic theory and uses empirical data to correlate the failure criteria it could be used for a variety of different composite material systems. The correlation coefficient which relates the isotropic theory to composite materials accounts for material orthotropy, pseudo-yielding capability, hole size and clearance effects. In some respects the coefficient can be thought of as a "catch all" factor accounting for all those effects which complicate the stress analysis of a loaded bolt-hole. It is therefore reasonable to expect that as the material systems and connection configurations used by civil engineers become more standardized, a data base of test results could be developed to allow the design engineer to "pick and choose" the appropriate "C" value from a design code without ever doing a single test. Considering the versatility and simplicity of this design procedure it is ideal for implementation in future design codes.

5.6 PRACTICAL APPLICATION

Given a connection made from EXTREN Flat Sheet /Series 500 with the dimensions w=130 mm, e=40 mm, t=12 mm, d=21 mm, d_{bolt}=19 mm and the material property F_{tu}=166 MPa, the structural efficiency can be determined from the envelopes in Fig. 5.22 for (d/w)=0.16 and (e/d)≈2 and is found to be 0.185. Consequently the ultimate load P_{ult}=Efficiency·t·w·F_{tu} is equal to 48 kN. Since the failure is located within the straight line portion of the envelope, the failure is a bearing or cleavage failure. In this case the failure is cleavage, since (e/d)<5.

The same results can be obtained using Eq.(5.12) and (5.21) with a correlation factor of C=0.33 and F_{br}=1.84 F_{tu}, determined experimentally for this type of material. The expression for net tension failure Eq.(5.12) gives an efficiency of 0.27 and a P_{ult} (net tension)=70 kN while expression (5.21) gives an efficiency of 0.18 and a P_{ult} (cleavage)=47 kN. Since Eq.(5.21) is critical the failure mode is cleavage.

By increasing the edge distance of the previous connection, the mode of failure can be changed from cleavage failure to a more desirable bearing failure. Setting e=110 mm so that (e/d)=5.2, the efficiency can be determined from Fig. 5.22 to be 0.28 and P_{ult}=72 kN. Since (e/d)≥5 the mode of failure will be bearing. Using Eq.(5.12) and (5.22) the net tension efficiency can be determined to be 0.31 and P_{ult} (net tension)=80 kN, while the bearing efficiency is found to be 0.27 and P_{ult} (bearing)=70 kN similar to that obtained from Fig. 5.22. Obviously bearing failure is critical.

If a similar connection is used except with w=40 mm and e=40 mm and thus

(d/w)=0.53 and (e/d)≈2, the efficiency is found from Fig. 5.22 to be 0.32 and hence the ultimate load is 25.5 kN with the governing mode of failure being net tension. Using Eq.(5.12) and (5.21) ,the net tension efficiency is determined to be 0.32 and P_{ult} (net tension)=25.7 kN, while the bearing/cleavage criterion predicts an efficiency of 0.59 and a P_{ult} (cleavage)=47 kN. Thus the net tension criterion is critical and therefore the mode of failure will be net tension.

Table 5.1 Bearing Strength of EXTREN Flat Sheet

Least Squares Regression Analysis

Fibre Angle (deg)	Fbr/Ftu	Standard Error	Bearing Strength (Fbr) (MPa)	Bearing Strength (Fbr) (ksi)
0	1.84	0.095	306	44.4
45	2.20	0.170	258	37.4
90	2.13	0.129	235	34.1

Simple Average of Tests

Fibre Angle (deg)	Fbr/Ftu	Standard Deviation	Bearing Strength (Fbr) (MPa)	Bearing Strength (Fbr) (ksi)
0	1.95	0.224	324	47.0
45	2.51	0.545	294	42.7
90	2.38	0.457	263	38.1

Table 5.2 Model Results

Test Designation	Experimental Ultimate Load kN	(lbs)	Predicted Ultimate Load kN	(lbs)	% Difference	Experimental Failure Mode Plate A	Plate B	Predicted Failure Mode
Series A								
A1	12.2	2750	13.2	2963	7.8	NT	NT	NT
A2	14.5	3250	13.5	3025	-6.9	NT	NT	NT
A3	44.0	9900	37.9	8511	-14.0	NT	NT	NT
A4	43.8	9850	38.6	8685	-11.8	NT	NT	NT
A5	39.4	8850	39.1	8787	-0.7	NT	NT	NT
A6	55.3	12425	58.4	13125	5.6	NT	NT	NT
A7	57.8	12990	60.4	13586	4.6	NT	NT	NT
A8	61.3	13775	61.6	13860	0.6	NT	NT	NT
A9	69.2	15550	73.0	16404	5.5	C	C	C
A10	95.3	21425	96.3	21641	1.0	B-NT	B-NT	C
A11	103.0	23150	111.2	24991	8.0	B-NT	B-NT	B
A12	100.5	22600	111.2	24991	10.6	B-NT	B-NT	B
A13	67.6	15200	73.0	16404	7.9	C	C	C
A14	109.4	24600	96.3	21641	-12.0	C	C	C
A15	129.0	29000	111.2	24991	-13.8	B-NT	B	B
A16	28.9	6500	28.8	6481	-0.3	C	C	C
A17	66.7	15000	73.0	16404	9.4	C	C	C
A18	113.0	25400	96.3	21641	-14.8	C	C	C
A19	116.8	26250	111.2	24991	-4.8	B	B	B
A20	113.9	25600	111.2	24991	-2.4	B	B	B
A21	92.1	20700	111.2	24991	20.7	B	B-NT	B
A22	122.8	27600	111.2	24991	-9.5	B	B	B
Series B								
B1	13.3	3000	14.8	3318	10.6	NT	NT	NT
B2	14.9	3350	15.1	3387	1.1	NT	NT	NT
B3	52.3	11750	50.5	11348	-3.4	NT	NT	NT
B4	60.5	13600	51.5	11581	-14.8	NT	NT	NT
B5	54.9	12350	52.1	11716	-5.1	NT	NT	NT
B6	72.9	16400	77.8	17500	6.7	NT	NT	NT
B7	75.4	16950	80.6	18115	6.9	NT	NT	NT
B8	83.4	18750	82.2	18480	-1.4	NT	NT	NT
B9	97.5	21925	97.3	21872	-0.2	C	C	C
B10	115.1	25870	128.3	28854	11.5	B-NT	B-NT	C
B11	145.0	32600	148.2	33322	2.2	B-NT	B-NT	B
B12	137.9	31010	148.2	33322	7.5	B-NT	B-NT	B
B13	95.2	21400	97.3	21872	2.2	C	C	C
B14	152.6	34300	128.3	28854	-15.9	C	C	C
B15	167.2	37600	148.2	33322	-11.4	B	B	B
B16	36.6	8225	38.4	8642	5.1	C	C	C
B17	101.1	22740	97.3	21872	-3.8	C	C	C
B18	133.9	30100	128.3	28854	-4.1	C	C	C
B19	184.1	41400	148.2	33322	-19.5	B-NT	B	B
B20	186.0	41810	148.2	33322	-20.3	B	B	B

Failure Modes: NT=Net Tension   C=Cleavage   B=Bearing   B-NT=Combined Bearing-Net Tension
B-C=Combined Bearing-Cleavage   C-NT=Combined Cleavage-Net Tension

Table 5.2 Model Results (cont'd)

Test Designation	Experimental Ultimate Load kN	(lbs)	Predicted Ultimate Load kN	(lbs)	% Difference	Experimental Failure Mode Plate A	Plate B	Predicted Failure Mode
Series C								
C1	11.8	2650	10.5	2356	-11.1	NT	NT	NT
C2	11.7	2630	10.7	2395	-8.9	NT	NT	NT
C3	34.9	7840	36.3	8162	4.1	NT	NT	NT
C4	28.7	6450	36.9	8298	28.7	NT	NT	NT
C5	32.1	7210	37.3	8377	16.2	NT	NT	NT
C6	57.8	12990	57.1	12835	-1.2	NT	NT	NT
C7	51.2	11500	58.8	13210	14.9	NT	NT	NT
C8	60.9	13690	59.7	13430	-1.9	NT	NT	NT
C9	78.8	17720	74.9	16848	-4.9	NT	NT	C
C10	81.2	18250	98.9	22226	21.8	NT	NT	C
C11	106.3	23890	114.2	25667	7.4	NT	NT	B
C12	107.7	24210	114.2	25667	6.0	NT	NT	B
C13	82.8	18620	74.9	16848	-9.5	NT	NT	C
C14	90.3	20300	98.9	22226	9.5	NT	NT	C
C15	120.4	27070	114.2	25667	-5.2	NT	NT	B
C16	39.9	8970	29.6	6657	-25.8	C	C	C
C17	84.2	18940	74.9	16848	-11.0	NT	NT	C
C18	114.2	25670	98.9	22226	-13.4	NT	NT	C
C19	135.8	30530	114.2	25667	-15.9	NT	NT	B
C20	165.1	37120	114.2	25667	-30.9	B	B	B
Series D								
D1	11.4	2570	11.5	2592	0.9	NT	NT	NT
D2	11.6	2600	11.7	2629	1.1	NT	NT	NT
D3	40.2	9040	40.2	9045	0.1	NT	NT	NT
D4	31.0	6975	40.8	9177	31.6	NT	NT	NT
D5	43.4	9750	41.2	9253	-5.1	NT	NT	NT
D6	64.9	14590	64.0	14384	-1.4	NT	NT	NT
D7	47.8	10750	65.6	14755	37.3	NT	NT	NT
D8	64.0	14390	66.6	14972	4.0	NT	NT	NT
D9	79.8	17930	82.0	18427	2.8	NT	NT	C
D10	96.5	21700	108.1	24309	12.0	NT	NT	C
D11	116.9	26280	124.9	28072	6.8	NT	NT	B
D12	109.7	24670	124.9	28072	13.8	NT	NT	B
D13	88.9	19990	82.0	18427	-7.8	NT	NT	C
D14	93.9	21100	108.1	24309	15.2	NT	NT	C
D15	143.2	32190	124.9	28072	-12.8	NT	NT	B
D16	36.3	8150	32.4	7280	-10.7	C	C	C
D17	89.3	20070	82.0	18427	-8.2	NT	C-NT	C
D18	126.8	28510	108.1	24309	-14.7	NT	NT	C
D19	157.6	35440	124.9	28072	-20.8	NT	B-NT	B
D20	185.6	41730	124.9	28072	-32.7	B	B	B

Failure Modes: NT=Net Tension C=Cleavage B=Bearing B-NT=Combined Bearing-Net Tension
B-C=Combined Bearing-Cleavage C-NT=Combined Cleavage-Net Tension

Table 5.2 Model Results (cont'd)

Test Designation	Experimental Ultimate Load kN	(lbs)	Predicted Ultimate Load kN	(lbs)	% Difference	Experimental Failure Mode Plate A	Plate B	Predicted Failure Mode
Series E								
E1	20.4	4580	22.1	4977	8.7	NT	NT	NT
E2	23.4	5270	22.6	5080	-3.6	NT	NT	NT
E3	76.7	17240	75.7	17022	-1.3	NT	NT	NT
E4	83.9	18870	77.3	17371	-7.9	NT	NT	NT
E5	84.0	18890	78.2	17573	-7.0	NT	NT	NT
E6	106.0	23830	116.8	26250	10.2	NT	NT	NT
E7	117.1	26330	120.9	27172	3.2	NT	NT	NT
E8	129.7	29150	123.3	27720	-4.9	NT	NT	NT
E9	133.5	30020	145.9	32809	9.3	C	C	C
E10	206.9	46520	192.5	43282	-7.0	B-NT	B-C	C
E11	228.3	51330	222.3	49983	-2.6	B-NT	B-NT	B
E12	236.1	53080	222.3	49983	-5.8	B	B	B
E13	135.7	30500	145.9	32809	7.6	C	C	C
E14	224.4	50460	192.5	43282	-14.2	B-C	B-C	C
E15	233.4	52480	222.3	49983	-4.8	B	B	B
E16	45.5	10240	57.7	12963	26.6	C	C	C
E17	129.1	29030	145.9	32809	13.0	C	C	C
E18	233.1	52400	192.5	43282	-17.4	B-C	B-C	C
E19	266.6	59940	222.3	49983	-16.6	B	B	B
E20	254.1	57130	222.3	49983	-12.5	B	B	B

Total=102 Connection Tests

Failure Modes: NT=Net Tension C=Cleavage B=Bearing B-NT=Combined Bearing-Net Tension
B-C=Combined Bearing-Cleavage   C-NT=Combined Cleavage-Net Tension
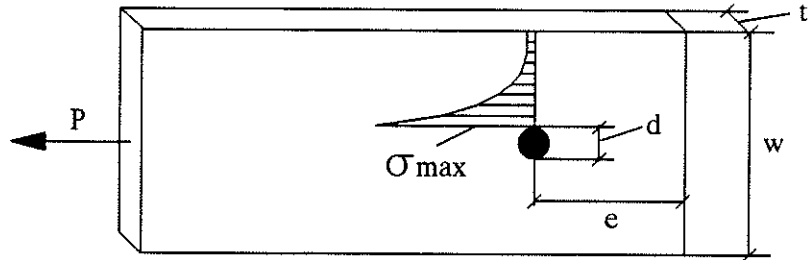
Figure 5.1 Connection Parameters
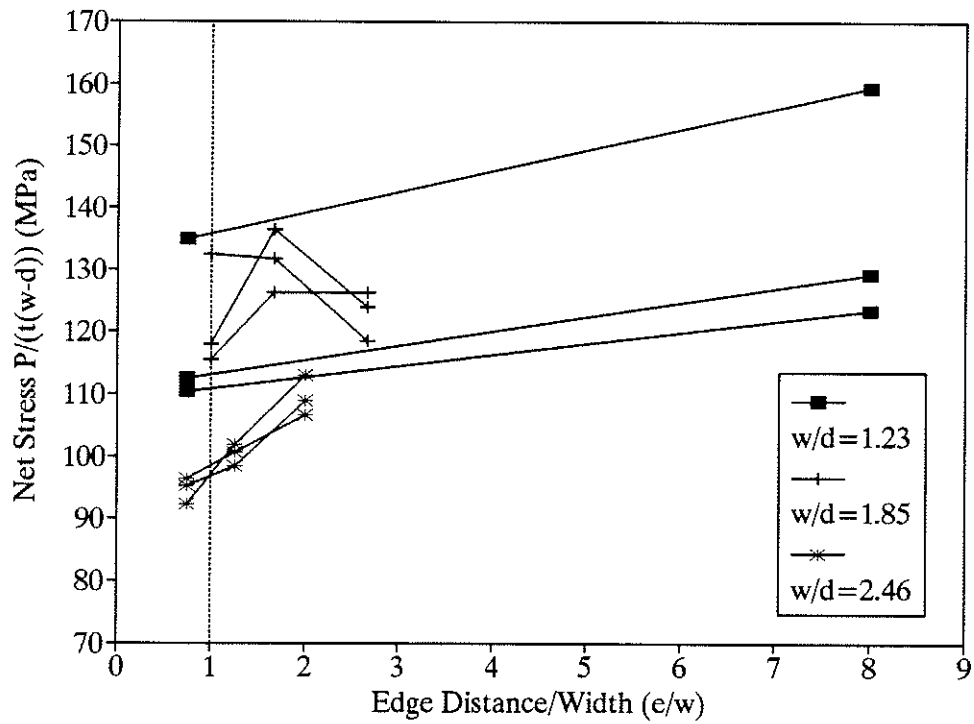
Figure 5.2 Effect of (e/w) on Net Stress
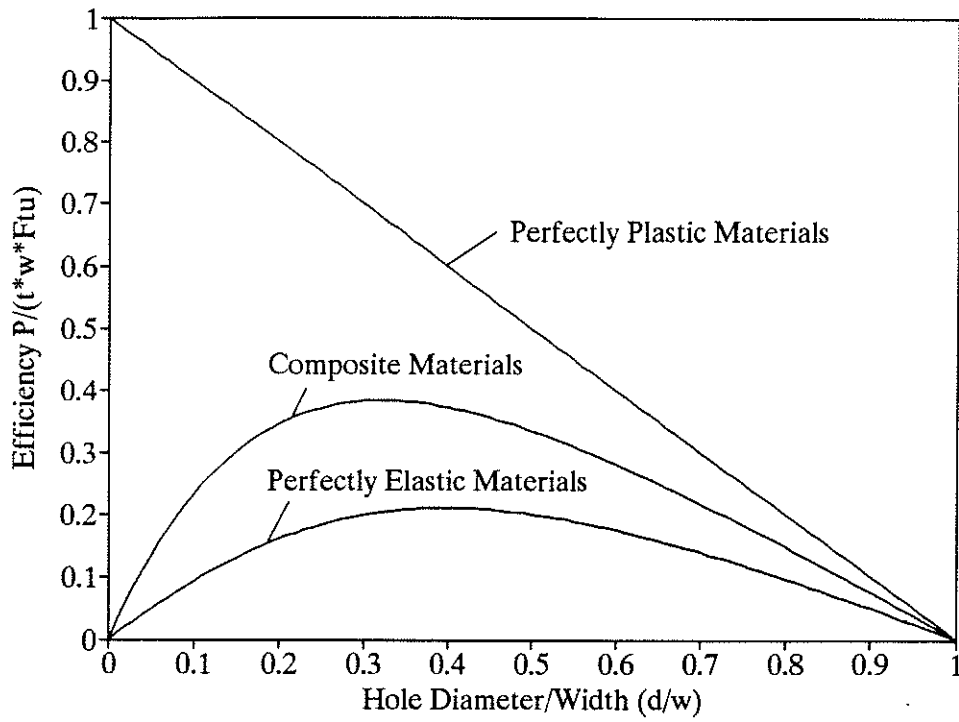
Figure 5.3 Net Tension Failure Criteria
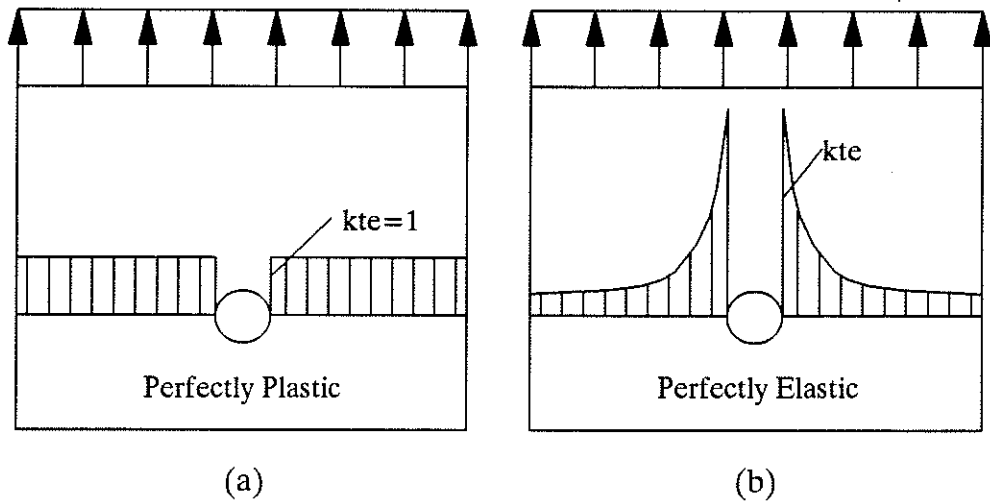
Figure 5.4 Difference in Plastic and Elastic Behaviours
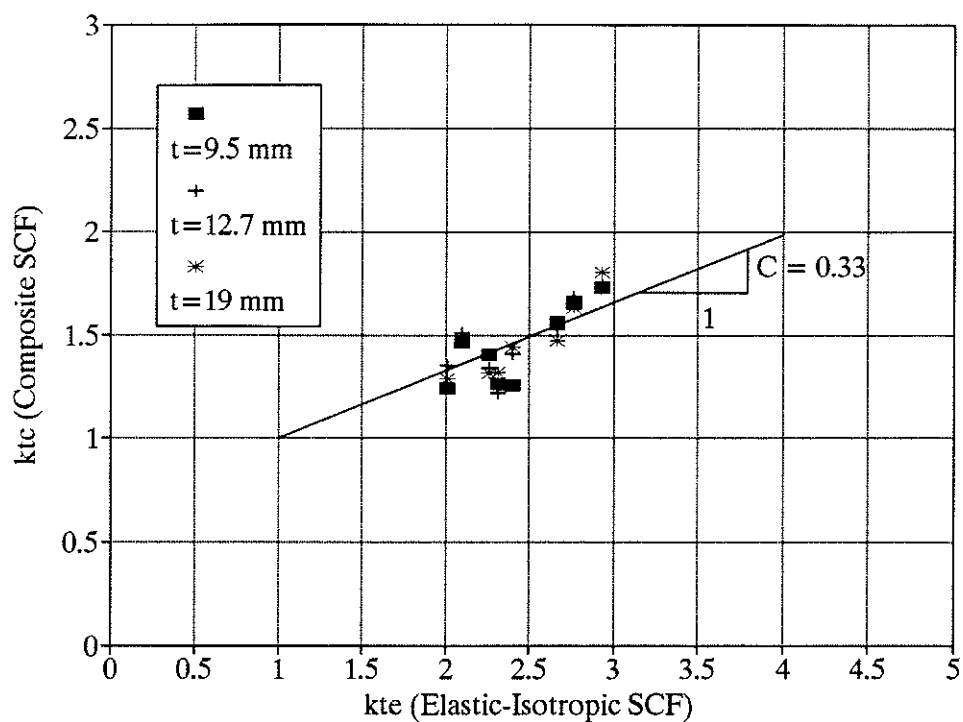
Figure 5.5 Correlation Coefficient for 0 deg. Connections
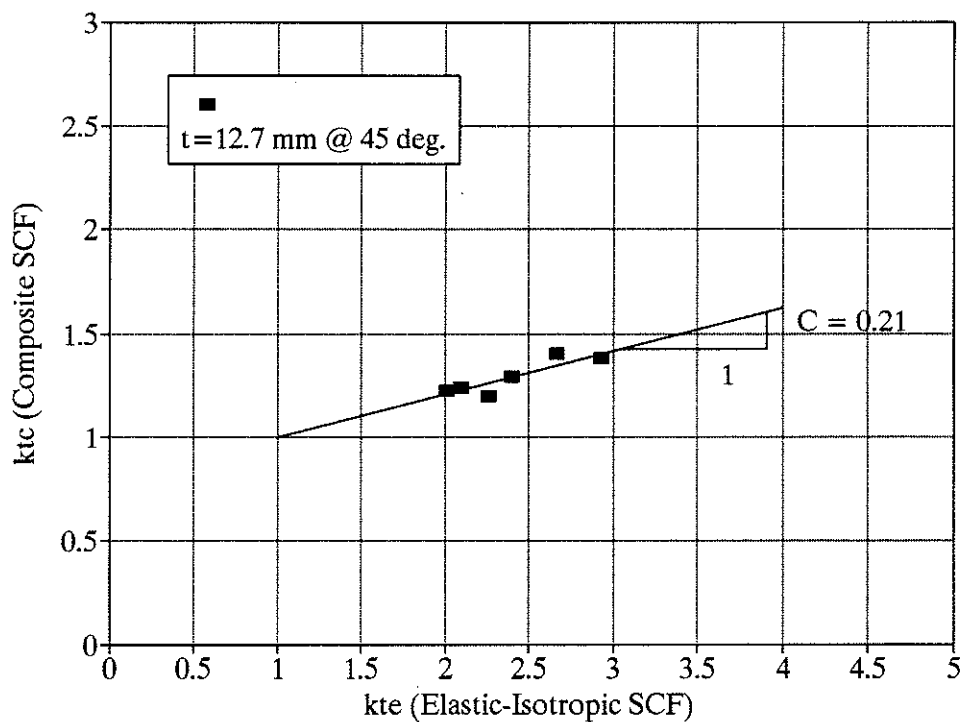
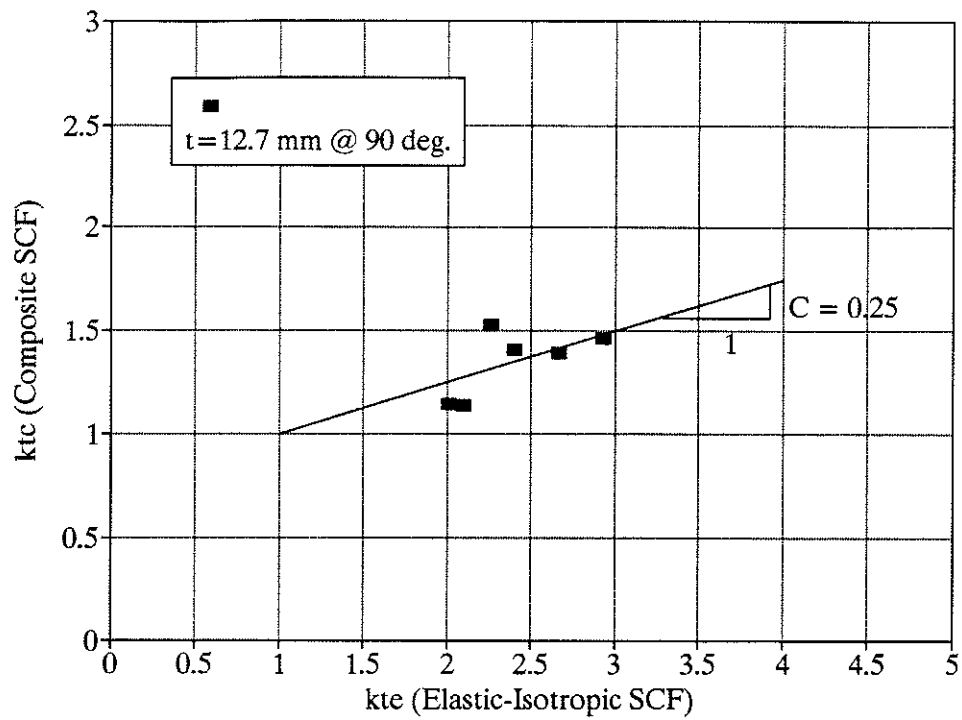Figure 5.6 Correlation Coefficient for 45 deg. Connections

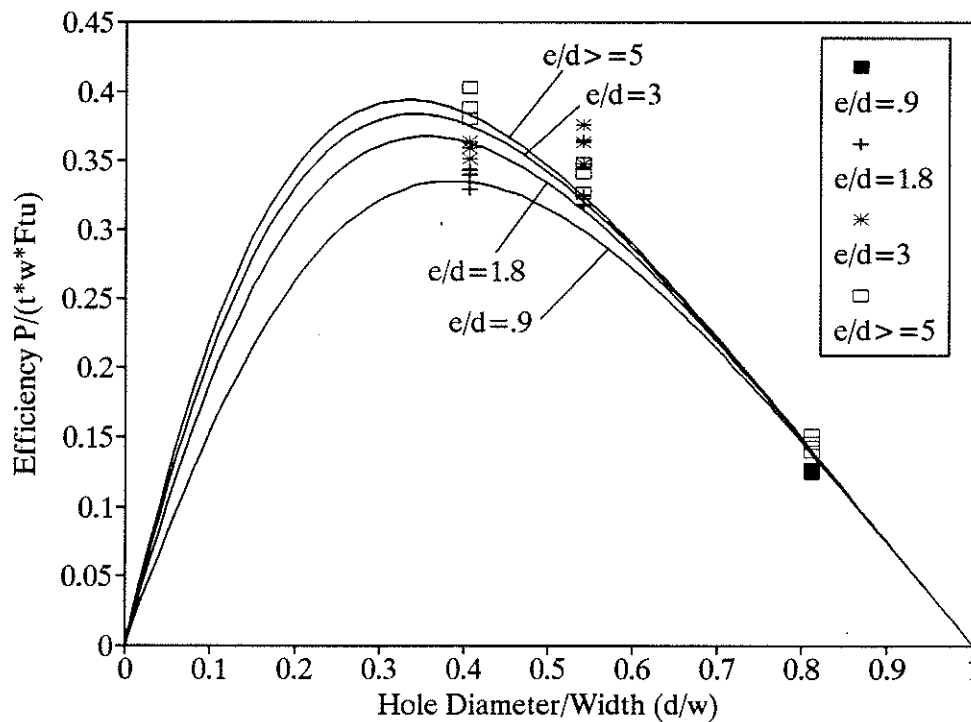Figure 5.7 Correlation Coefficient for 90 deg. Connections

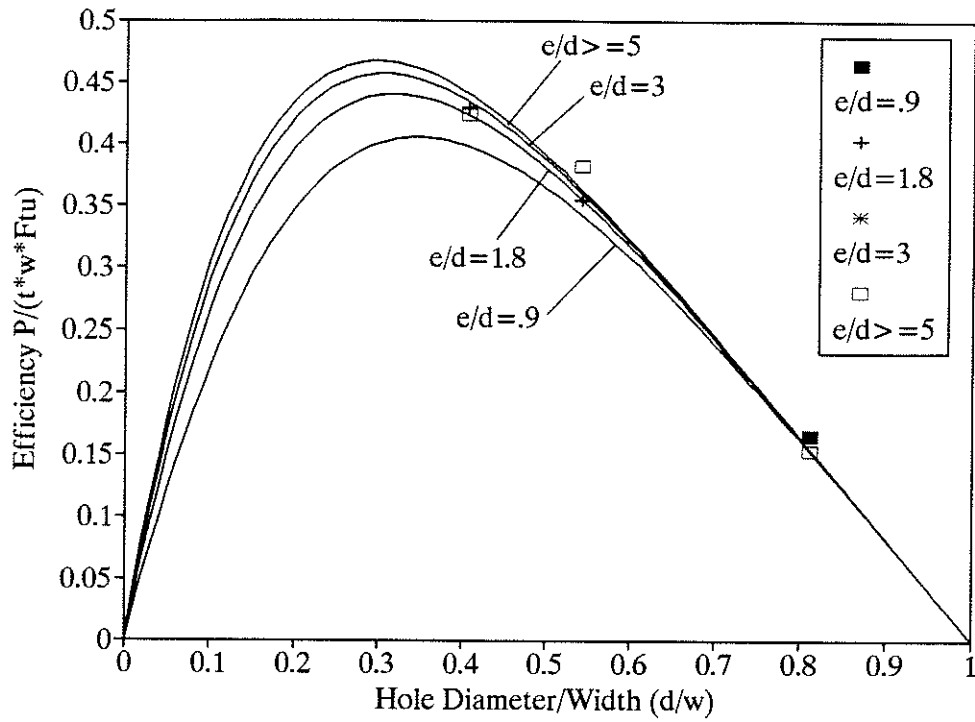Figure 5.8 Net Tension Failure Envelopes for 0 deg. Connections
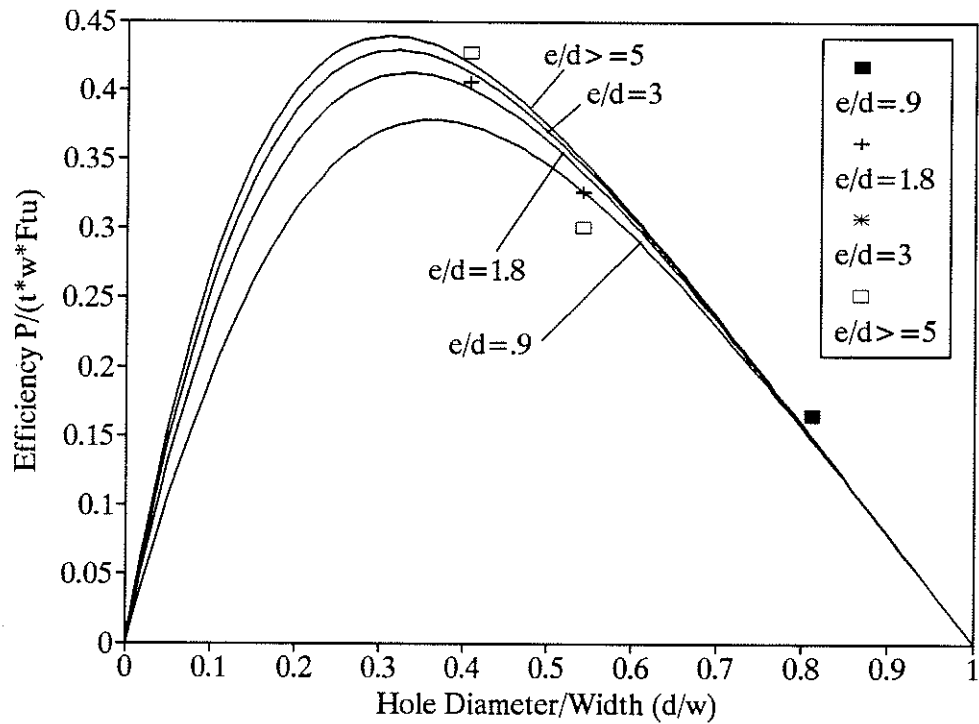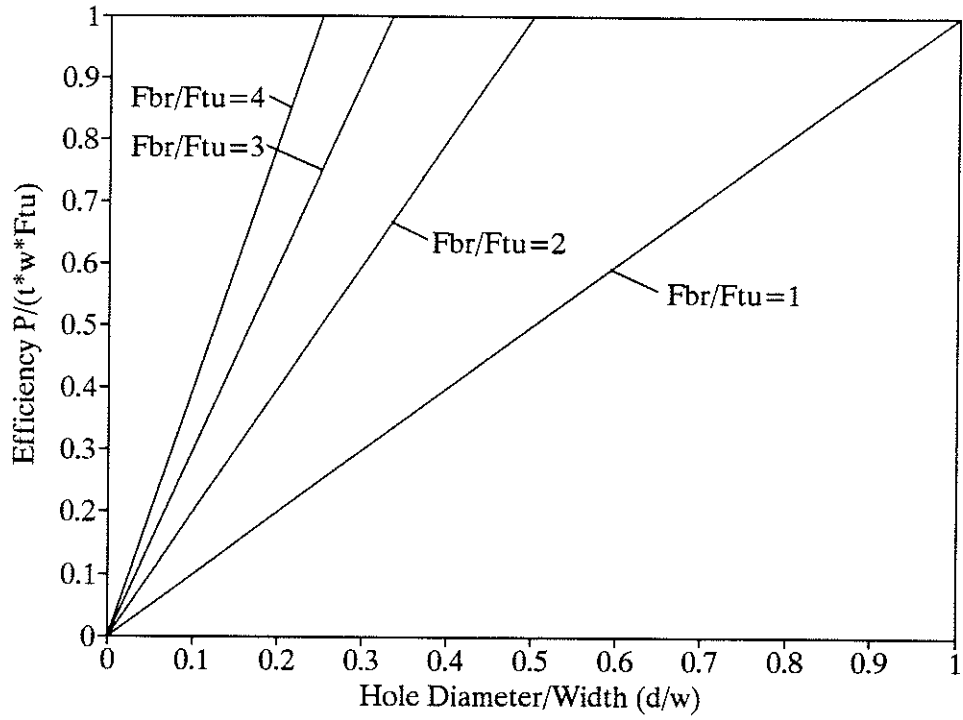
Figure 5.9 Net Tension Failure Envelopes for 45 deg. Connections

Figure 5.10 Net Tension Failure Envelopes for 90 deg. Connections

Figure 5.11 Bearing Criteria for Various Fbr/Ftu Ratios
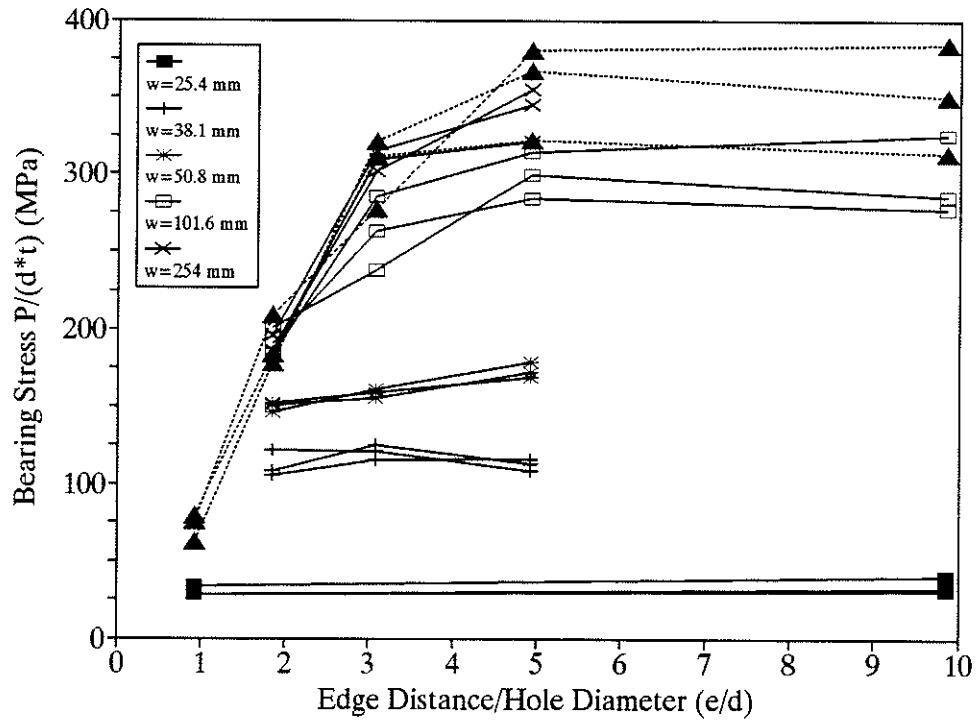
Figure 5.12 Effect of (e/d) on Bearing Stresses
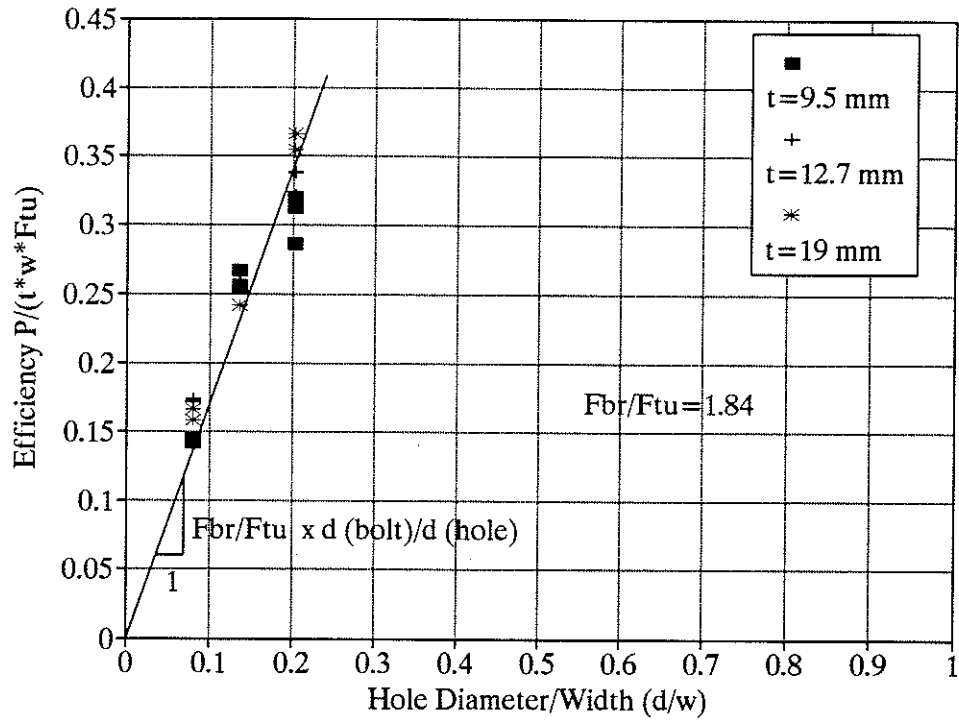
Figure 5.13 Bearing Strength for 0 deg. Connections
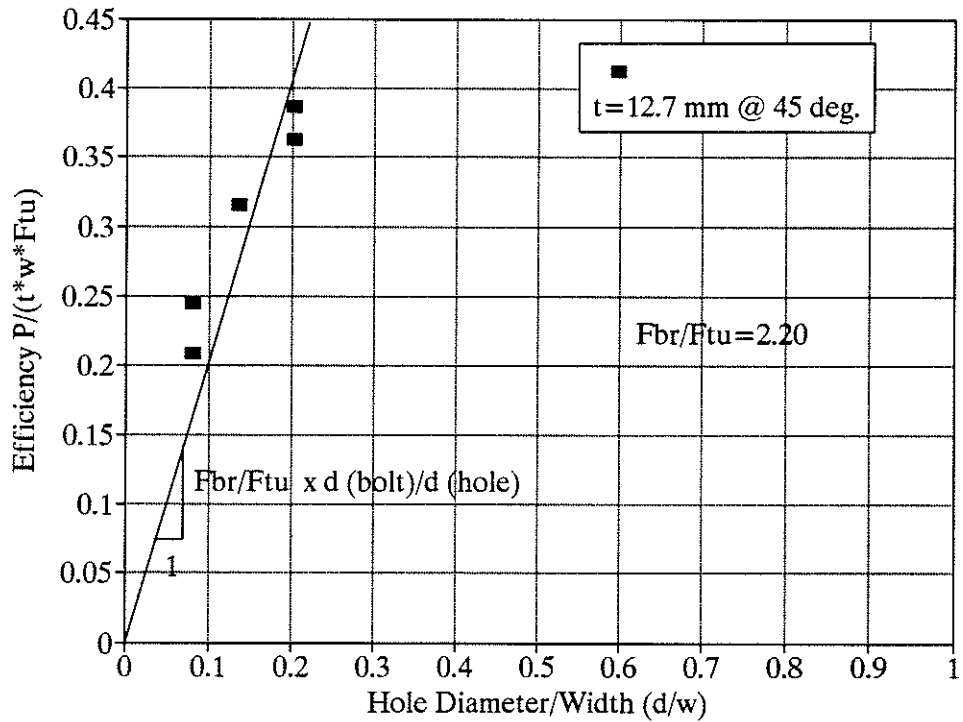
Figure 5.14 Bearing Strength for 45 deg. Connections
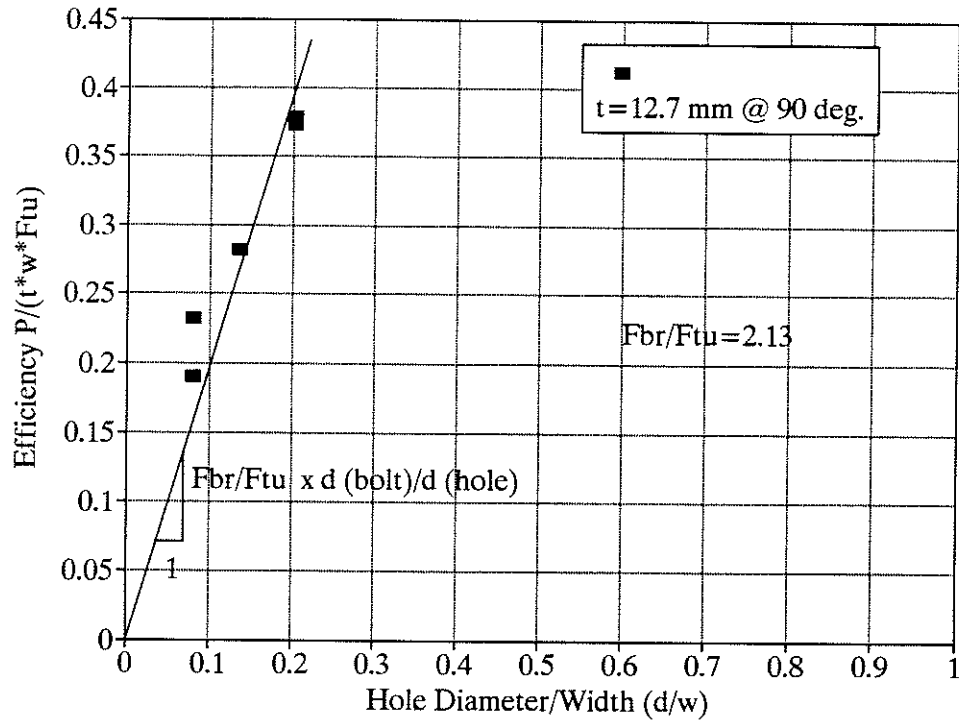
Figure 5.15 Bearing Strength for 90 deg. Connections
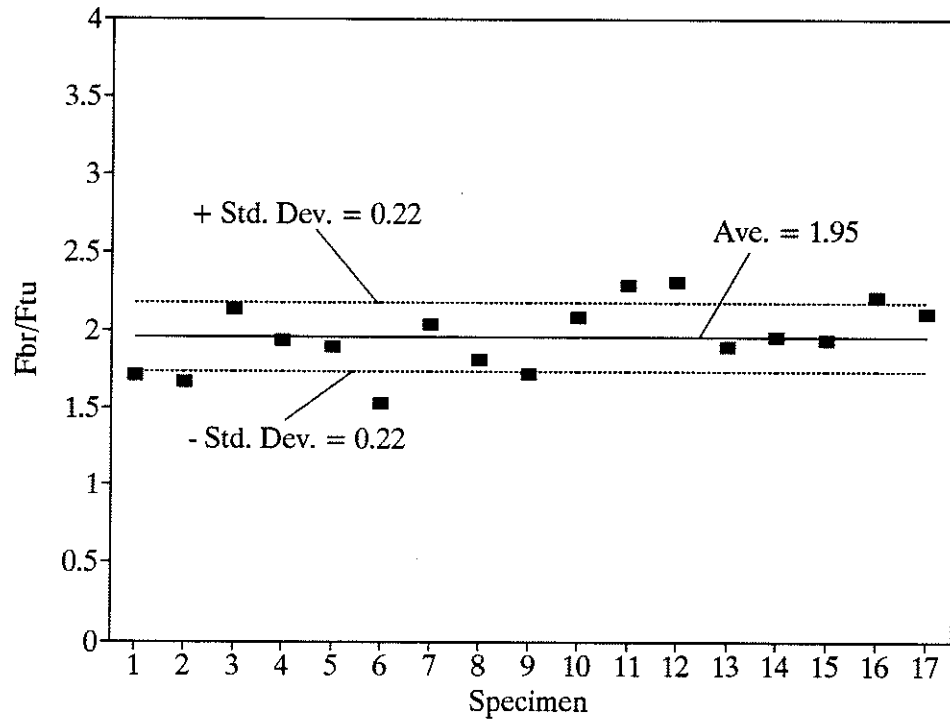
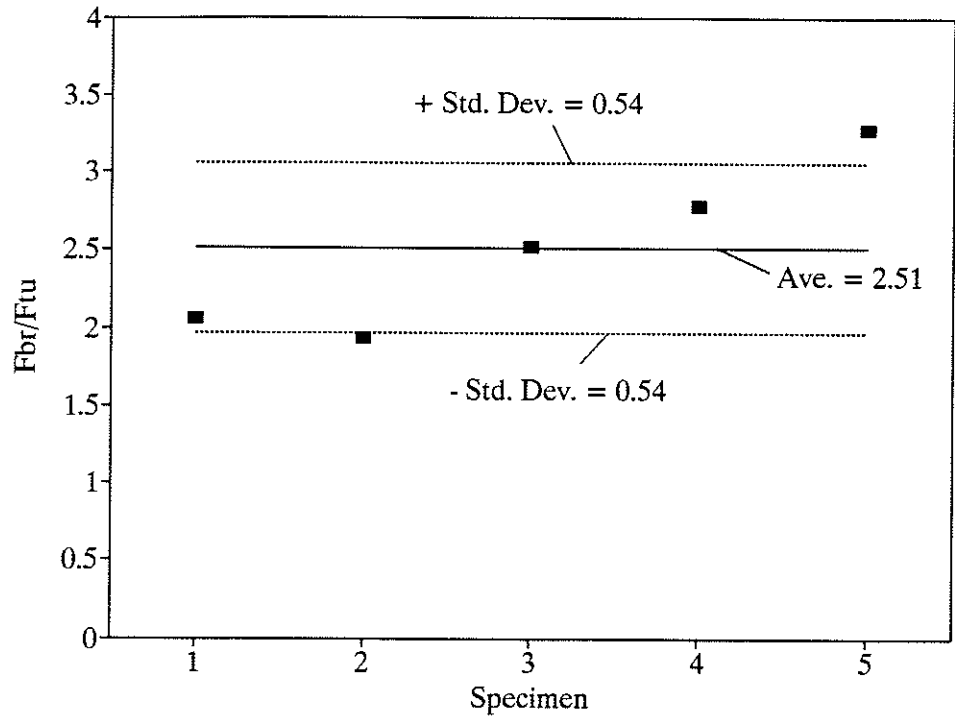

Figure 5.16 Average Fbr/Ftu Ratio for 0 deg. Connections

Figure 5.17   Average Fbr/Ftu Ratio for 45 deg. Connections
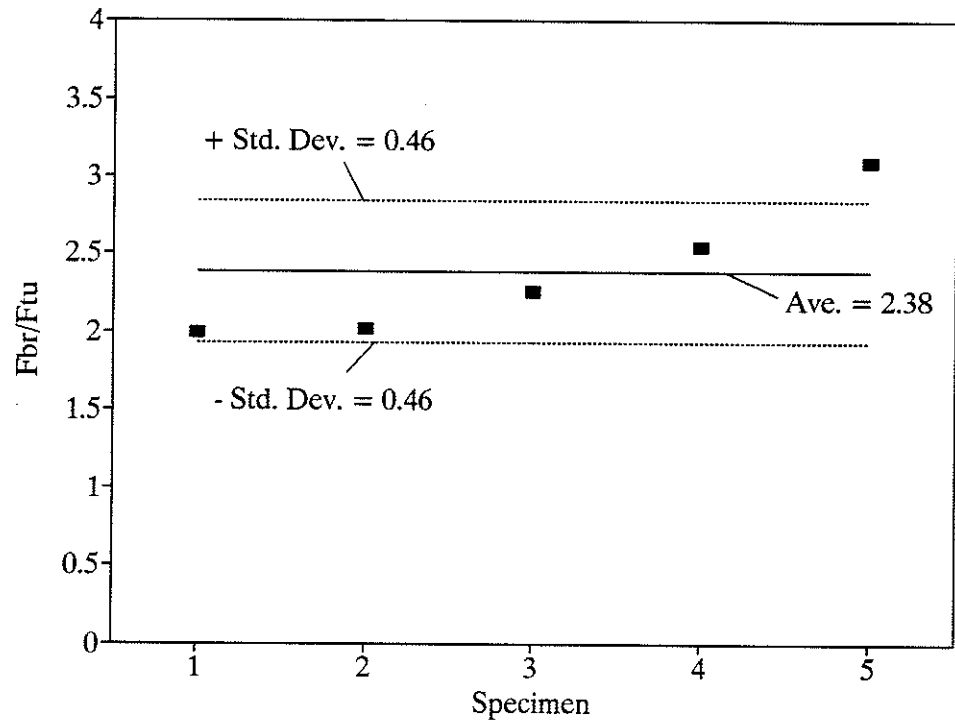

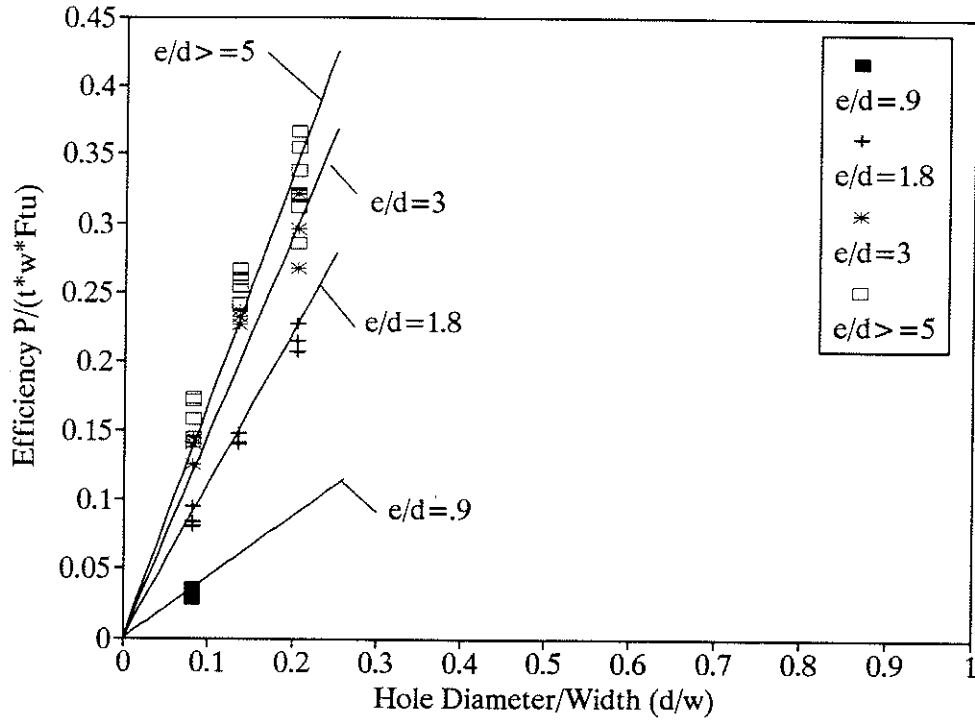Figure 5.18   Average Fbr/Ftu Ratio for 90 deg. Connections

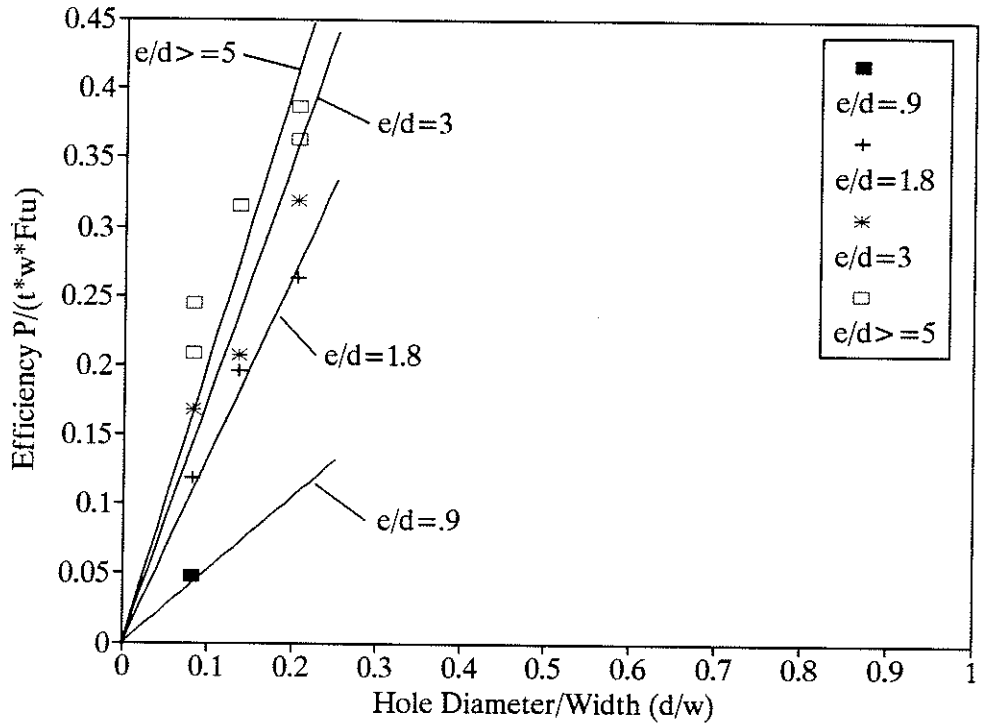Figure 5.19 Bearing Failure Envelopes for 0 deg. Connections

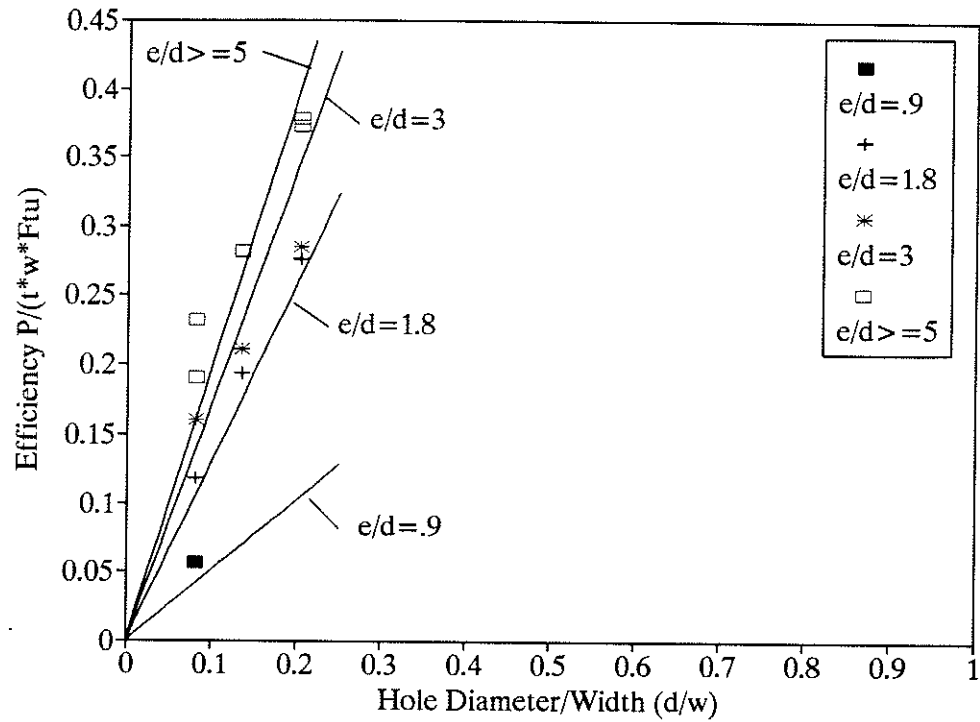Figure 5.20 Bearing Failure Envelopes for 45 deg. Connections

Figure 5.21 Bearing Failure Envelopes for 90 deg. Connections
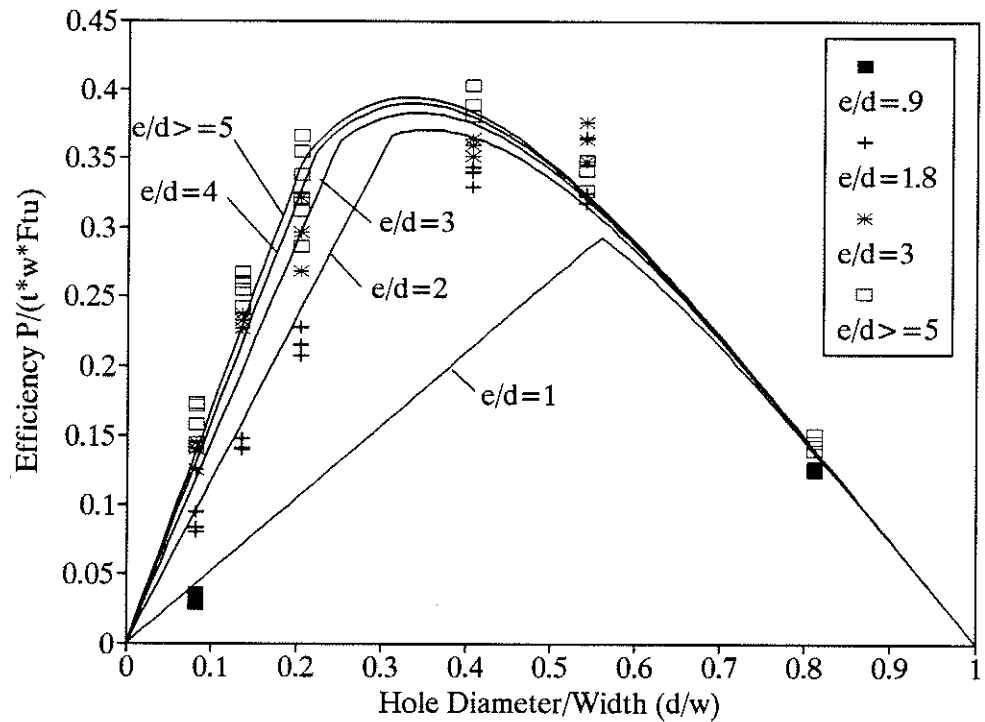

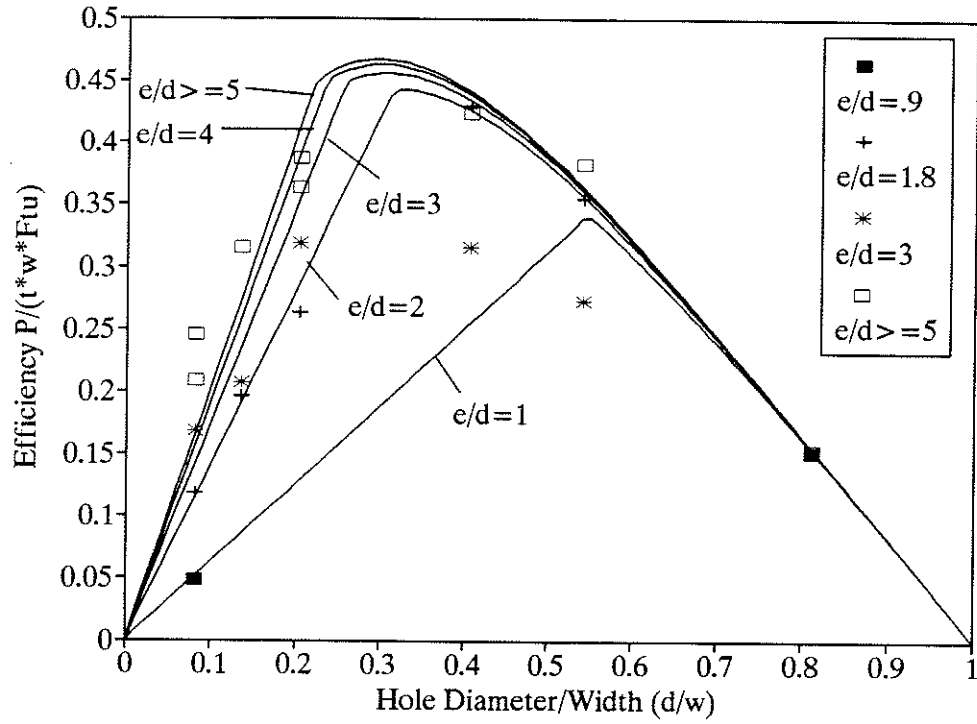Figure 5.22 Design Envelopes for 0 deg. Connections

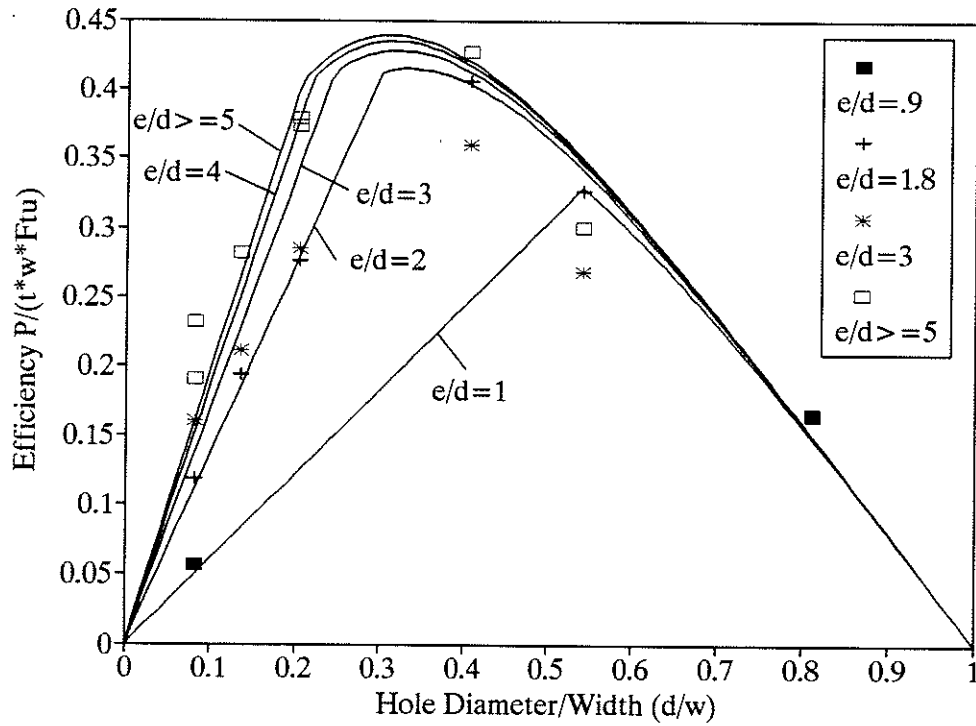Figure 5.23 Design Envelopes for 45 deg. Connections

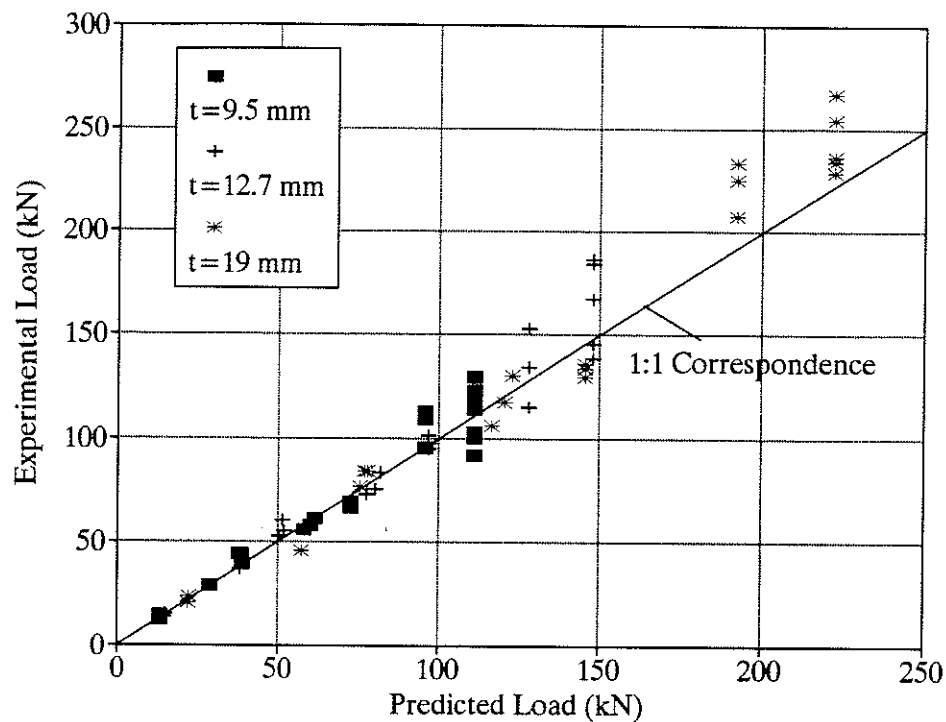Figure 5.24 Design Envelopes for 90 deg. Connections

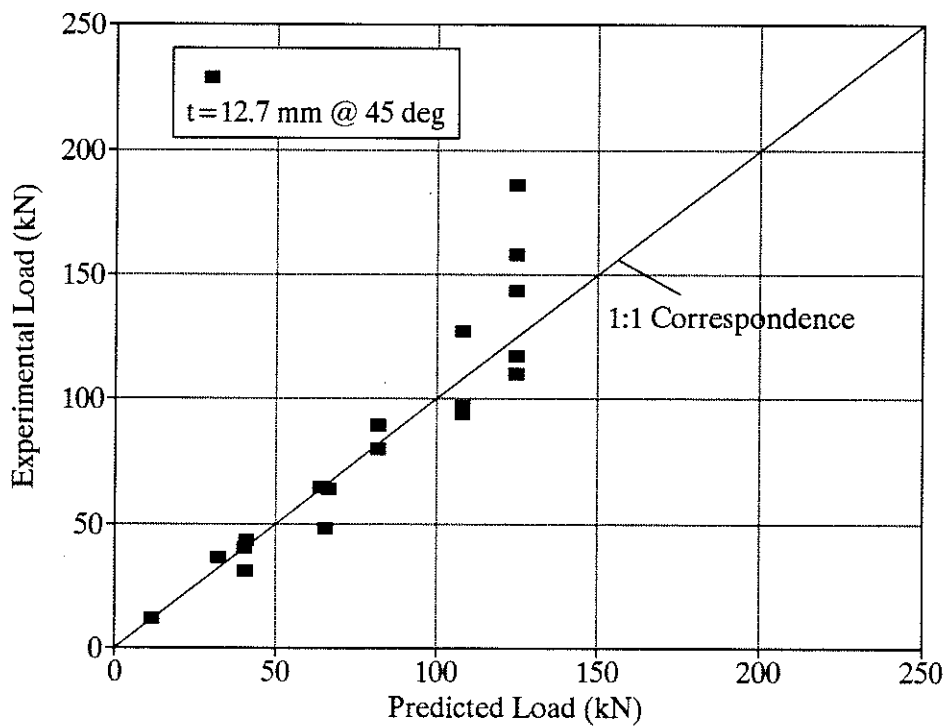Figure 5.25 Experimental vs. Model Results for 0 deg. Connections

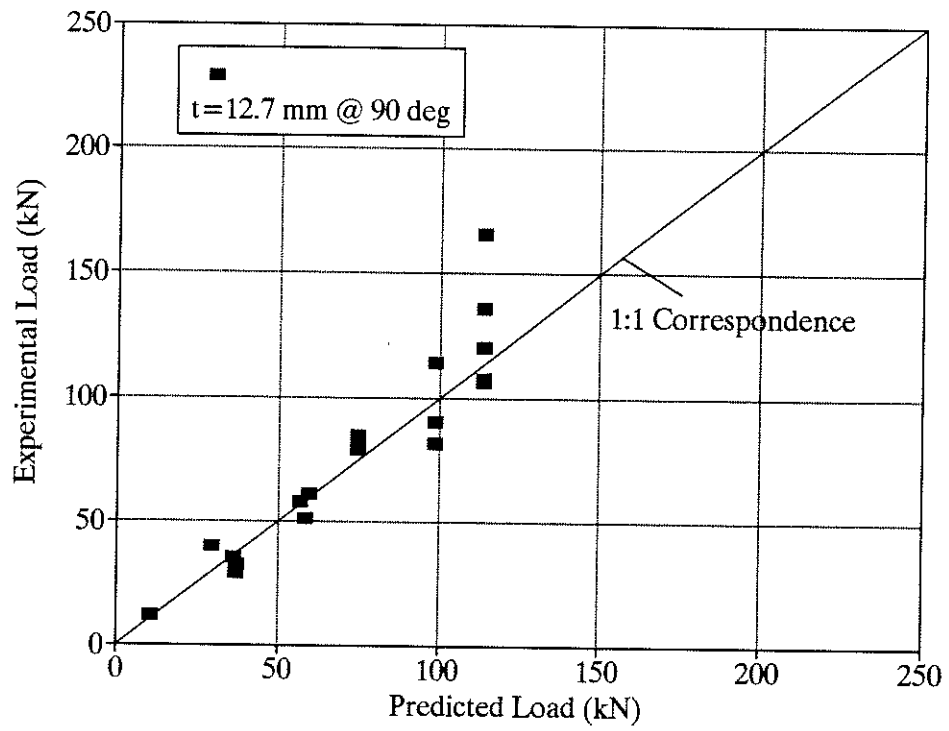Figure 5.26 Experimental vs. Model Results for 45 deg. Connections

Figure 5.27 Experimental vs. Model Results for 90 deg. Connections

CHAPTER 6 CONCLUSIONS

6.1 SUMMARY

The high strength-to-weight ratio and non-corrosion characteristics of fibre-reinforced composites makes them extremely attractive as a structural material. However, the lack of understanding of the behaviour of advanced composite materials has limited their acceptance and use. The structural integrity and the capacity of buildings fabricated from fibre reinforced composite materials are mainly controlled by the behaviour of the connections. In civil structural applications, bolted connections are the most practical, since they are easily assembled and disassembled, and usually cost-effective when compared to other types of connections. Therefore an understanding of the behaviour of bolted connections is necessary for the full potential of this material to be realized in civil structural applications.

An experimental program was undertaken at the University of Manitoba to investigate the behaviour of bolted connections for fibre-reinforced composite materials. A total of 102 single-bolt double-lap connections were tested to determine the effects of various geometric parameters on the ultimate strength and mode of failure. In addition, an extensive material test program was conducted to characterize the material properties and utilize them in the proposed design procedure.

148

Based on the experimental results, a mathematical model and a design procedure are proposed to predict the ultimate load and failure modes of single-bolt connections in fibre-reinforced composite materials. The model can be applied to other composite materials through the use of a correlation coefficient which can be evaluated by limited test data. The procedure is simple and is ideal for implementation in design codes.

6.2 CONCLUSIONS

Based on the observed and measured behaviour of 102 single-bolt connections, the following conclusions can be made:

1. Slipping resistance is negligible at the specified bolt torque of 32.5 N-m (24 ft-lbs) used in this investigation.

2. Connection load-displacement behaviour is linear up to failure regardless of the modes of failure.

3. Connections that failed in a catastrophic manner, such as in net tension and cleavage failure, experienced a sudden drop in load carrying capacity followed by large displacements represented by a "step" in the load-displacement curve.

4. For connections with a 0° fibre orientation (loaded parallel to the unidirectional fibres), the member width-to-hole-diameter ratio (w/d) had a significant effect on the mode of failure. For relatively small edge distances the mode of failure changed from net tension to cleavage failure by

increasing the (w/d) ratio. For relatively large edge distances the mode of failure changed from net tension to bearing failure by increasing the (w/d) ratio.

5. The bearing strength for connections loaded parallel to the unidirectional fibres increased with increasing (w/d) ratios up to a limiting value of (w/d)=5. Therefore, a minimum (w/d) ratio of 5 is recommended.

6. For connections loaded parallel to the unidirectional fibres with a relatively narrow width, the mode of failure is net tension failure, regardless of the magnitude of the edge distance. For relatively wide connections the mode of failure changed from cleavage to bearing failure with increasing edge distance-to-hole diameter ratios (e/d).

7. The bearing strength of connections loaded parallel to the unidirectional fibres increased with increasing (e/d) ratios up to a limiting value of (e/d)=5. Therefore, a minimum (e/d) ratio of 5 is recommended.

8. Increasing the thickness of the members increased the ultimate load capacity of the connection. It was found that the member thickness had little effect on the bearing stresses and the mode of failure. Results suggest that high strength structural bolts, tightened to a torque of 32.5 N-m (24 ft-lbs) as used in this investigation, were adequate to remove most of the influence of the material thickness.

9. Connections with members having fibre orientations of 45° and 90° to the direction of the applied load tend to be more susceptible to net tension

failure. Due to the transverse reinforcement of the unidirectional fibres at angles with respect to the applied load, the cleavage mode of failure was suppressed. Only at extreme geometric ratios could the cleavage and bearing modes of failure be induced.

10.   The bearing strengths of connections with members having fibre orientations of 45° and 90° to the applied load tend to increase with increasing (w/d) and (e/d) ratios. Similar to the connections with fibre orientations parallel to the applied load, the strength increases tended to level off at values of 5 for both the (w/d) and (e/d) ratios. However, to achieve bearing failure, the results seem to indicate the minimum (w/d) and (e/d) ratios are larger.

11.   The ultimate strength of connections with fibre orientations of 45° and 90° with respect to the applied load were respectively, 18% and 24% lower than the corresponding connections with a 0° fibre orientation (parallel to the applied load).

12.   The magnitude of the stress concentrations along the net section perpendicular to the applied load are highly influenced by the width of the connections. The stress concentrations tend to increase with increasing width. For relatively narrow specimens the stress concentrations adjacent to the hole are in the order of 2 to 3 and for relatively wide connections are in the order of 5 to 6. The member width is the dominant geometric variable affecting the efficiency of a connection.

13.   The effects of connection edge distance and thickness on the stress concentrations are less than the effect of member width. Stress concentrations tended to decrease with increasing edge distance and were negligibly affected by the member thickness.

14.   The stress concentrations seemed to increase with change in fibre orientation from $0°$ to $90°$ with respect to the applied load.

15.   The proposed design procedure predicts the ultimate load and failure mode of the connections with an adequate degree of accuracy. On average, the predicted loads were within 10% of the experimentally determined values. For connections with a $0°$ fibre orientation, parallel to the applied load, the correspondence between the predicted and experimental modes of failure is excellent.

16.   Because the procedure is based on isotropic theory and uses empirical data to correlate the failure criteria it could be used for a variety of different composite material systems.

17   Considering the versatility and simplicity of the proposed design procedure, it is ideal for implementation in design codes.

6.3 RECOMMENDATIONS FOR FUTURE STUDY

1. The parametric study conducted in this investigation could be repeated, except with intermediate values of the geometric dimensions with respect to the ones selected in this investigation.

2. The parametric study may be extended to include more connections that fall within the transition zones of the various failure modes to study the behaviour of combined failure.

3. The parametric study may be extended to include the effects of other parameters such as hole diameter, bolt diameter, clearance, bolt stiffness, clamping force, and environmental effects.

4. The study of stress and strain distributions may be extended to include the instrumentation of strain gauges to narrow connections, with a width less than 100 mm (4 in.). Strain gauges may be placed at locations other than the net section to record maximum radial strains in the bearing area around the hole and the maximum tensile strains that occur at the free edge of the connections where cleavage cracks initiate.

5. To help characterize the behaviour of beam-column connections, tests may be conducted to investigate the effects of prying action and the bolt pulling through the thickness direction of the material.

6. The experimental program may be extended to include multi-bolt connections and effects of such factors as number of bolts per row, number of bolts per column, bolt pattern, load bearing/bypass ratios, and stress field

interactions between bolt holes.

7.   Combined bolted and bonded connections may be investigated to study the general behaviour as well as the load sharing between the bolts and the adhesive.

REFERENCES

1.   Green, A., Glass-Fibre-Reinforced Composites in Building Construction. *Transportation Research Record 1118*, pp.73-76.

2.   Sheard, P. ,1992 , Expansion of Composite Material Applications. *Advanced Materials Technology International 1992* London, Sterling Publications Limited.

3.   Ahmad, S.H. and Plecnik, J.M., Transfer of Composite Technology to Design and Construction of Bridges. *Final Report. Prepared for U.S. Department of Transportation Federal Highway Administration.* Feb. 1988.

4.   Meier, U., Proposal for a Carbon Fibre Reinforced Composite Bridge Across the Straight of Gibraltar at its Narrowest Site. *Proc Instn Mech Engrs*, Vol.201, No.B2, 1987, pp.73-78.

5.   Meier, U., Topic 2 Designing and Producing Materials by Combination. *Materials and Structures*, Vol.21, 1988, pp.85-89.

6.   Plecnik, J.M., Ballinger, E., Rao, J.K. and Ahmad, S., State-of-the-Art: Composite Materials for Bridges. *Proceedings of a Workshop on Research Needs for Short and Medium-Span Bridges*, Computech Engineering Services, 1987, CES Report No. 5518.2, Berkeley, California.

7.   Barbero, E.J., Pultruded Structural Shapes-From the Constituents to the Structural Behaviour. *SAMPE Journal*, Vol. 27, No. 1, January/February 1991, pp.25-30.

8.   Meier, U., Muller, R. and Puck, A., FRP-Box Beams Under Static and Fatigue Loading. *Proceedings of the International Conference on Testing, Evaluation and Quality Control of Composite*, ed. T. Feest, 1983, Butterworth, Guilord.

9.   Bank, L.C., Flexural and Shear Moduli of Full-Section Fibre Reinforced Plastic (FRP) Pultruded Beams. *Journal of Testing and Evaluation*, JTEVA, Vol. 17, No. 1, Jan., 1989, pp.40-45.

10.   Bank, L.C., Properties of Pultruded Fibre Reinforced Plastic Structural Members. *Transportation Research Record 1223, Bridge Design and Performance and Composite Materials*, Transportation Research Board, Washington, D.C., 1989, pp. 117-124.

11. Mosallam, A.S., Short and Long-Term Behaviour of a Pultruded Fibre Reinforced Plastic Frame. *PhD. Dissertation School of Engineering and Architecture, Catholic University of America*, Washington, D.C., Oct., 1990.

12. Mallick, P.K.,1988. *Fibre-Reinforced Composites: Materials, Manufacturing, and Design*. New York:Marcel Decker, Inc.

13. Cosenza, F., Mechanical Fasteners for Composites. *Materials Engineering*, Aug. 1987, pp.32-37.

14. Godwin, E.W. and Matthews, F.L., A Review of the Strength of Joints in Fibre-Reinforced Plastics Part 1. Mechanically Fastened Joints. *Composites*, July 1980, pp.155-160.

15. Bickford, J.H., Bolt Torque: Getting it Right. *Machine Design*, June 21, 1990, pp.67-71.

16. Bank, L.C., Mosallam, A.S., and McCoy, G.T., Design and Performance of Connections for Pultruded Frame Structures. *47th Annual Conference, Composites Institute, The Society of the Plastics Industry, Inc.* February 3-6, 1992 Session 2-B pp.1-8.

17. Tsiang, T., Survey of Bolted-Joint Technology in Composite Laminates. *Composite Technology Review*, Vol.6, No.2, 1984, pp.74-77.

18. Vinson, J.R., Mechanical Fastening of Polymer Composites, *Polymer Engineering and Science*, Mid-October, 1989, Vol. 29 No. 19, pp.1332-1339.

19. Matthews, F.L., Load Carrying Joints. *Composite Materials in Aircraft Structures*. D. Middleton, Ed., Longman Group UK Limited, 1990. Ch. 9. pp.142-155.

20. Bord, C., Les Materiaux Composites. *CEP Edition (Editions de l'Usine nouvelle)*, 1983, Paris.

21. Oplinger, D.W., On the Structural Behaviour of Mechanically Fastened Joints in Composite Structures *Proceedings of the Fourth Conference on Fibrous Composites in Structural Design*, San Diego, California, November 14-17 1978, New York, Plenum Press 1980, pp.575-601.

22. Timoshenko, S.P., and Goodier, J.N., *Theory of Elasticity*. Third Edition, McGraw-Hill, New York, 1951, pp.90-97.

23.   Lekhnitskii, S.G., *Anisotropic Plates*, Translated from the Second Russian Edition by S.W. Tsai and T. Cheron, Gordon and Breach, Science Publishers, New York, 1968.

24.   Bickley, W.G., The Distribution of Stress Round a Circular Hole in a Plate, *Philosophical Transactions of the Royal Society (London)*, Series A, Vol. 227, 1928, pp.383-415.

25.   De Jong, T., Stresses Around Pin-Loaded Holes in Elastically Orthotropic or isotropic Plates, *Journal of Composite Materials*, Vol. 11, July, 1977, pp.313-331.

26.   Collings, T.A., The Strength of Bolted Joints in Multi-Directional CFRP Laminates. *Composites*, Vol.8, No.1, Jan. 1977, pp.43-55.

27.   Kretsis, G. and Matthews, F.L., The Strength of Bolted Joints in Glass Fibre/Epoxy Laminates. *Composites*, April 1985.

28.   Smith, P.A., Ashby, M.F., and Pascoe, K.J., Modelling Clamp-Up Effects in Composite Bolted Joints. *Journal of Composite Materials*, Vol. 21 Oct., 1987, pp.878-897.

29.   Ramkumar, R.L., Bolted Joint Design, *Test Methods and Design Allowables for Fibrous Composites, ASTM STP 734*, C. C. Chamis Ed., American Society for Testing and Materials, 1981, pp.376-395.

30.   Tang, S., Failure of Composite Joints Under Combined Tension and Bolt Loads. *Journal of Composite Materials*, Vol.15, July 1981, pp.329-335.

31.   Agarwal, B.L., Behaviour of Multifastener Bolted Joints in Composite Materials. *AIAA 18th Aerospace Sciences Meeting*, Pasadena, California, Paper No. 80-0307, Jan., 1980.

32.   Pyner, G.R. and Matthews, F.L., Comparison of Single and Multi-Holed Bolted Joints in Glass Fibre Reinforced Plastic. *J. Composite Materials*, Vol.13, July 1979, pp.232-239.

33.   Kim, R.Y. and Whitney, J.M., Effect of Temperature and Moisture on Pin Bearing Strength of Composite Laminates. *J. Composite Materials*, Vol.10, April 1976, pp.149-155.

34.   Bailie, J.A., Duggan, M.F., Bradshaw, N.C. and McKenzie, T.G., Design Data for Graphite Cloth Epoxy Bolted Joints at Temperatures up to 450 K. *Joining of Composite Materials, ASTM STP 749*, K.T. Kedward, Ed., American Society for Testing and Materials, 1981, pp.165-180.

35.   Crews, J.R., Jr., Bolt-Bearing Fatigue of a Graphite/Epoxy Laminate, *Joining of Composite Materials, ASTM STP 749*, K.T. Kedward, Ed., American Society for Testing and Materials, 1981, pp.131-144.

36.   Tanis, C. and Poullos, M., Composite Fastener Applications for Helicopter Composite Structure *Proceedings of the Fourth Conference on Fibrous Composites in Structural Design*, San Diego, California, November 14-17 1978, New York, Plenum Press 1980, pp.652-657.

37.   Chamis, C.C., Simplified Procedures for Designing Composite Bolted Joints. *43rd Annual Conference, Composites Institute, The Society of the Plastics Industry, Inc.*, Feb., 1988, pp.1-5 : Session 23-D.

38.   Johnson, M. and Matthews, F.L., Determination of Safety Factors for Use When Designing Bolted Joints in GRP, *Composites*, Vol. 10, No. 2, Apr. 1979, pp.73-76.

39.   Hart-Smith, L.J., Mechanically-Fastened Joints for Advanced Composites - Phenomenological Considerations and Simple Analyses. *Proceedings of the Fourth Conference on Fibrous Composites in Structural Design*, San Diego, California, November 14-17 1978, New York, Plenum Press 1980, pp.543-574.

40.   Hart-Smith, L.J., Joints, *Composite Structures Analysis and Design*, Vol. 1, 1987, pp.479-495.

41.   Whitney, J.M. and Nuismer, R.J., Stress Fracture Criteria for Laminated Composites Containing Stress Concentrations. *Journal of Composite Materials*, Vol.8, July 1974, pp.254-265.

42.   Nuismer, R.J. and Whitney, J.M., Uniaxial Failure of Composites Laminates Containing Stress Concentrations. *Fracture Mechanics of Composites, ASTM STP 593*, American Society for Testing and Materials, 1975, pp.117-142.

43.   Waddoups, M.E., Eisenmann, J.R., and Kaminski, B.E., Macroscopic Fracture Mechanics of Advanced Composite Materials, *Journal of Composite Materials*, Vol.8, Oct. 1971, pp.446-454.

44. Pipes, R.B., Wetherhold, R.C., and Gillespie, J.W., Notched Strength of Composite Materials. *Journal of Composite Materials*, Vol.13, April 1979, pp.148-160.

45. Hill, R., 1950, *The Mathematical Theory of Plasticity*. London, Oxford University Press.

46. Azzi, V.D. and Tsai, S.W., Anisotropic Strength of Composites. *Experimental Mechanics*, Vol.5, Sept. 1965, pp.283-288.

47. Tsai, S.W. and Wu, E.M., A General Theory of Strength for Anisotropic Materials. *Journal of Composite Materials*, Vol.5, January 1971, pp.58-80.

48. Yamada, S.E. and Sun, C.T., Analysis of Laminate Strength and Its Distribution. *Journal of Composite Materials*, Vol.12, July 1978, pp.275-284.

49. Snyder, B.D., Burns, J.G. and Venkayya, V.B., Composite Bolted Joint Analysis Programs. Paper No. 88-2423, 1988, pp.1648-1655.

50. Garbo, S.P., Design and Analysis of Composite Structures with Stress Concentrations. McDonnell Aircraft Co., McDonnell Douglas Corp., St. Louis, MO, pp.95-127.

51. Pataro, R.N., Stress Concentrations in Composite Structures. Chrysler Corp., Detroit, Michigan. pp.271-280.

52. Agarwal, B.L., Static Strength Prediction of Bolted Joints in Composite Material. *AIAA Journal*, Vol.18, No.11, Nov. 1980, pp.1371-1375.

53. Soni, S.R., Failure Analysis of Composite Laminates with a Fastener Hole. *Joining of Composite Materials. ASTM STP 749*, Ed. K.T. Edward, American Society for Testing and Materials, Philadelphia. 1981, pp.145-164.

54. Garbo, S.P., Hong, S.W. and Kim, W., Strength Evaluation of Helicopter Composite Bolted Joints. American Institute of Aeronautics and Astronautics, Inc., Paper No. 86-0973, 1986, pp.486-494.

55. Lee, Y.J. and Chen, W.H., Failure Process and Bolted Joint Strength of Composite Laminates. *Journal of the Chinese Society of Mechanical Engineers*, Vol.9, No.3, 1988, pp.169-182.

56. Waszczak, J.P., and Cruse, T.A., A Synthesis Procedure for Mechanically Fastened Joints in Advanced Composite Materials. *Technical Report AFML-TR-73-145*, Vol. 2, Air Force Materials Laboratory, Sept., 1973.

57. York, J.L., Wilson, D.W. and Pipes, R.B., Analysis of the Net Tension Failure Mode in Composite Bolted Joints. *Journal of Reinforced Plastics and Composites*, Vol.1, April 1982, pp.141-152.

58. Chang, F.K., Scott, R.A., and Springer, G.S., Strength of Mechanically Fastened Composite Joints. *J. Composite Materials*, Vol.16, Nov. 1982, pp.470-494.

59. Chang, F.K., Scott, R.A., and Springer, G.S., Failure of Composite Laminates Containing Pin Loaded Holes-Method of Solution, *Journal of Composite Materials*. Vol. 18, No. 3, May 1984, pp.255-278.

60. Chang, F.K., Scott, R.A., and Springer, G.S., Design of Composite Laminates Containing Pin Loaded Holes, *Journal of Composite Materials*. Vol. 18, No. 3, May 1984, pp.279-289.

61. Wong, C.M.S. and Matthews, F.L., A Finite Element Analysis of Single and Two-Hole Bolted Joints in Fibre Reinforced Plastic. *Journal of Composite Materials*, Vol.15, Sept. 1981, pp.481-491.

62. Rowlands, R.E., Rahman, M.U., Wilkinson, T.L., and Chiang, Y.I., Single- and Multiple-Bolted Joints in Orthotropic Materials. *Composites*, Vol. 13, No. 3, July, 1982, pp.273-279.

63. Wang, S. and Han, Y., Finite Element Analysis for Load Distribution of Multi-Fastener Joints. *J. Composite Materials*, Vol.22, Feb. 1988, pp.124-135.

64. Lucking, W.M., Hoa, S.V., and Sankar, T.S., The Effect of Geometry on Interlaminar Stresses of [0/90]$_s$ Composite Laminates with Circular Holes. *Journal of Composite Materials*, Vol. 17, March, 1984, pp.188-198.

65. Dutta, A., 1990, Modelling the Behaviour of Bolted Composite Material Connections. M.Eng. Thesis, Department of Civil Engineering, Carlton University.

66. Naik, R.A. and Crews, J.H., Stress Analysis Method for a Clearance Fit Bolt Under Bearing Loads. NASA, No. 85-0746, 1985, pp.522-527.

67. Hyer, M.W. and Klang, E.C., Stresses Around Holes in Pin-Loaded Orthotropic Plates. *J. Aircraft*, Vol.22, No.12, Dec. 1985, pp.1099-1101.

68. Eriksson, L.I., Contact Stresses in Bolted Joints of Composite Materials. *Composite Structures*, Vol.6, 1986, pp.57-75.

69. Rosner, C.N., Mechanical Properties of GFRP Material Used for Single-Bolted Connections. *Technical Paper for MSc. Thesis: Single-Bolted Connections for Orthotropic Fibre-Reinforced Composite Structural Members.* Civil Engineering Department, University of Manitoba, Winnipeg, Manitoba, Sept., 1992.

70. Morrison Molded Fibre Glass Company, Extren Fibreglass Structural Shapes Design Manual.

71. Rosner, C.N., Experimental Results of GFRP Single-Bolted Connections. *Technical Paper for MSc. Thesis: Single-Bolted Connections for Orthotropic Fibre-Reinforced Composite Structural Members.* Civil Engineering Department, University of Manitoba, Winnipeg, Manitoba, Sept., 1992.

APPENDIX
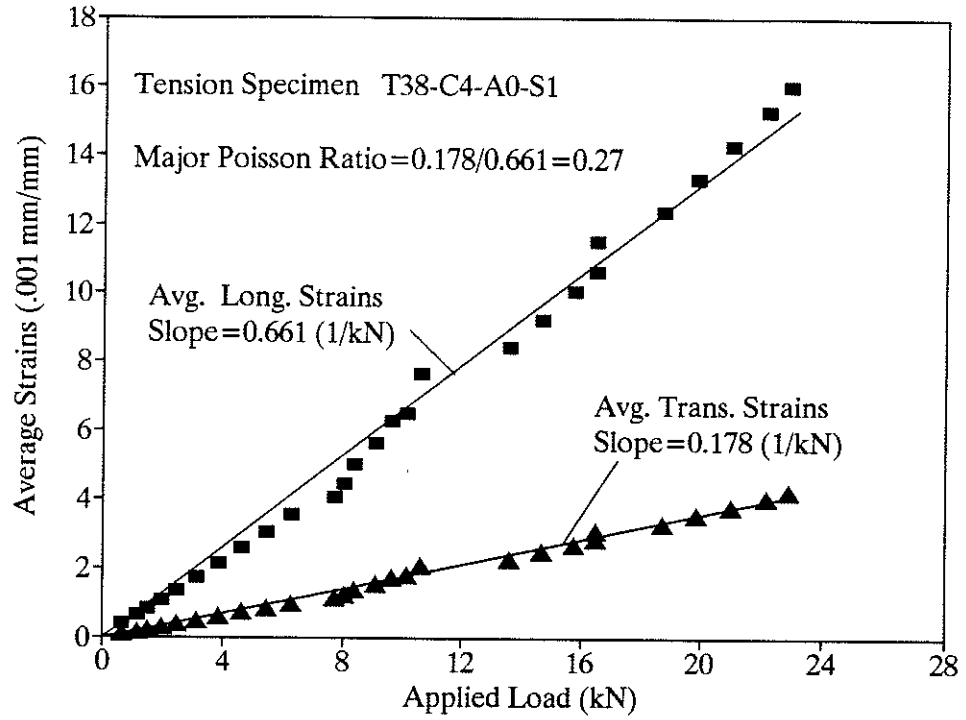
Figure A1 Determination of Major Poisson Ratio (Specimen #1)
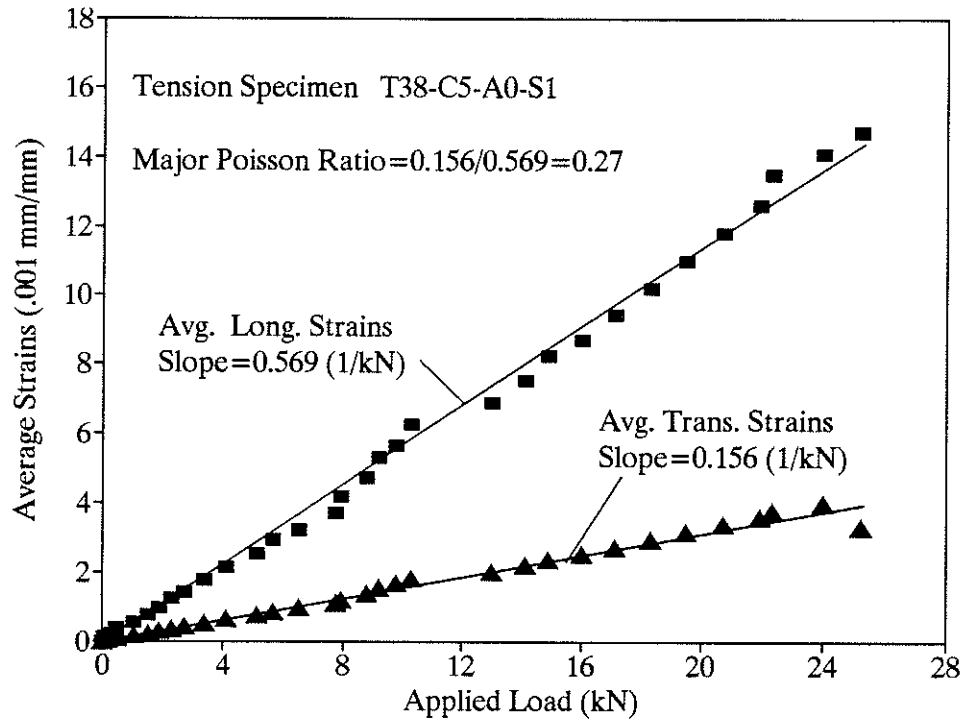
Figure A2 Determination of Major Poisson's Ratio (Specimen #2)
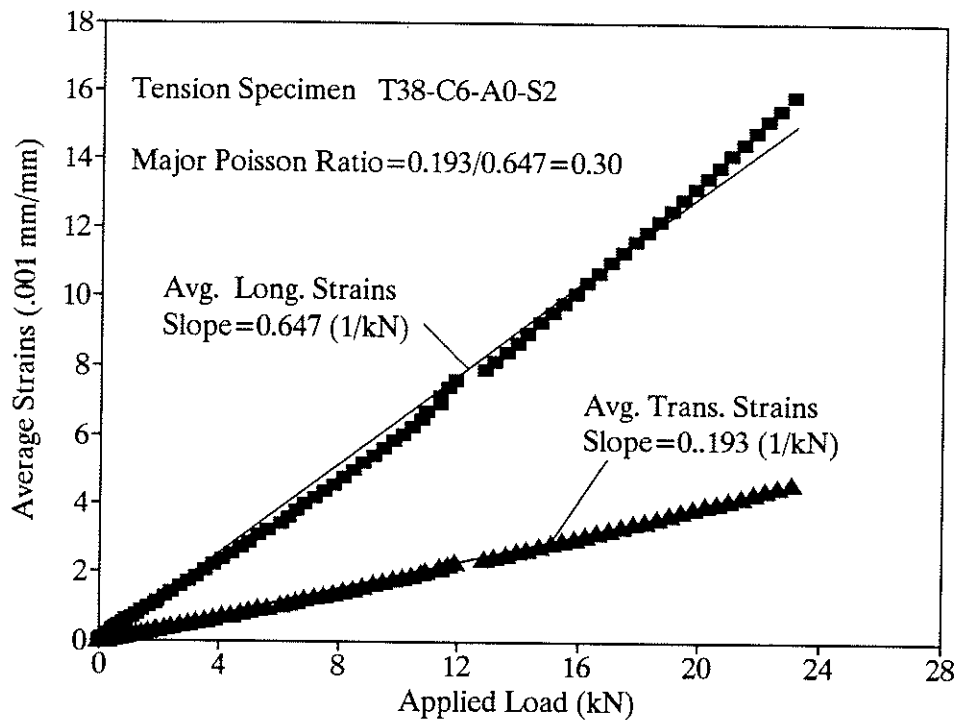
Figure A3 Determination of Major Poisson's Ratio (Specimen #3)
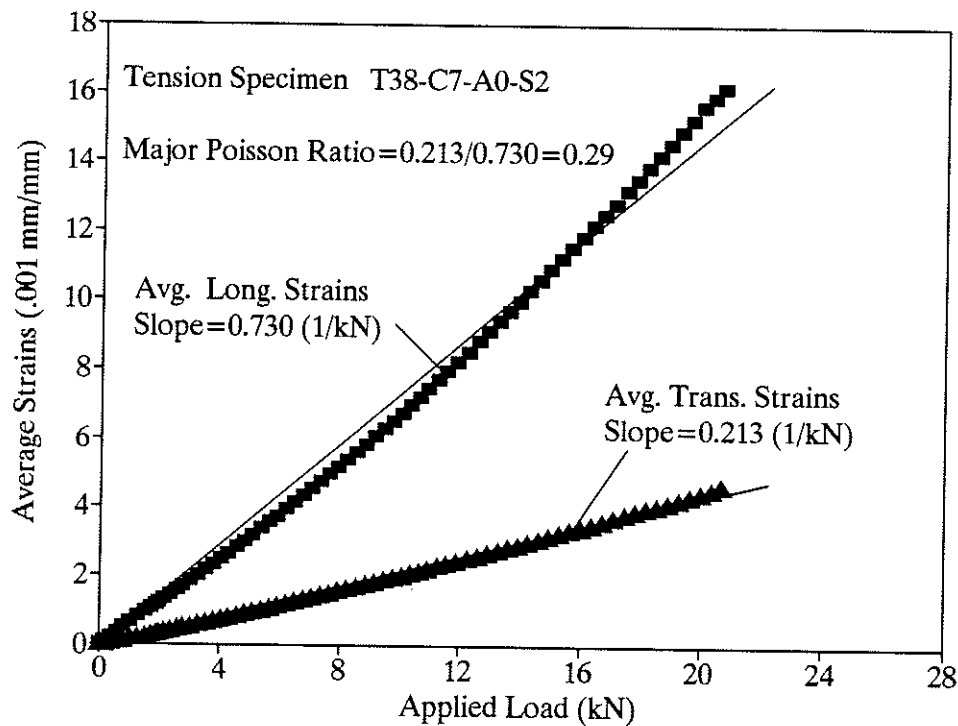

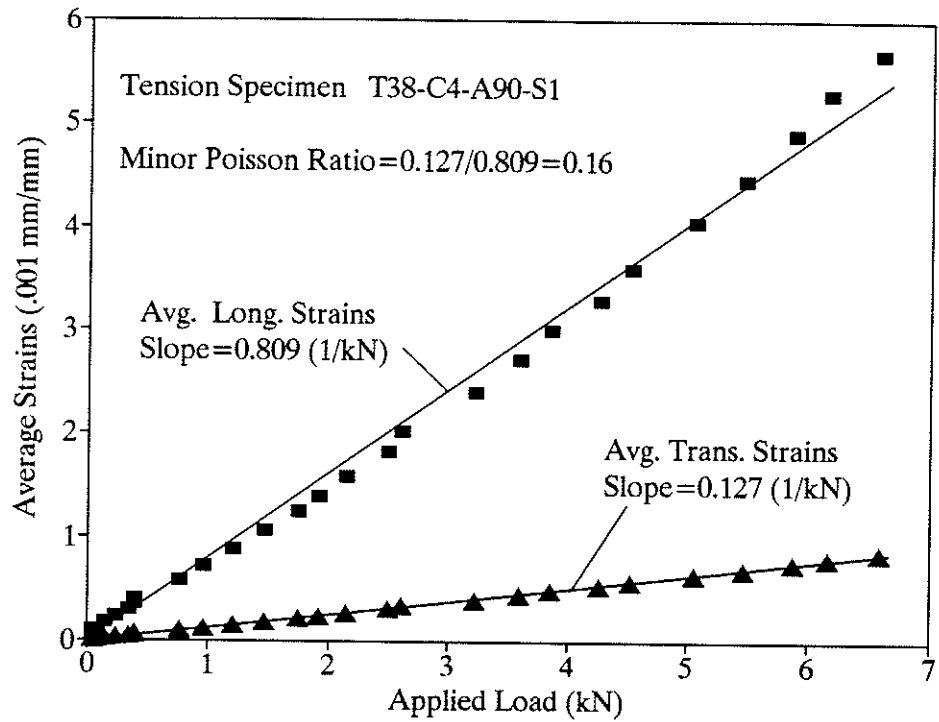Figure A4 Determination of Major Poisson's Ratio (Specimen #4)

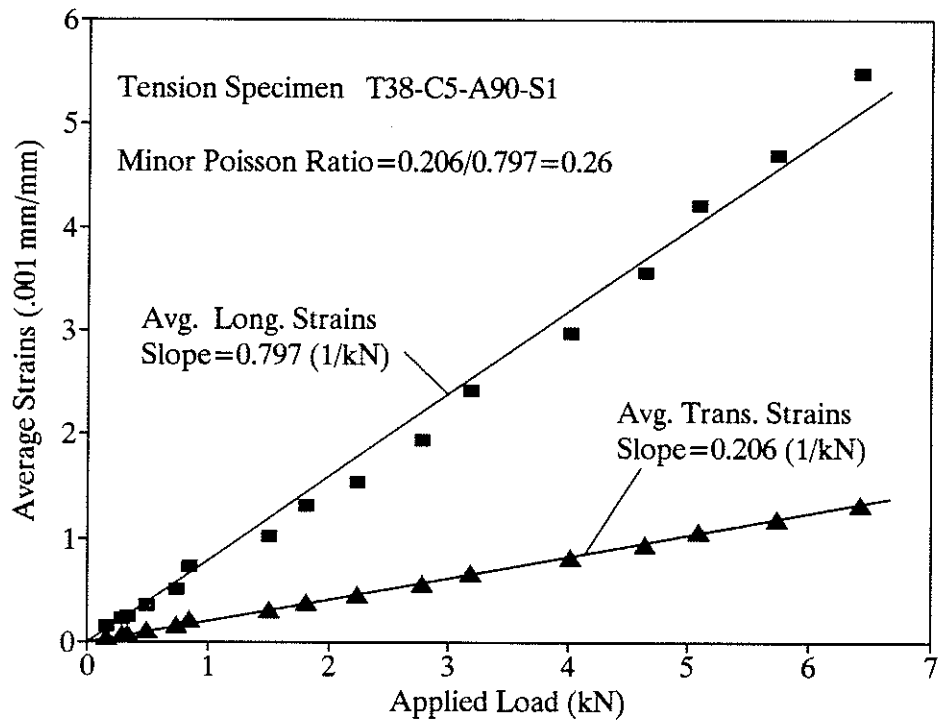Figure A5 Determination of Minor Poisson's Ratio (Specimen #1)

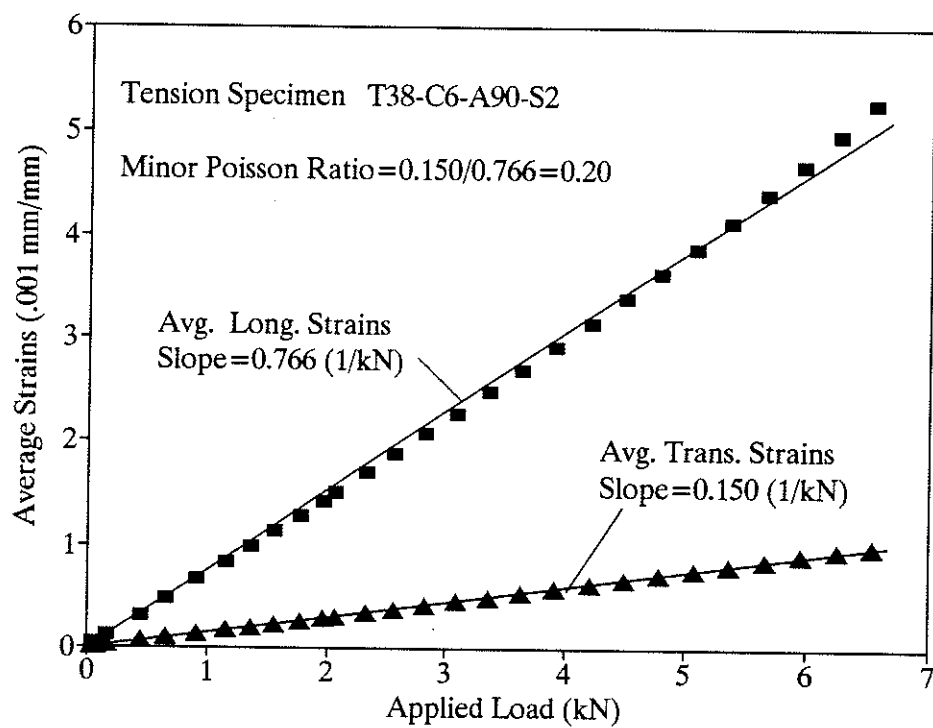
Figure A6 Determination of Minor Poisson's Ratio (Specimen #2)

Figure A7 Determination of Minor Poisson's Ratio (Specimen #3)